Università degli studi di Genova

Scuola di Scienze Matematiche, Fisiche e Naturali

Corso di Laurea Magistrale in Fisica

Modelling thermal transport in non-collinear magnets

Supervisors:
Prof. Sergey Artyukhin
Prof. Riccardo Ferrando
Co-Supervisor:
Prof. Francesco Bisio

Candidate:
Margherita Parodi

Defended on October 17, 2022

Contents

Chapter 1

Abstract

Magnetic memory and logic devices, including prospective ones based on skyrmions and other non-collinear spin textures, inevitably produce heat. Thus, controlling heat flow is essential for the performance. Here we study thermal conductivity in the most basic non-collinear magnet with a spin spiral ground state.

Non-collinearity of spins leads to anharmonic three-magnon interactions, absent in collinear magnets, that give rise to scattering processes where one magnon may split into two or two magnons can merge into one. These additional scattering events imply lower magnon lifetime and the lowering of thermal conductivity compared to a collinear case. Indeed, recent experiments show a significant decrease of thermal conductivity upon the transition from ferromagnetic to spiral state in multiferroic GaV_4S_8.

In order to study the most basic effects of spin non-collinearity on thermal transport, we focus on the magnon scattering in a quasi-one dimensional spiral magnet. We start from a model Hamiltonian with competing nearest and next-nearest neighbor interactions and expand the spin-spin interaction up to the third order in bosonic operators using the Holstein-Primakoff transformation. This results in the magnon scattering matrix that is used in the description of the dynamics of the excitations via a kinetic equation. Since the scattering matrix has non-diagonal elements in the magnon basis, magnons are not the eigenmodes. By diagonalizing the symmetrized collision matrix, we obtain linear combinations of magnons, relaxons, that describe exponential decay of non-equilibrium magnon distribution to the equilibrium one, and can be interpreted as heat carriers. We develop relaxon formalism for magnets and compute the magnetic contribution to the thermal conductivity.

Due to complex features of the scattering function, computations require fine k-space grid. We have developed a Mathematica code that implements the procedure, as well as a parallel C++/OpenMP version of the code that allows to scale the calculations to a large number of cores.

The work paves the path to realistic modelling of magnetic contribution to thermal transport in non-collinear magnets.

Chapter 2

Introduction

Competing spin interactions, or magnetic frustration, is an ideal playground for non-collinear magnetic states, such as spin spirals and skyrmions. They are actively discussed as a potential platform for information technology, and arise in many materials, for example, due to competition between nearest and next-nearest neighbor exchange interactions, spin-orbit-driven anisotropic interactions, or thermal fluctuations. Spin spirals break inversion symmetry and may give rise to ferroelectric polarization, which holds a promise for electric control of magnetism [1–4].

Recent advent of ultrafast experiments allowed us to observe and manipulate magnetic and structural orders on their natural timescale. Complex switching dynamics and excitations, such as magnons, phonons and combined magnon-polar phonon excitations ("electromagnons") can be excited by external fields [5]. Switching is crucial for memory devices and is usually facilitated by domain nucleation and domain wall motion [6, 7]. Dynamics of localized spin textures, domain walls and skyrmions is in the focus of active experimental investigations [8].

Recent ultrafast experiments observed strong change of thermal conductivity upon the phase transition from ferromagnetic to spiral and skyrmion states [9], as seen in Fig. 2.1. The origin of the effect is still debated, and one possible explanation is the scattering of magnons and phonons off the domain walls formed in abundance in non collinear states.

While phonon contribution to the thermal conductivity is usually significant, in magnetic logic and memory devices energy is mostly dissipated as magnons. Thus controlling magnon thermal transport is crucial to keep the devices operating.

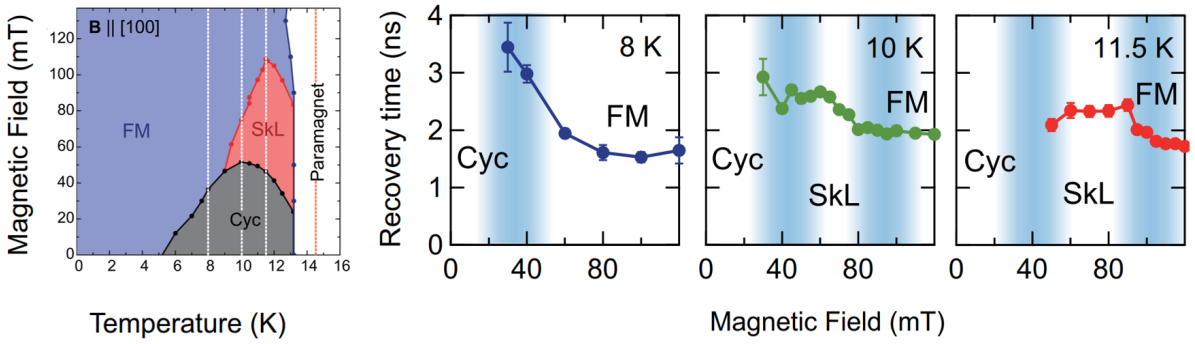

Figure 2.1: Non-collinear magnetic phases in GaV_4S_8 and variation of thermal conductivity, as represented by the inverse magnetization recovery time, across the phase diagram. 50% increase of the thermal conductivity in the spiral phase is observed [9].

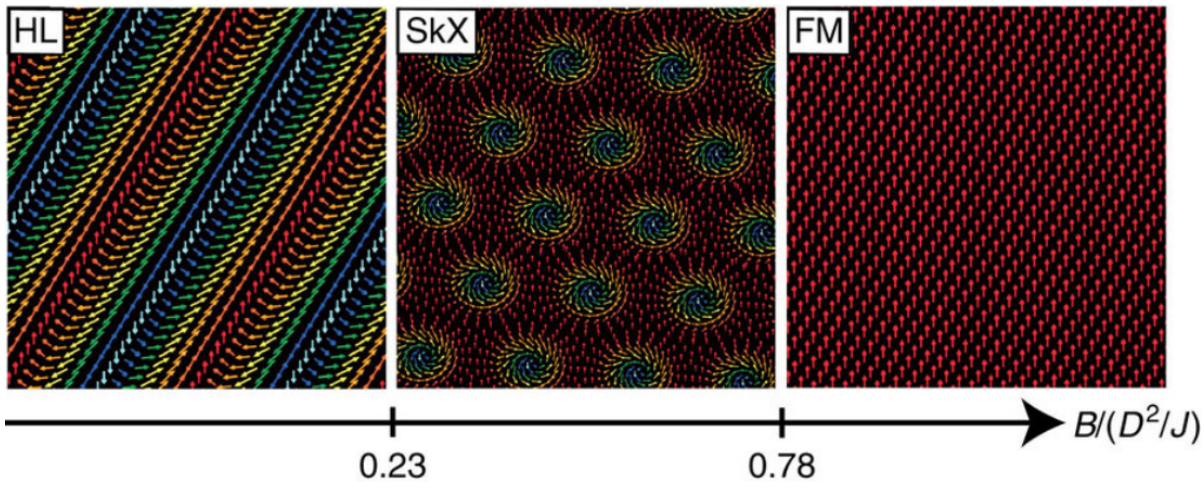

Figure 2.2: Non-collinear magnetic structures, helimagnetic (HL) and skyrmion lattice (SkX) as compared to a collinear ferromagnetic state (FM). Image adopted from [10].

In a collinear spin structure, such as a ferromagnet or an antiferromagnet, the magnon Hamiltonian has no third order terms. However, non-collinearity of spins leads to cubic anharmonic terms [11]. To put it in simple terms, since commutation relations of spin operators are neither bosonic nor fermionic, transformation to bosonic operators is often used to diagonalize the spin Hamiltonian. The number of bosons on a site describes the deviation of spin from the quantization axis and aligning the axis with the classical spin direction leads to low number of bosons at low temperatures and allows to expand in the number of bosons and to neglect higher-order terms. S_x and S_y are expressed via single bosonic operators and S_z – via $a^\dagger a$. For collinear spins the quantization axes are parallel and therefore the terms in the exchange operator involving $S_x S'_x$ and $S_y S'_y$ contain two bosonic operators, while $S_z S'_z$ contains four. In a non-collinear state, however, quantization axes of neighboring spins are tilted with respect to each other, which leads to three-magnon terms. These terms describe events where a magnon splits into two or two magnons merge into one. This leads to magnon scattering and a finite magnon mean free path, and thus a finite magnetic contribution to thermal conductivity.

The description of thermal transport is based on Boltzmann transport equation [12]. In its right-hand side, the collision matrix accounts for the scattering on magnons with different wave vectors. Since it is non-diagonal, magnons are not eigenvectors of the matrix, and thus not heat carriers – there is no relaxation time for a single magnon! The collision matrix can be diagonalized and its eigenvectors describe actual heat carriers – relaxons, which are linear combinations of many magnons. The inverse eigenvalues are the relaxation times. Comparing the thermal conductivity estimated from magnon and relaxon pictures, we see that magnons give lower thermal conductivity. That is because the relaxation time for a magnon in a single mode approximation corresponds to the scattering to the state with another wave vector, which may also contribute to thermal conductivity. At the same time, a relaxon combines many such magnons and its relaxation time is thus higher.

Another consequence of non-collinearity is the appearance of anomalous terms of the form $aa + a^\dagger a^\dagger$ in the Hamiltonian. Diagonalizing such terms with a Bogoliubov transformation leads to enhanced scattering amplitudes into low-energy states at $k = 0$ and $k = \pm Q$, with Q being the spiral wave vector. The Goldstone mode at $k = \pm Q$ is

gapped by easy-plane anisotropy. It will be therefore essential to study the effects of this anisotropy and the spiral wave vector, that determines the degree on non-collinearity, on the thermal conductivity. An important technical aspect is the convergence of the results with respect to the reciprocal space grids.

This Thesis is structured in the following way: we start with the introduction on the Boltzmann transport equation and on the elementary excitations in magnets. We then derive the magnetic Hamiltonian, describing the magnons in a spiral magnet, and diagonalize its second-order part. The resulting Hamiltonian, including third-order terms, is used to formulate the kinetic equation. Its solution is obtained in the basis of eigenvectors of the symmetrized scattering matrix (the relaxon basis). We develop Mathematica [13] code to calculate the thermal conductivity, and then turn it into a C++/OpenMP code optimized for speed, which allows to use much finer reciprocal space grids. We conclude with the description of the results.

2.1 Thermal conductivity

2.1.1 Boltzmann transport equation

If a material is subject to a thermal gradient, there will be a heat flux $\mathbf{Q}$, defined as the energy per unit time per unit area (perpendicular to $\mathbf{Q}$), from the hot to the cold environment.

Thermal conductivity κ is defined as the proportionality coefficient between the thermal gradient and the heat flux:

$$Q_i \equiv -\kappa_{ij}(\nabla T)_j. \tag{2.1}$$

In the harmonic approximation, discussed by Hardy [14], the heat flux can be written as:

$$\mathbf{Q} = \int d\boldsymbol{k} E_{\boldsymbol{k}} \mathbf{v}_{\boldsymbol{k}} \Delta f_{\boldsymbol{k}}, \tag{2.2}$$

where $E_{\boldsymbol{k}}$ and $\mathbf{v}_{\boldsymbol{k}}$ are respectively the energy and velocity of the excitations with the wave vector $\boldsymbol{k}$, and $\Delta f_{\boldsymbol{k}}$ is the deviation of the magnon distribution function from the thermal equilibrium, $f^0_{\boldsymbol{k}}$, computed at the temperature $T(\mathbf{r}, t)$:

$$\Delta f_{\boldsymbol{k}} = f_{\boldsymbol{k}} - f^0_{\boldsymbol{k}}. \tag{2.3}$$

Integrating the distribution function, we get the total number of excitations:

$$\int d\boldsymbol{k} \int d\mathbf{r}\, f_{\boldsymbol{k}}(\mathbf{r}) = N_{\text{exc}}. \tag{2.4}$$

Putting together Eq. (2.1) and Eq. (2.2), we can find the thermal conductivity of the system if we know $\Delta f_{\boldsymbol{k}}$. The equation for $\Delta f_{\boldsymbol{k}}$ is the Boltzmann transport equation, that describes the evolution of the distribution function.

Let us consider what can cause the distribution function to change: first of all, diffusion processes, where a magnon with momentum $\boldsymbol{k}$, in a time t, moves from position $\mathbf{r}$ to $\mathbf{r} + \mathbf{v}_{\boldsymbol{k}} t$:

$$\left(\frac{\partial f_{\boldsymbol{k}}(\mathbf{r})}{\partial t}\right)_{diff} = -\mathbf{v}_{\boldsymbol{k}} \cdot \nabla f_{\boldsymbol{k}}(\mathbf{r}). \tag{2.5}$$

Analogously, if there are external forces, the wave vector will change according to $\mathbf{F} = \hbar\dot{\boldsymbol{k}}$. Consequently, $f_{\boldsymbol{k}}(\mathbf{r}, t) = f_{\boldsymbol{k}+t\dot{\boldsymbol{k}}}(\mathbf{r}, t)$ and

$$\left(\frac{\partial f_{\boldsymbol{k}}(\mathbf{r})}{\partial t}\right)_{forces} = -\frac{\mathbf{F}}{\hbar} \cdot \frac{\partial f_{\boldsymbol{k}}(\mathbf{r})}{\partial \boldsymbol{k}}. \tag{2.6}$$

The last term accounts for the fact that carriers can interact with each other and with defects in the lattice, and these scattering events can cause them to change their state:

$$\left(\frac{\partial f_{\boldsymbol{k}}(\mathbf{r})}{\partial t}\right)_{\text{coll}}. \tag{2.7}$$

By summing all the contributions,

$$\frac{\partial f_{\boldsymbol{k}}(\mathbf{r})}{\partial t} = \left(\frac{\partial f_{\boldsymbol{k}}(\mathbf{r})}{\partial t}\right)_{\text{diff}} + \left(\frac{\partial f_{\boldsymbol{k}}(\mathbf{r})}{\partial t}\right)_{\text{forces}} + \left(\frac{\partial f_{\boldsymbol{k}}(\mathbf{r})}{\partial t}\right)_{\text{coll}}, \tag{2.8}$$

we get the Boltzmann transport equation:

$$\frac{\partial f_{\boldsymbol{k}}(\mathbf{r})}{\partial t} + \mathbf{v}_{\boldsymbol{k}} \cdot \nabla f_{\boldsymbol{k}}(\mathbf{r}) + \frac{\mathbf{F}}{\hbar} \cdot \frac{\partial f_{\boldsymbol{k}}(\mathbf{r})}{\partial \boldsymbol{k}} = \left(\frac{\partial f_{\boldsymbol{k}}(\mathbf{r})}{\partial t}\right)_{\text{coll}}. \tag{2.9}$$

In writing down the collision term, we assume that interactions are local in space, and that the time between two collisions is much longer than the collision time. In this case, the scattering term is an integral of the rate P of such processes over the wave vectors of particles that can be involved in the collisions in the initial and final states. For example, in the case of a two-particle scattering $\boldsymbol{k} + \mathbf{k}_2 \to \mathbf{k}_3 + \mathbf{k}_4$:

$$\left(\frac{\partial f_{\boldsymbol{k}}(\mathbf{r})}{\partial t}\right)_{\text{coll}} = \int\int\int d\mathbf{k}_2 d\mathbf{k}_3 d\mathbf{k}_4 \left(P_{\mathbf{k}_3\mathbf{k}_4 \to \boldsymbol{k}\mathbf{k}_2} - P_{\boldsymbol{k}\mathbf{k}_2 \to \mathbf{k}_3\mathbf{k}_4}\right). \tag{2.10}$$

where the plus or minus sign in front of the rates depends on the creation or annihilation of $\boldsymbol{k}$ in the scattering.

The collision rate is given by a product of the scattering function $\Gamma_{\boldsymbol{k}\boldsymbol{p} \to \boldsymbol{k}'\boldsymbol{p}'}$ and distribution functions of the particles involved in the process:

$$P_{\boldsymbol{k}\boldsymbol{p} \to \boldsymbol{k}'\boldsymbol{p}'} = \Gamma_{\boldsymbol{k}\boldsymbol{p} \to \boldsymbol{k}'\boldsymbol{p}'} f_{\boldsymbol{k}} f_{\boldsymbol{q}} (f_{\boldsymbol{k}'} \pm 1)(f_{\boldsymbol{q}'} \pm 1) \tag{2.11}$$

$\Gamma_{\boldsymbol{k}\boldsymbol{p} \to \boldsymbol{k}'\boldsymbol{p}'}$ gives the rate in the case where the states $\boldsymbol{k}$ and $\boldsymbol{p}$ are known to be full and $\boldsymbol{k}'$, $\boldsymbol{q}'$ are known to be empty. $f_{\boldsymbol{k}}$ and $f_{\boldsymbol{q}}$ take into account the actual occupations in the initial state, while for the final state there are two cases: if the particles are fermions, the factor $(f_{\boldsymbol{k}'} - 1)(f_{\boldsymbol{q}'} - 1)$ ensures that the final states are empty, while if we are working with bosons, $(f_{\boldsymbol{k}'} + 1)(f_{\boldsymbol{q}'} + 1)$ accounts for the stimulated emission.

2.1.2 Single Mode Approximation

In principle, to write the collision integral, one needs to know which scattering events are allowed and relevant in the system, and their transition rates. Given the complexity of the problem, the single-mode relaxation time approximation (SMA) is often used. It consists in identifying single magnons (in our case) as heat carriers, with a well defined lifetime and mean free path. In other words, it is assumed that the gas of excitations

responsible for thermal conductivity is composed by magnons. The consequence of this approximation on the collision integral is that we neglect the non-diagonal elements:

$$\int \frac{d\boldsymbol{p}}{(2\pi)^3}\Omega_{\boldsymbol{kp}}\Delta f_{\boldsymbol{p}} \approx -\frac{\Delta f_{\boldsymbol{k}}}{\tau_{\boldsymbol{k}}^{\mathrm{SMA}}}. \tag{2.12}$$

Here, $\tau_{\boldsymbol{k}}^{SMA}$ is the lifetime of a magnon with momentum $\boldsymbol{k}$. To see this, we can rewrite the left hand side of the Boltzmann equation in terms of $\Delta f_{\boldsymbol{k}}$, using $f_{\boldsymbol{k}} = f_{\boldsymbol{k}}^0 + \Delta f_{\boldsymbol{k}}$ and the fact that $f_{\boldsymbol{k}}^0$ depends on space and time only through the temperature $T(\mathbf{x}, t)$. If there are no external forces, we get:

$$\frac{\partial f_{\boldsymbol{k}}^0}{\partial T}\left(\frac{\partial T(\mathbf{x},t)}{\partial t} + \mathbf{v}_{\boldsymbol{k}}\cdot\nabla T(\mathbf{x},t)\right) + \frac{\partial(\Delta f_{\boldsymbol{k}})}{\partial t} + \mathbf{v}_{\boldsymbol{k}}\cdot\nabla(\Delta f_{\boldsymbol{k}}) \approx -\frac{\Delta f_{\boldsymbol{k}}}{\tau_{\boldsymbol{k}}^{\mathrm{SMA}}}. \tag{2.13}$$

We start from a situation of thermal equilibrium, where $\frac{\partial T(\mathbf{X},t)}{\partial t} = 0$ and $\nabla T(\mathbf{x}, t) = 0$. If we excite a magnon $\boldsymbol{k}$ at $t = t_0$, there is an initial deviation $\Delta f_{\boldsymbol{k}}(t_0, t)$ that we assume uniform in space. Then, its evolution is described by

$$\frac{\partial(\Delta f_{\boldsymbol{k}})}{\partial t} = -\frac{\Delta f_{\boldsymbol{k}}}{\tau_{\boldsymbol{k}}^{\mathrm{SMA}}}, \tag{2.14}$$

and the solution is an exponential decay:

$$\Delta f_{\boldsymbol{k}}(t) = \left(f_{\boldsymbol{k}}(t_0) - f_{\boldsymbol{k}}^0\right) e^{-t/\tau_{\boldsymbol{k}}^{\mathrm{SMA}}}. \tag{2.15}$$

This simple result and its transparent interpretation are the reasons this approximation is often used. However, when interactions between the excitations are not negligible, it does not give accurate values of thermal conductivity [15]. This happens because if we cannot drop the non-diagonal elements in the collision matrix, single magnons cannot be considered as heat carriers, as they will not have a well defined lifetime and mean free path anymore. Instead, as we will see in the following the linear combinations of magnons that diagonalize the symmetrized scattering matrix ("relaxons") decay purely exponentially and are the actual heat carriers.

When a uniform temperature gradient ∇T is present, in a steady state, Eq. (2.13) reduces to

$$\frac{\partial f_{\boldsymbol{k}}^0}{\partial T}\mathbf{v}_{\boldsymbol{k}}\cdot\nabla T \approx -\frac{\Delta f_{\boldsymbol{k}}}{\tau_{\boldsymbol{k}}^{\mathrm{SMA}}}. \tag{2.16}$$

Expressing $\Delta f_{\boldsymbol{k}}$ from here and substituting it in the expression for the heat flux $\boldsymbol{Q}$, we obtain

$$Q_i = \int \frac{d\boldsymbol{k}}{(2\pi)^3}E_{\boldsymbol{k}}\mathrm{v}_{\boldsymbol{k}}^i\Delta f_{\boldsymbol{k}} = -\int \frac{d\boldsymbol{k}}{(2\pi)^3}E_{\boldsymbol{k}}\mathrm{v}_{\boldsymbol{k}}^i\tau_{\boldsymbol{k}}^{\mathrm{SMA}}\frac{\partial f_{\boldsymbol{k}}^0}{\partial T}\mathrm{v}_{\boldsymbol{k}}^j\nabla_j T. \tag{2.17}$$

In the presented SMA picture, for every $\boldsymbol{k}$ we have a specific heat contribution of

$$C_{\boldsymbol{k}} \equiv \frac{\partial f_{\boldsymbol{k}}^0}{\partial T}E_{\boldsymbol{k}} = -\frac{f_{\boldsymbol{k}}\left(f_{\boldsymbol{k}}^0 + 1\right)E_{\boldsymbol{k}}^2}{k_B T^2}, \tag{2.18}$$

which we use to simplify Eq. (2.17):

$$Q_i = -\int \frac{d\boldsymbol{k}}{(2\pi)^3}C_{\boldsymbol{k}}\mathrm{v}_{\boldsymbol{k}}^i\tau_{\boldsymbol{k}}^{\mathrm{SMA}}\mathrm{v}_{\boldsymbol{k}}^j\nabla_j T. \tag{2.19}$$

We now compare the latter equation with the definition of the thermal conductivity as a proportionality tensor between the temperature gradient and a heat flux, $Q_i = -\sum_j \kappa_{ij} \nabla_j T$, hence

$$\kappa_{ij}^{\mathrm{SMA}} = \int \frac{d\boldsymbol{k}}{(2\pi)^3} C_{\boldsymbol{k}} \mathrm{v}_{\boldsymbol{k}}^i \mathrm{v}_{\boldsymbol{k}}^j \tau_{\boldsymbol{k}}^{\mathrm{SMA}}. \tag{2.20}$$

This expression gives the thermal conductivity in a single mode approximation in terms of specific heat contributions $C_{\boldsymbol{k}}$, velocities $\mathbf{v}_{\boldsymbol{k}}$ and relaxation times $\tau_{\boldsymbol{k}}^{\mathrm{SMA}}$ of individual excitations.

2.2 Magnons in ferromagnets

Since commutation relations for spin operators $[S_x, S_y] = iS_z$ are neither bosonic nor fermionic, it is customary to transition to fermionic or bosonic operators in order to diagonalize spin Hamiltonians[16][17]. Here we use Holstein-Primakoff transformation of the form [18]:

$$\begin{aligned} S_i^z &= S - a_i^\dagger a_i \\ S_i^+ &= \sqrt{2S - a_i^\dagger a_i} a_i \\ S_i^- &= a_i^\dagger \sqrt{2S - a_i^\dagger a_i} \end{aligned} \tag{2.21}$$

The operator $a_i^\dagger$ creates a boson on site i, that is describing a unit deviation of the spin projection from z axis. In the low temperature limit the number of bosons is low, $\langle a_i^\dagger a_i \rangle \ll 2S$, and hence the square roots may be expanded as $\sqrt{1 - \frac{a_i^\dagger a_i}{2S}} \approx 1 - \frac{a_i^\dagger a_i}{4S}$, leading to

$$\begin{aligned} S_i^z &= S - a_i^\dagger a_i, \\ S_i^+ &\approx \sqrt{2S} \left(1 - \frac{a_i^\dagger a_i}{4S}\right) a_i, \\ S_i^- &\approx \sqrt{2S} a_i^\dagger \left(1 - \frac{a_i^\dagger a_i}{4S}\right). \end{aligned} \tag{2.22}$$

Then, for a ferromagnet, the Hamiltonian takes the form

$$\mathcal{H} = \sum_{\boldsymbol{r},\boldsymbol{\delta}} J_{\boldsymbol{\delta}} S_{\boldsymbol{r}} \cdot S_{\mathbf{r}+\boldsymbol{\delta}} = \sum_{\boldsymbol{r},\boldsymbol{\delta}} J_{\boldsymbol{\delta}} \left[S_{\boldsymbol{r}}^z S_{\boldsymbol{r}+\boldsymbol{\delta}}^z + \frac{1}{2} \left(S_{\mathbf{r}}^+ S_{\boldsymbol{r}+\boldsymbol{\delta}}^- + S_{\boldsymbol{r}}^- S_{\boldsymbol{r}+\boldsymbol{\delta}}^+ \right) \right] \tag{2.23}$$

The transformation 2.22 then leads to

$$\begin{aligned} S_{\boldsymbol{r}}^z S_{\boldsymbol{r}+\boldsymbol{\delta}}^z &= (S - a_{\boldsymbol{r}}^\dagger a_{\boldsymbol{r}})(S - a_{\boldsymbol{r}+\boldsymbol{\delta}}^\dagger a_{\boldsymbol{r}+\boldsymbol{\delta}}) \approx S^2 - S(a_{\boldsymbol{r}}^\dagger a_{\boldsymbol{r}} + a_{\boldsymbol{r}+\boldsymbol{\delta}}^\dagger a_{\boldsymbol{r}+\boldsymbol{\delta}}) \\ \frac{1}{2} \left(S_{\mathbf{r}}^+ S_{\boldsymbol{r}+\boldsymbol{\delta}}^- + S_{\boldsymbol{r}}^- S_{\boldsymbol{r}+\boldsymbol{\delta}}^+ \right) &\approx S(a_{\boldsymbol{r}}^\dagger a_{\boldsymbol{r}+\boldsymbol{\delta}} + a_{\boldsymbol{r}} a_{\boldsymbol{r}+\boldsymbol{\delta}}^\dagger). \end{aligned}$$

Overall, we obtain, neglecting terms of fourth and higher order in magnon operators,

$$\mathcal{H} = \sum_{\boldsymbol{r},\boldsymbol{\delta}} S J_{\boldsymbol{\delta}} (a_{\boldsymbol{r}}^\dagger a_{\boldsymbol{r}+\boldsymbol{\delta}} + a_{\boldsymbol{r}} a_{\boldsymbol{r}+\boldsymbol{\delta}}^\dagger - a_{\boldsymbol{r}}^\dagger a_{\boldsymbol{r}} - a_{\boldsymbol{r}+\boldsymbol{\delta}}^\dagger a_{\boldsymbol{r}+\boldsymbol{\delta}}), \tag{2.24}$$

and, after the Fourier transform,

$$\mathcal{H} = \sum_{\boldsymbol{k},\boldsymbol{\delta}} S J_{\boldsymbol{\delta}} a_{\boldsymbol{k}}^\dagger a_{\boldsymbol{k}} (\cos \boldsymbol{\delta} \cdot \boldsymbol{k} - 1) = \sum_{\boldsymbol{k},\boldsymbol{\delta}} -2S J_{\boldsymbol{\delta}} a_{\boldsymbol{k}}^\dagger a_{\boldsymbol{k}} \sin^2 \frac{\boldsymbol{\delta} \cdot \boldsymbol{k}}{2}, \tag{2.25}$$

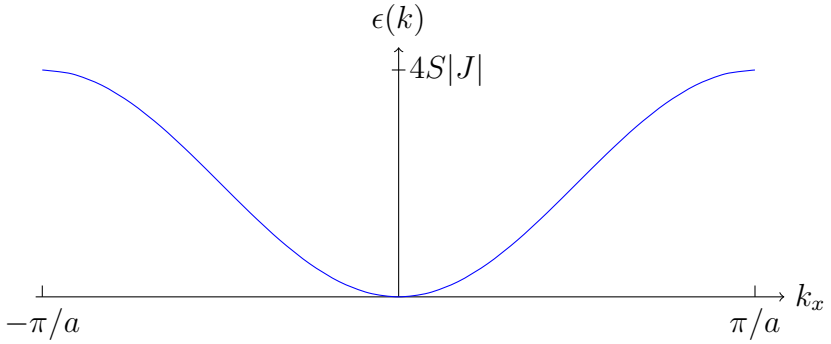

Figure 2.3: Dispersion of magnons in a ferromagnet with nearest-neighbor exchange J

hence, for a cubic lattice with the nearest neighbor ferromagnetic exchange $J_{\pm\boldsymbol{x}} = J_{\pm\boldsymbol{y}} = J_{\pm\boldsymbol{z}} = J < 0$ the Hamiltonian takes the form $\mathcal{H} = \sum_{\boldsymbol{k}} \epsilon_{\boldsymbol{k}} a^\dagger_{\boldsymbol{k}} a_{\boldsymbol{k}}$ with

$$\epsilon_{\boldsymbol{k}} = 4S|J|\left(\sin^2\frac{k_x}{2} + \sin^2\frac{k_y}{2} + \sin^2\frac{k_z}{2}\right), \tag{2.26}$$

a quadratic dispersion with the bandwidth of $4S|J|$, as illustrated in Fig. 2.3. The magnon creation operators $a^\dagger_{\boldsymbol{k}} = \sum_{\boldsymbol{r}} e^{i\boldsymbol{k}\cdot\boldsymbol{r}} a^\dagger_{\boldsymbol{r}}$ induce a spin wave with wave vector $\boldsymbol{k}$, so that spins start precessing, leading to an oscillating magnetization component at this wave vector.

Chapter 3

Magnons in spin spirals

In this Chapter, we will define the non-collinear system of interest, a quasi one-dimensional spin spiral. Then, we will describe its magnetic excitations, and the interactions between them.

The most important point is that in a non-collinear system there are scattering events involving three magnons, while in collinear systems the first allowed processes involve four magnons, and that is the reason for the decrease in thermal conductivity when going from the ferromagnetic to the spiral phase, observed in experiments (2.1).

3.1 Model

Non-collinear spin textures can be found in frustrated systems, and the simplest model that leads to a spin spiral includes competing interactions between nearest neighbors (J_1) and next-nearest-neighbors (J_2) along the a axis. No matter the sign of J_1, alone it would make next nearest neighbors ferromagnetic. An antiferromagnetic J_2 creates frustration, which may lead to spiral states. The system we want to study is a quasi-one dimensional spin spiral where one-dimensional chains along the a axis with spiral ordering are ferromagnetically coupled between each other. This ferromagnetic coupling is given by two exchange interactions between nearest-neighbors in the directions perpendicular to the chain, J_3 and J_4, respectively in direction b and c; clearly, $J_3, J_4 < 0$.

We also include an easy plane anisotropy, $\Delta > 0$, that favors spins to lie in the ac plane.

Hence, the complete Hamiltonian is:

$$H = \sum_{\boldsymbol{i}} J_1 \mathbf{S}_{\boldsymbol{i}} \cdot \mathbf{S}_{\boldsymbol{i}+\mathbf{a}} + J_2 \mathbf{S}_{\boldsymbol{i}} \cdot \mathbf{S}_{\boldsymbol{i}+2\mathbf{a}} + J_3(\mathbf{S}_{\boldsymbol{i}} \cdot \mathbf{S}_{\boldsymbol{i}+\mathbf{b}} + \mathbf{S}_{\boldsymbol{i}} \cdot \mathbf{S}_{\boldsymbol{i}+\mathbf{c}}) + \Delta \left(S_{\boldsymbol{i}}^{y}\right)^2 \tag{3.1}$$

where $\mathbf{S}_{\boldsymbol{i}}$ is the spin ($S \gg \frac{1}{2}$) on the site $\boldsymbol{R}_i$; $\mathbf{a}, \mathbf{b}, \mathbf{c}$ are the translational vectors along the Cartesian directions.

To see how the spiral ordering arises, let us focus only on the $J_1 - J_2$ Hamiltonian, so that we are ignoring coupling between the chains:

$$H = \sum_{n} J_1 \mathbf{S}_n \cdot \mathbf{S}_{n+1} + J_2 \mathbf{S}_n \cdot \mathbf{S}_{n+2} \tag{3.2}$$

where the exchanges are ferromagnetic between nearest-neighbors, $J_1 < 0$, and antiferromagnetic between next-nearest-neighbors, $J_2 > 0$. For different values of the ratio J_1/J_2, the competition between the two interactions gives rise to different ground states.

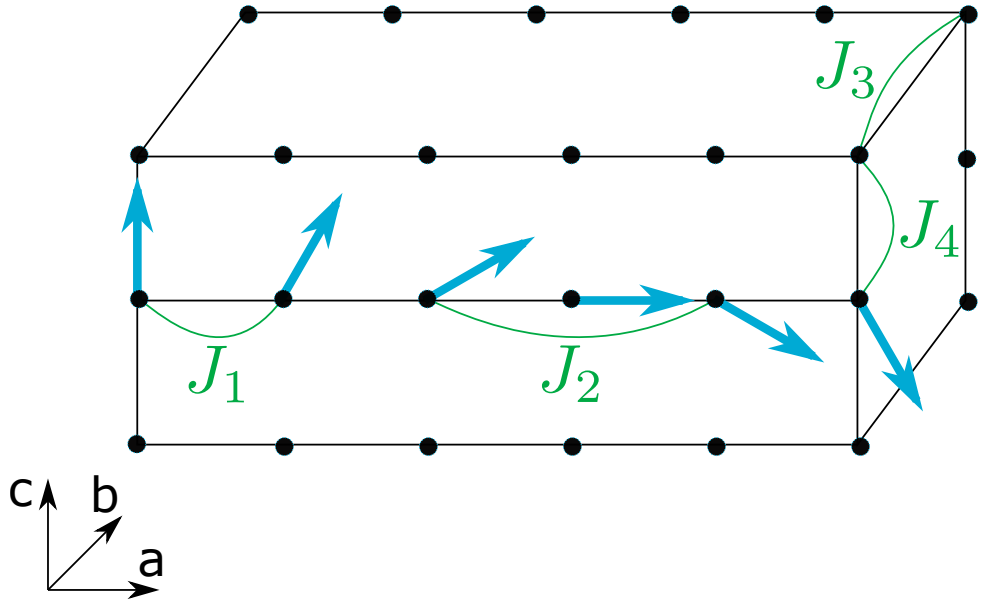

Figure 3.1: Caption

To compare the energies of the ferromagnetic, antiferromagnetic, and spiral states as J_1 and J_2 are varied, we write $\boldsymbol{S}_n$ in polar coordinates, in the xz plane:

$$\mathbf{S}_n = \begin{pmatrix} \sin\phi_n \\ 0 \\ \cos\phi_n \end{pmatrix}. \tag{3.3}$$

The scalar product becomes

$$\mathbf{S}_n \cdot \mathbf{S}_m = \cos(\phi_n - \phi_m). \tag{3.4}$$

Assuming a uniform spiral, i.e. that the angle between two neighboring spins is a constant, ϕ, the energy of the system is:

$$E = N(J_1 \cos\phi + J_2 \sin 2\phi) \tag{3.5}$$

Minimizing with respect to ϕ, we find

$$\sin\phi = 0, \tag{3.6}$$

describing a ferromagnet with energy $E = N(J_1 + J_2)$, where N is the number of sites, or an antiferromagnet with $E = N(-J_1 + J_2)$, and

$$\cos\phi = -\frac{J_1}{4J_2}, \tag{3.7}$$

which describes a spiral with an angle $\phi = \pm\arccos\left(-\frac{J_1}{4J_2}\right)$ between neighboring spins. If this state exists, that is, if

$$\left|\frac{J_1}{4J_2}\right| < 1, \tag{3.8}$$

it has the energy $E = N(-\frac{J_1^2}{8J_2} - J_2)$ and is therefore favorable compared to the ferromagnetic and antiferromagnetic phases.

Since we want to study the effect of non-collinearity on thermal transport, the system we are describing must fulfill the condition (3.8), so that along every chain there is a spin spiral.

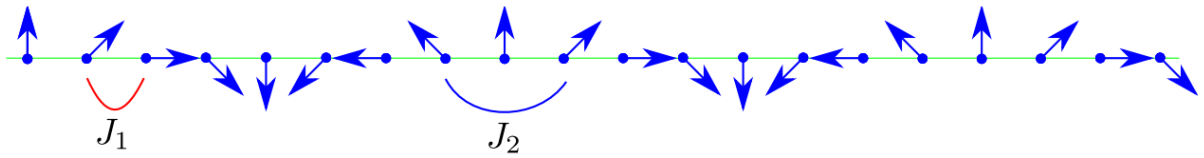

Figure 3.2: Spin spiral ordering is stabilized by competing nearest-neighbor J_1 and next-nearest-neighbor antiferromagnetic J_2 exchange interactions.

3.2 Holstein-Primakoff transformation for a spin spiral

We would like now to describe the magnetic excitations in our system. However, simply applying (2.21) to (3.1) would mean that we are expanding around the ferromagnetic state $S_z = S$, while we want to expand around the classical directions of the spins in the spiral. Therefore, we apply a rotation around y axis, $\hat{R}_i \equiv \hat{R}(\theta_i)$, where θ_i is the deviation of the i-th spin from the z axis, to align the state with zero bosons with a classical spin direction on site i. The rotation matrix is then

$$\hat{R}_{\boldsymbol{i}} = \hat{R}(\theta_{\boldsymbol{i}}) = \begin{pmatrix} \cos\theta_{\boldsymbol{i}} & 0 & -\sin\theta_{\boldsymbol{i}} \\ 0 & 1 & 0 \\ \sin\theta_{\boldsymbol{i}} & 0 & \cos\theta_{\boldsymbol{i}} \end{pmatrix}. \tag{3.9}$$

In the collinear case, $\theta_{\boldsymbol{i}} = 0$ for every $\boldsymbol{R}_i$, and the rotation matrix would be just the identity:

$$\hat{R}_{\boldsymbol{i}}^{coll} = \begin{pmatrix} 1 & 0 & 0 \\ 0 & 1 & 0 \\ 0 & 0 & 1 \end{pmatrix}. \tag{3.10}$$

A non-zero $\sin\theta_i$ makes an important difference in the scattering events between magnons that are allowed, and consequently in thermal conductivity, as will be discussed later.

The spin on site $\boldsymbol{R}_i$ is now $\hat{R}_{\boldsymbol{i}}\mathbf{S}_{\boldsymbol{i}}$ and the scalar product of the two spins

$$(\hat{R}_{\boldsymbol{i}}\mathbf{S}_{\boldsymbol{i}}) \cdot \hat{R}_{\boldsymbol{j}}\mathbf{S}_{\boldsymbol{j}} = (\hat{R}_{\boldsymbol{i}}\mathbf{S}_{\boldsymbol{i}})^T \hat{R}_{\boldsymbol{j}}\mathbf{S}_{\boldsymbol{j}} = \mathbf{S}_{\boldsymbol{i}}^T \hat{R}_{\boldsymbol{i}}^T \hat{R}_{\boldsymbol{j}}\mathbf{S}_{\boldsymbol{j}} = \mathbf{S}_{\boldsymbol{i}}^T \hat{R}(\theta_{\boldsymbol{j}} - \theta_{\boldsymbol{i}})\mathbf{S}_{\boldsymbol{j}}. \tag{3.11}$$

Here we took into account $R(\theta)^T = R(-\theta)$ and transitivity of rotations $R(\alpha)R(\beta) = R(\alpha+\beta)$. Ultimately,

$$(\hat{R}_{\boldsymbol{i}}\mathbf{S}_{\boldsymbol{i}}) \cdot \hat{R}_{\boldsymbol{j}}\mathbf{S}_{\boldsymbol{j}} = \begin{pmatrix} \cos\theta_{\boldsymbol{i}} S_{\boldsymbol{i}}^x - \sin\theta_{\boldsymbol{i}} S_{\boldsymbol{i}}^z & S_{\boldsymbol{i}}^y & \sin\theta_{\boldsymbol{i}} S_{\boldsymbol{i}}^x + \cos\theta_{\boldsymbol{i}} S_{\boldsymbol{i}}^z \end{pmatrix} \begin{pmatrix} \cos\theta_{\boldsymbol{j}} S_{\boldsymbol{j}}^x - \sin\theta_{\boldsymbol{j}} S_{\boldsymbol{j}}^z \\ S_{\boldsymbol{j}}^y \\ \sin\theta_{\boldsymbol{j}} S_{\boldsymbol{j}}^x + \cos\theta_{\boldsymbol{j}} S_{\boldsymbol{j}}^z \end{pmatrix}.$$

Then the Hamiltonian takes the form:

$$H = \sum_{\boldsymbol{ij}} J_{\boldsymbol{ij}} \left[S_{\boldsymbol{i}}^y S_{\boldsymbol{j}}^y + \cos\theta_{\boldsymbol{ij}} \left(S_{\boldsymbol{i}}^x S_{\boldsymbol{j}}^x + S_{\boldsymbol{i}}^z s_{\boldsymbol{j}}^z \right) + \sin\theta_{\boldsymbol{ij}} \left(S_{\boldsymbol{i}}^x S_{\boldsymbol{j}}^z - S_{\boldsymbol{i}}^z S_{\boldsymbol{j}}^x \right) \right] + \Delta \left(S_{\boldsymbol{i}}^y \right)^2 \tag{3.12}$$

Substituting $S_{\boldsymbol{i}}^x$ and $S_{\boldsymbol{i}}^y$ in terms of the ladder operators $S_\pm$, defined as [12]

$$S_\pm \equiv S_x \pm i S_y \tag{3.13}$$

we obtain:

$$\begin{aligned} H = \frac{1}{4}\sum_{\boldsymbol{ij}} J_{\boldsymbol{ij}} \big[& (1+\cos\theta_{\boldsymbol{ij}}) \left(S_{\boldsymbol{i}}^{+}S_{\boldsymbol{j}}^{-} + S_{\boldsymbol{i}}^{-}S_{\boldsymbol{j}}^{+}\right) - (1-\cos\theta_{\boldsymbol{ij}}) \left(S_{\boldsymbol{i}}^{+}S_{\boldsymbol{j}}^{+} + S_{\boldsymbol{i}}^{-}S_{\boldsymbol{j}}^{-}\right) \\ & +4\cos\theta_{\boldsymbol{ij}} S_{\boldsymbol{i}}^{z}S_{\boldsymbol{j}}^{z} + 2\sin\theta_{\boldsymbol{ij}} \left[\left(S_{\boldsymbol{i}}^{+}+S_{\boldsymbol{i}}^{-}\right)S_{\boldsymbol{j}}^{z} - S_{\boldsymbol{i}}^{z}\left(S_{\boldsymbol{j}}^{+}+S_{\boldsymbol{j}}^{-}\right)\right]\big] \\ & - \Delta\left(S_{\boldsymbol{i}}^{+}S_{\boldsymbol{i}}^{+} + S_{\boldsymbol{i}}^{-}S_{\boldsymbol{i}}^{-} - S_{\boldsymbol{i}}^{+}S_{\boldsymbol{i}}^{-} - S_{\boldsymbol{i}}^{-}S_{\boldsymbol{i}}^{+}\right) \end{aligned} \tag{3.14}$$

where $\theta_{\boldsymbol{ij}} \equiv \theta_{\boldsymbol{j}} - \theta_{\boldsymbol{i}}$ takes the values

$$\theta_{\boldsymbol{ij}} = \begin{cases} Q, & \text{if } \boldsymbol{j} = \boldsymbol{i} \pm \mathbf{a} \\ 2Q, & \text{if } \boldsymbol{j} = \boldsymbol{i} \pm 2\mathbf{a} \\ 0, & \text{otherwise} \end{cases} \tag{3.15}$$

with Q defined as the angle between two neighboring spins in the spiral:

$$Q = \arccos\left(-\frac{J_1}{4J_2}\right) \tag{3.16}$$

and

$$J_{\boldsymbol{ij}} = \begin{cases} J_1, & \text{if } \boldsymbol{j} = \boldsymbol{i} \pm \mathbf{a} \\ J_2, & \text{if } \boldsymbol{j} = \boldsymbol{i} \pm 2\mathbf{a} \\ J_3, & \text{if } \boldsymbol{j} = \boldsymbol{i} \pm \mathbf{b} \\ J_4, & \text{if } \boldsymbol{j} = \boldsymbol{i} \pm \mathbf{c} \\ 0, & \text{otherwise} \end{cases} \tag{3.17}$$

3.3 Second order Hamiltonian

Performing the Holstein-Primakoff transformation [18] Eq. (2.21) in Eq. (3.14) and collecting the second-order terms, we obtain:

$$\begin{aligned} H^{(2)} = \frac{S}{2}\sum_{\boldsymbol{ij}} J_{\boldsymbol{ij}} \Big[& (1+\cos\theta_{\boldsymbol{ij}}) \left(a_{\boldsymbol{i}}a_{\boldsymbol{j}}^{\dagger} + a_{\boldsymbol{i}}^{\dagger}a_{\boldsymbol{j}}\right) - (1-\cos\theta_{\boldsymbol{ij}}) \left(a_{\boldsymbol{i}}a_{\boldsymbol{j}} + a_{\boldsymbol{i}}^{\dagger}a_{\boldsymbol{j}}^{\dagger}\right) \\ & -2\cos\theta_{\boldsymbol{ij}} \left(a_{\boldsymbol{i}}^{\dagger}a_{\boldsymbol{i}} + a_{\boldsymbol{j}}^{\dagger}a_{\boldsymbol{j}}\right)\Big] - \Delta\left(a_{\boldsymbol{i}}a_{\boldsymbol{i}} + a_{\boldsymbol{i}}^{\dagger}a_{\boldsymbol{i}}^{\dagger} - a_{\boldsymbol{i}}a_{\boldsymbol{i}}^{\dagger} - a_{\boldsymbol{i}}^{\dagger}a_{\boldsymbol{i}}\right) \end{aligned} \tag{3.18}$$

To diagonalize this Hamiltonian, we start with the Fourier transform,

$$a_{\boldsymbol{i}} = \frac{1}{\sqrt{N}}\sum_{\boldsymbol{k}} a_{\boldsymbol{k}} e^{i\boldsymbol{k}\cdot\mathbf{R}_i} \tag{3.19}$$

to obtain:

$$\begin{aligned} H^{(2)} = \frac{S}{2N}\sum_{\boldsymbol{ij}}\sum_{\boldsymbol{kq}} J_{\boldsymbol{ij}} \Big[& (1+\cos\theta_{\boldsymbol{ij}}) \left(a_{\boldsymbol{k}}a_{\boldsymbol{q}}^{\dagger} e^{i\boldsymbol{k}\cdot\mathbf{R}_i} e^{-i\boldsymbol{q}\cdot\mathbf{R}_j} + a_{\boldsymbol{k}}^{\dagger}a_{\boldsymbol{q}} e^{-i\boldsymbol{k}\cdot\mathbf{R}_i} e^{i\boldsymbol{q}\cdot\boldsymbol{R}_j}\right) \\ & - (1-\cos\theta_{\boldsymbol{ij}}) \left(a_{\boldsymbol{k}}a_{\boldsymbol{q}} e^{i\boldsymbol{k}\cdot\mathbf{R}_i} e^{i\boldsymbol{q}\cdot\boldsymbol{R}_j} + a_{\boldsymbol{k}}^{\dagger}a_{\boldsymbol{q}}^{\dagger} e^{-i\boldsymbol{k}\cdot\mathbf{R}_i} e^{-i\boldsymbol{q}\cdot\mathbf{R}_j}\right) \\ & -2\cos\theta_{\boldsymbol{ij}} \left(a_{\boldsymbol{k}}^{\dagger}a_{\boldsymbol{q}} e^{i(\boldsymbol{q}-\boldsymbol{k})\cdot\boldsymbol{R}_i} + a_{\boldsymbol{k}}^{\dagger}a_{\boldsymbol{q}} e^{i(\boldsymbol{q}-\boldsymbol{k})\cdot\boldsymbol{R}_j}\right)\Big] \\ & - \Delta\left(a_{\boldsymbol{k}}a_{\boldsymbol{q}} e^{i(\boldsymbol{k}+\boldsymbol{q})\cdot\boldsymbol{R}_i} + a_{\boldsymbol{k}}^{\dagger}a_{\boldsymbol{q}}^{\dagger} e^{-i(\boldsymbol{k}+\boldsymbol{q})\cdot\boldsymbol{R}_i} - 2a_{\boldsymbol{k}}a_{\boldsymbol{q}}^{\dagger} e^{i(\boldsymbol{k}-\boldsymbol{q})\cdot\boldsymbol{R}_i}\right), \end{aligned} \tag{3.20}$$

where in the last term we used the commutation relation for magnons, $\left[a_{\boldsymbol{k}}, a_{\boldsymbol{q}}^\dagger\right] = \delta_{\boldsymbol{k},\boldsymbol{q}}$, to write $a_{\boldsymbol{k}}^\dagger a_{\boldsymbol{q}}$ as $a_{\boldsymbol{k}} a_{\boldsymbol{q}}^\dagger$ plus a constant, that we can drop.

Let us start from the first term. The sum of the interactions in the direction of the spiral, that is $\boldsymbol{j} = \boldsymbol{i} + \mathbf{a}, \boldsymbol{i} + 2\mathbf{a}$, gives:

$$\begin{aligned}\frac{S}{2N}\sum_{\boldsymbol{i}}\sum_{\boldsymbol{kq}}\Big[&J_1\left(1+\cos Q\right)\left(a_{\boldsymbol{k}}a_{\boldsymbol{q}}^\dagger e^{i(\boldsymbol{k}-\boldsymbol{q})\cdot\boldsymbol{R}_i}e^{-iq_x a} + a_{\boldsymbol{k}}^\dagger a_{\boldsymbol{q}} e^{i(\boldsymbol{q}-\boldsymbol{k})\cdot\boldsymbol{R}_i}e^{iq_x a}\right)\\ &+J_2\left(1+\cos 2Q\right)\cos 2q_x a\left(a_{\boldsymbol{k}}a_{\boldsymbol{q}}^\dagger e^{i(\boldsymbol{k}-\boldsymbol{q})\cdot\boldsymbol{R}_i}e^{-2iq_x a} + a_{\boldsymbol{k}}^\dagger a_{\boldsymbol{q}} e^{i(\boldsymbol{q}-\boldsymbol{k})\cdot\boldsymbol{R}_i}e^{2iq_x a}\right)\Big]\end{aligned} \tag{3.21}$$

Using the relation

$$\sum_{\boldsymbol{i}} e^{i(\boldsymbol{k}-\boldsymbol{q})\cdot\boldsymbol{R}_i} = N\delta_{\boldsymbol{k},\boldsymbol{q}} \tag{3.22}$$

we can sum over $\boldsymbol{i}$:

$$\begin{aligned}\frac{S}{2}\sum_{\boldsymbol{k}}\Big[&J_1\left(1+\cos Q\right)\left(a_{\boldsymbol{k}}a_{\boldsymbol{k}}^\dagger e^{-ik_x a} + a_{\boldsymbol{k}}^\dagger a_{\boldsymbol{k}} e^{ik_x a}\right)\\ &+J_2\left(1+\cos 2Q\right)\left(a_{\boldsymbol{k}}a_{\boldsymbol{k}}^\dagger e^{-2ik_x a} + a_{\boldsymbol{k}}^\dagger a_{\boldsymbol{k}} e^{2ik_x a}\right)\Big]\end{aligned} \tag{3.23}$$

Finally, dropping the constant that comes from the commutation relation between magnons, we get:

$$\frac{S}{2}\sum_{\boldsymbol{k}}\left[2J_1\left(1+\cos Q\right)\cos k_x a + 2J_2\left(1+\cos 2Q\right)\cos 2k_x a\right]a_{\boldsymbol{k}}^\dagger a_{\boldsymbol{k}} \tag{3.24}$$

We still have to sum over $\boldsymbol{j} = \boldsymbol{i}+\mathbf{b}, \boldsymbol{i}+\mathbf{c}$. In this case, the angle between two neighboring spins is zero:

$$\frac{S}{2}\sum_{\boldsymbol{i}}\sum_{\boldsymbol{kq}} 2\left(a_{\boldsymbol{k}}a_{\boldsymbol{q}}^\dagger e^{i(\boldsymbol{k}-\boldsymbol{q})\cdot\boldsymbol{R}_i}\left(J_3 e^{iq_y b} + J_4 e^{iq_z c}\right) + a_{\boldsymbol{k}}^\dagger a_{\boldsymbol{q}} e^{i(\boldsymbol{q}-\boldsymbol{k})\cdot\boldsymbol{R}_i}\left(J_3 e^{-iq_y b} + J_4 e^{-iq_z c}\right)\right) \tag{3.25}$$

Again, the sum over $\boldsymbol{i}$ with Eq. (3.22) gives:

$$\begin{aligned}&S\sum_{\boldsymbol{k}} a_{\boldsymbol{k}}a_{\boldsymbol{k}}^\dagger\left(J_3 e^{ik_y b} + J_4 e^{ik_z c}\right) + a_{\boldsymbol{k}}^\dagger a_{\boldsymbol{k}}\left(J_3 e^{-ik_y b} + J_4 e^{-ik_z c}\right)\\ &\quad = S\sum_{\boldsymbol{k}}\left(2J_3\cos k_y b + 2J_4\cos k_z c\right)a_{\boldsymbol{k}}^\dagger a_{\boldsymbol{k}}\end{aligned} \tag{3.26}$$

The first term is then:

$$\begin{aligned}\frac{S}{2}\sum_{\boldsymbol{k}}\Big[&2J_1((1+\cos Q)\cos k_x a)\\ &+2J_2((1+\cos 2Q)\cos 2k_x a) + 4J_3\cos k_y b + 4J_4\cos k_z c\Big]a_{\boldsymbol{k}}^\dagger a_{\boldsymbol{k}}\end{aligned} \tag{3.27}$$

The second term of the Hamiltonian is analogous, but since there is $1-\cos\theta_{ij}$ in front,

the sums over $\boldsymbol{j} = \boldsymbol{i} + \mathbf{b}, \boldsymbol{i} + \mathbf{c}$ do not contribute, since there is no rotation angle in the perpendicular directions:

$$\begin{aligned}
&-\frac{S}{2N}\sum_{\boldsymbol{ij}}\sum_{\boldsymbol{kq}} J_{\boldsymbol{ij}}(1-\cos\theta_{\boldsymbol{ij}})\left(a_{\boldsymbol{k}}a_{\boldsymbol{q}}e^{i\boldsymbol{k}\cdot\mathbf{R}_i}e^{i\boldsymbol{q}\cdot\boldsymbol{R}_j}+a^\dagger_{\boldsymbol{k}}a^\dagger_{\boldsymbol{q}}e^{-i\boldsymbol{k}\cdot\mathbf{R}_i}e^{-i\boldsymbol{q}\cdot\mathbf{R}_j}\right)\\
&=-\frac{S}{2N}\sum_{\boldsymbol{i}}\sum_{\boldsymbol{kq}} J_1(1-\cos Q)\left(a_{\boldsymbol{k}}a_{\boldsymbol{q}}e^{i(\boldsymbol{k}+\boldsymbol{q})\cdot\boldsymbol{R}_i}e^{iq_xa}+a^\dagger_{\boldsymbol{k}}a^\dagger_{\boldsymbol{q}}e^{-i(\boldsymbol{k}+\boldsymbol{q})\cdot\boldsymbol{R}_i}e^{-iq_xa}\right)\\
&+J_2(1-\cos Q)\left(a_{\boldsymbol{k}}a_{\boldsymbol{q}}e^{i(\boldsymbol{k}+\boldsymbol{q})\cdot\boldsymbol{R}_i}e^{2iq_xa}+a^\dagger_{\boldsymbol{k}}a^\dagger_{\boldsymbol{q}}e^{-i(\boldsymbol{k}+\boldsymbol{q})\cdot\boldsymbol{R}_i}e^{-2iq_xa}\right)
\end{aligned}\tag{3.28}$$

Summing over $\boldsymbol{i}$:

$$\begin{aligned}
&-\frac{S}{2}\sum_{\boldsymbol{k}} J_1(1-\cos Q)\left(a_{\boldsymbol{k}}a_{-\boldsymbol{k}}e^{-ik_xa}+a^\dagger_{\boldsymbol{k}}a^\dagger_{-\boldsymbol{k}}e^{ik_xa}\right)\\
&+J_2(1-\cos Q)\left(a_{\boldsymbol{k}}a_{-\boldsymbol{k}}e^{-2ik_xa}+a^\dagger_{\boldsymbol{k}}a^\dagger_{-\boldsymbol{k}}e^{2ik_xa}\right)\\
&=-\frac{S}{2}\sum_{\boldsymbol{k}}\left[J_1(1-\cos Q)\cos k_xa+J_2(1-\cos Q)\cos 2k_xa\right]\left(a_{\boldsymbol{k}}a_{-\boldsymbol{k}}+a^\dagger_{\boldsymbol{k}}a^\dagger_{-\boldsymbol{k}}\right)
\end{aligned}\tag{3.29}$$

The third term is:

$$\begin{aligned}
&-\frac{S}{2N}\sum_{\boldsymbol{ij}}\sum_{\boldsymbol{kq}} J_{\boldsymbol{ij}}\left[2\cos\theta_{\boldsymbol{ij}}\left(a^\dagger_{\boldsymbol{k}}a_{\boldsymbol{q}}e^{i(\boldsymbol{q}-\boldsymbol{k})\cdot\boldsymbol{R}_i}+a^\dagger_{\boldsymbol{k}}a_{\boldsymbol{q}}e^{i(\boldsymbol{q}-\boldsymbol{k})\cdot\boldsymbol{R}_j}\right)\right]\\
&=-\frac{S}{N}\sum_{i}\sum_{\boldsymbol{kq}}\left[J_1\cos Q\left(1+e^{i(q_x-k_x)a}\right)+J_2\cos 2Q\left(1+e^{2i(q_x-k_x)a}\right)\right.\\
&\left.+J_3\left(1+e^{i(q_y-k_y)b}\right)+J_4\left(1+e^{i(q_z-k_z)c}\right)\right]\left(a^\dagger_{\boldsymbol{k}}a_{\boldsymbol{q}}e^{i(\boldsymbol{q}-\boldsymbol{k})\cdot\boldsymbol{R}_i}\right)\\
&=-2S\sum_{\boldsymbol{k}}\left(J_1\cos Q+J_2\cos 2Q+J_3+J_4\right)a^\dagger_{\boldsymbol{k}}a_{\boldsymbol{k}}
\end{aligned}\tag{3.30}$$

In the fourth term there is no sum over $\boldsymbol{j}$, and we get:

$$\begin{aligned}
&-\frac{S}{2N}\sum_{\boldsymbol{i}}\sum_{\boldsymbol{kq}}\Delta\left(a_{\boldsymbol{k}}a_{\boldsymbol{q}}e^{i(\boldsymbol{k}+\boldsymbol{q})\cdot\boldsymbol{R}_i}+a^\dagger_{\boldsymbol{k}}a^\dagger_{\boldsymbol{q}}e^{-i(\boldsymbol{k}+\boldsymbol{q})\cdot\boldsymbol{R}_i}-2a_{\boldsymbol{k}}a^\dagger_{\boldsymbol{q}}e^{i(\boldsymbol{k}-\boldsymbol{q})\cdot\boldsymbol{R}_i}\right)\\
&-\frac{S}{2}\sum_{\boldsymbol{k}}\Delta\left(a_{\boldsymbol{k}}a_{-\boldsymbol{k}}+a^\dagger_{\boldsymbol{k}}a^\dagger_{-\boldsymbol{k}}-2a_{\boldsymbol{k}}a^\dagger_{\boldsymbol{k}}\right)
\end{aligned}\tag{3.31}$$

The second order Hamiltonian is the sum of the four terms:

$$\begin{aligned}
H^{(2)}=&\frac{S}{2}\sum_{\boldsymbol{k}}a^\dagger_{\boldsymbol{k}}a_{\boldsymbol{k}}\left\{2J_1\left[(1+\cos Q)\cos k_xa-2\cos Q\right]\right.\\
&\left.+2J_2\left[(1+\cos 2Q)\cos 2k_xa-2\cos 2Q\right]+4J_3\left(\cos k_yb-1\right)+4J_4\left(\cos k_zc-1\right)+2\Delta\right\}\\
&+\left(a_{\boldsymbol{k}}a_{-\boldsymbol{k}}+a^\dagger_{\boldsymbol{k}}a^\dagger_{-\boldsymbol{k}}\right)\left[J_1\left(\cos Q-1\right)\cos k_xa+J_2\left(\cos 2Q-1\right)\cos 2k_xa-\Delta\right]
\end{aligned}\tag{3.32}$$

We introduce [19]

$$\begin{aligned}
A(\boldsymbol{k})=&J_1\left[(1+\cos Q)\cos k_xa-2\cos Q\right]+J_2\left[(1+\cos 2Q)\cos 2k_xa-2\cos 2Q\right]\\
&+2J_3\left(\cos k_yb-1\right)+2J_4\left(\cos k_zc-1\right)+\Delta\\
B(\boldsymbol{k})=&J_1\left(\cos Q-1\right)\cos k_xa+J_2\left(\cos 2Q-1\right)\cos 2k_xa-\Delta
\end{aligned}\tag{3.33}$$

and we get

$$H^{(2)} = \frac{S}{2}\sum_{\boldsymbol{k}}\left[2A(\boldsymbol{k})a^{\dagger}_{\boldsymbol{k}}a_{\boldsymbol{k}} + B(\boldsymbol{k})\left(a_{\boldsymbol{k}}a_{-\boldsymbol{k}} + a^{\dagger}_{\boldsymbol{k}}a^{\dagger}_{-\boldsymbol{k}}\right)\right] \tag{3.34}$$

In order to eliminate the anomalous terms we perform a Bogoliubov transformation [20]:

$$a_{\boldsymbol{k}} \to \alpha_{\boldsymbol{k}}\cosh\theta_{\boldsymbol{k}} - \alpha^{\dagger}_{-\boldsymbol{k}}\sinh\theta_{\boldsymbol{k}} \tag{3.35}$$

where the coefficients $\theta_{\boldsymbol{k}}$ must satisfy $\theta_{\boldsymbol{k}} = \theta_{-\boldsymbol{k}}$ in order for the transformation to preserve the commutation relations. Substituting Eq. (3.35) in the Hamiltonian Eq. (3.34), we obtain:

$$\begin{aligned} H^{(2)} = \frac{S}{2}\sum_{\boldsymbol{k}} & 2A_{\boldsymbol{k}}\left(\alpha^{\dagger}_{\boldsymbol{k}}\alpha_{\boldsymbol{k}}\cosh^2\theta_{\boldsymbol{k}} - \alpha^{\dagger}_{\boldsymbol{k}}\alpha^{\dagger}_{-\boldsymbol{k}}\cosh\theta_{\boldsymbol{k}}\sinh\theta_{\boldsymbol{k}}\right. \\ & \left.-\alpha_{-\boldsymbol{k}}\alpha_{\boldsymbol{k}}\cosh\theta_{\boldsymbol{k}}\sinh\theta_{\boldsymbol{k}} + \alpha_{-\boldsymbol{k}}\alpha^{\dagger}_{-\boldsymbol{k}}\sinh^2\theta_{\boldsymbol{k}}\right) \\ & + B_{\boldsymbol{k}}\left[\cosh^2\theta_{\boldsymbol{k}}\left(\alpha_{\boldsymbol{k}}\alpha_{-\boldsymbol{k}} + \alpha_{\boldsymbol{k}}\alpha_{-\boldsymbol{k}}\right) + \sinh^2\theta_{\boldsymbol{k}}\left(\alpha^{\dagger}_{-\boldsymbol{k}}\alpha^{\dagger}_{\boldsymbol{k}} + \alpha_{-\boldsymbol{k}}\alpha_{\boldsymbol{k}}\right)\right. \\ & \left.-\cosh\theta_{\boldsymbol{k}}\sinh\theta_{\boldsymbol{k}}\left(\alpha_{\boldsymbol{k}}\alpha^{\dagger}_{\boldsymbol{k}} + \alpha^{\dagger}_{-\boldsymbol{k}}\alpha_{-\boldsymbol{k}} + \alpha^{\dagger}_{\boldsymbol{k}}\alpha_{\boldsymbol{k}} + \alpha_{-\boldsymbol{k}}\alpha^{\dagger}_{-\boldsymbol{k}}\right)\right] \end{aligned} \tag{3.36}$$

This expression can be simplified by first taking into account the commutation relation $[\alpha_{\boldsymbol{k}}, \alpha_{\boldsymbol{q}}] = \delta_{\boldsymbol{k},\boldsymbol{q}}$ and the parity of the functions $\theta_{\boldsymbol{k}}$, $A(\boldsymbol{k})$ and $B(\boldsymbol{k})$:

$$\begin{aligned} H^{(2)} = \frac{S}{2}\sum_{\boldsymbol{k}} & 2\alpha^{\dagger}_{\boldsymbol{k}}\alpha_{\boldsymbol{k}}\left[A(\boldsymbol{k})\left(\cosh^2\theta_{\boldsymbol{k}} + \sinh^2\theta_{\boldsymbol{k}}\right) - 2B(\boldsymbol{k})\cosh\theta_{\boldsymbol{k}}\sinh\theta_{\boldsymbol{k}}\right] \\ & + \left(\alpha^{\dagger}_{\boldsymbol{k}}\alpha^{\dagger}_{-\boldsymbol{k}} + (\alpha_{\boldsymbol{k}}\alpha_{-\boldsymbol{k}}\right)\left[-2A(\boldsymbol{k})\cosh\theta_{\boldsymbol{k}}\sinh\theta_{\boldsymbol{k}} + B(\boldsymbol{k})\left(\cosh^2\theta_{\boldsymbol{k}} + \sinh^2\theta_{\boldsymbol{k}}\right)\right], \end{aligned} \tag{3.37}$$

and then the relations $\cosh^2\theta_{\boldsymbol{k}} + \sinh^2\theta_{\boldsymbol{k}} = \cosh 2\theta_{\boldsymbol{k}}$, $2\cosh\theta_{\boldsymbol{k}}\sinh\theta_{\boldsymbol{k}} = \sinh 2\theta_{\boldsymbol{k}}$:

$$\begin{aligned} H^{(2)} = \frac{S}{2}\sum_{\boldsymbol{k}} & 2\alpha^{\dagger}_{\boldsymbol{k}}\alpha_{\boldsymbol{k}}\left(A(\boldsymbol{k})\cosh 2\theta_{\boldsymbol{k}} - B(\boldsymbol{k})\sinh 2\theta_{\boldsymbol{k}}\right) \\ & + \left(\alpha_{\boldsymbol{k}}\alpha_{-\boldsymbol{k}} + \alpha^{\dagger}_{\boldsymbol{k}}\alpha^{\dagger}_{-\boldsymbol{k}}\right)\left(B(\boldsymbol{k})\cosh 2\theta_{\boldsymbol{k}} - A(\boldsymbol{k})\sinh 2\theta_{\boldsymbol{k}}\right). \end{aligned} \tag{3.38}$$

In order to diagonalize the Hamiltonian, we set the coefficient of the anomalous terms to zero, that is, choosing $\theta_{\boldsymbol{k}}$ such that:

$$\tanh 2\theta_{\boldsymbol{k}} = \frac{B(\boldsymbol{k})}{A(\boldsymbol{k})}. \tag{3.39}$$

From this relation and the property $\cosh^2 2\theta_{\boldsymbol{k}} - \sinh^2\theta_{\boldsymbol{k}} = 1$, we can find the expression for $\cosh 2\theta_{\boldsymbol{k}}$ and $\sinh 2\theta_{\boldsymbol{k}}$ in terms of $A(\boldsymbol{k})$ and $B(\boldsymbol{k})$:

$$\cosh 2\theta_{\boldsymbol{k}} = \frac{A(\boldsymbol{k})}{\sqrt{A^2(\boldsymbol{k}) - B^2(\boldsymbol{k})}} \tag{3.40}$$

$$\sinh 2\theta_{\boldsymbol{k}} = \frac{B(\boldsymbol{k})}{\sqrt{A^2(\boldsymbol{k}) - B^2(\boldsymbol{k})}} \tag{3.41}$$

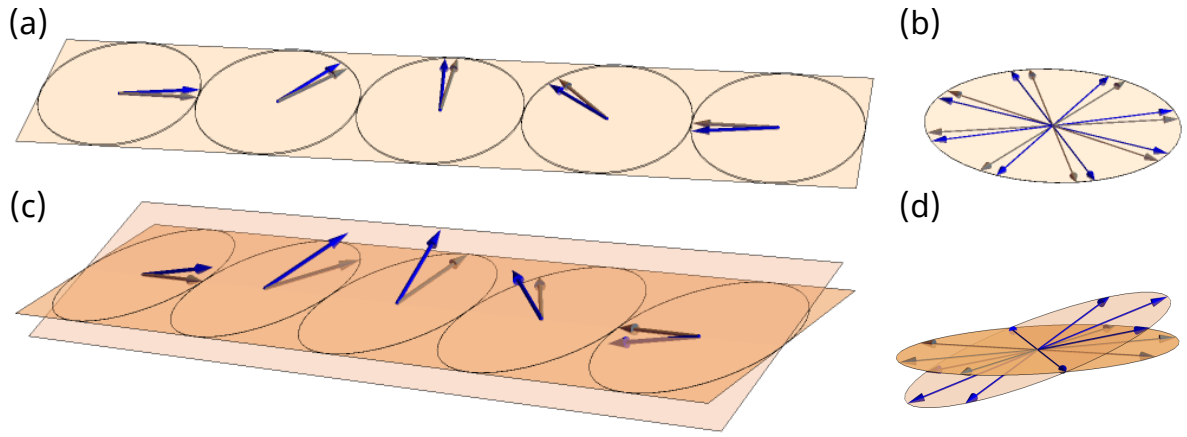

Figure 3.3: Low-energy modes of a spin spiral: (a,b) $k = 0$ phason mode, corresponding to the rotation of all spins. Spins along a direction are shown with arrows. The initial state is indicated in gray, the phason mode moves spins into the state, indicated by blue arrows. In panel (b) all spins are brought to a common center. (c,d) $k = \pm Q$ spiral plane tilting mode is shown in a similar way. The initial and final spiral planes are indicated by transparent polygons.

Substituting these relations in Eq. (3.38), we get the diagonalized second order Hamiltonian:

$$H^{(2)} = S \sum_{\boldsymbol{k}} \sqrt{A(\boldsymbol{k})^2 - B(\boldsymbol{k})^2} \alpha^\dagger_{\boldsymbol{k}} \alpha_{\boldsymbol{k}} \tag{3.42}$$

We can now plot the dispersion relation as a function of k_x, k_y and k_z.

Without an easy-plane anisotropy, $\Delta = 0$, and with $k_y, k_z = 0$, there are three Goldstone bosons, as can be seen in Fig. (3.6). One, at $k = 0$, is associated with the uniform rotation of all spins by the same angle, which implies the shift of the spiral (a phason mode), and is represented in Fig. 3.3. The other two Goldstone modes are at $k_x = \pm Q$. They are associated with a tilting of the spiral plane and are therefore gapped by an easy plane anisotropy Δ.

According to Mermin-Wagner theorem [21], long range order in one dimension is not possible in a system with a continuous symmetry, because of the fluctuations associated with Goldstone modes. This is the reason we introduced weak ferromagnetic couplings in the directions perpendicular to the spiral wave vector, instead of studying a single one-dimensional chain.

With an easy plane anisotropy, the Goldstone modes at $k_x = \pm Q$ are gapped as illustrated for $\Delta = 0.01$ meV by the dispersion plot in Fig. (3.6).

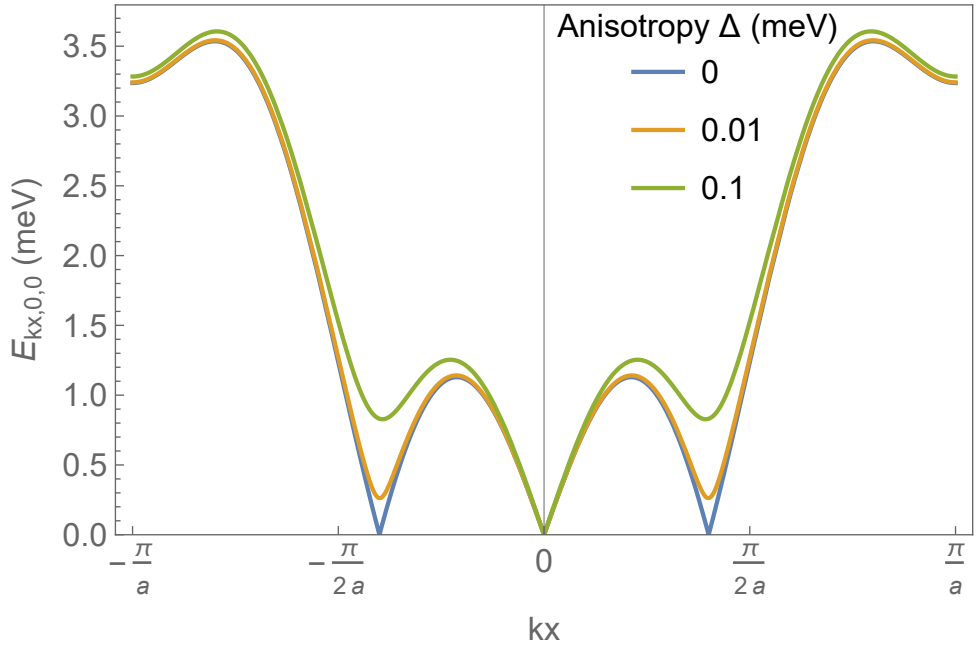

Figure 3.4: Magnon dispersion along the spiral wave vector $E(k_x, k_y = 0, k_z = 0)$. The model parameters are $J_2 = 1$ meV, $Q = \frac{2\pi}{5}$ and $J_1 = -4J_2 \cos Q$ and the easy plane anisotropy Δ is indicated in the legend. The easy plane anisotropy favors one plane for the spiral (in our case, the xz plane), so the Goldstone modes associated with the continuous rotational symmetry, broken by the anisotropy, are now gapped.

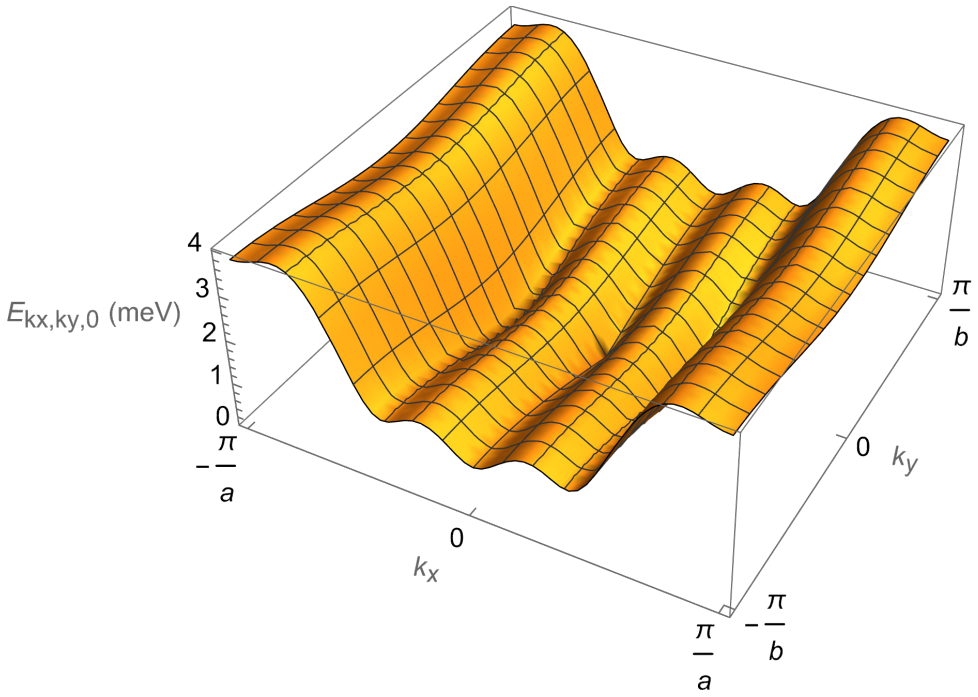

Figure 3.5: Magnon dispersion for the wave vector in ab plane $E(k_x, k_y, k_z = 0)$. The spiral wave vector points in a direction. The model parameters are $J_2 = 1meV$, $Q = \frac{2\pi}{5}$ and $J_1 = -4J_2 \cos Q$ and the easy plane anisotropy $\Delta = 0$.

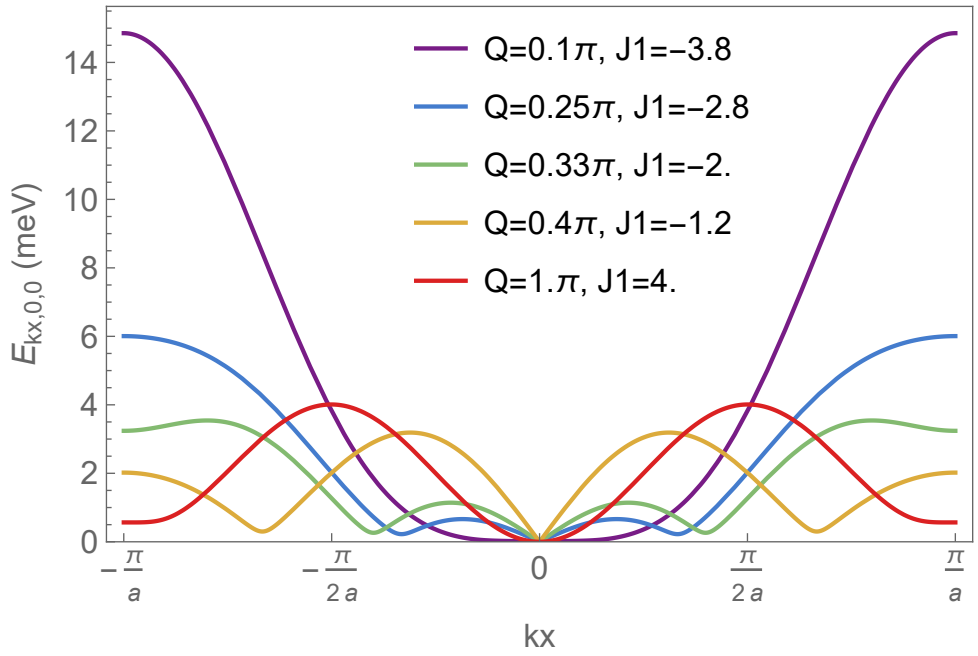

Figure 3.6: Magnon dispersion along the spiral wave vector $E(k_x, k_y = 0, k_z = 0)$ for the spirals with different pitch Q, with $J_2 = 1$ meV and $J_1 = -4J_2 \cos Q$. The spiral pitch Q and the corresponding value of J_1 are indicated in the legend. The easy plane anisotropy $\Delta = 0.01$ meV. The quasi-Goldstone mode at $k = Q$, corresponding to the spiral plane oscillations, is shifting with changing Q.

3.4 Third order Hamiltonian

Now we study the scattering events allowed in our system, in order to understand which processes must be included in the collision integral appearing in the Boltzmann transport equation Eq. (2.9).

Note that the Holstein-Primakoff transformation [18] Eq. (2.21), with the square root expanded up to the first order in $1/S$, is

$$\begin{aligned} S_{\boldsymbol{i}}^x &= \frac{\sqrt{2S}}{2}\left[\left(a_{\boldsymbol{i}} - \frac{a_{\boldsymbol{i}}^\dagger a_{\boldsymbol{i}} a_{\boldsymbol{i}}}{4S}\right) + \left(a_{\boldsymbol{i}}^\dagger - \frac{a_{\boldsymbol{i}}^\dagger a_{\boldsymbol{i}}^\dagger a_{\boldsymbol{i}}}{4S}\right)\right], \\ S_{\boldsymbol{i}}^y &= \frac{\sqrt{2S}}{2i}\left[\left(a_{\boldsymbol{i}} - \frac{a_{\boldsymbol{i}}^\dagger a_{\boldsymbol{i}} a_{\boldsymbol{i}}}{4S}\right) - \left(a_{\boldsymbol{i}}^\dagger - \frac{a_{\boldsymbol{i}}^\dagger a_{\boldsymbol{i}}^\dagger a_{\boldsymbol{i}}}{4S}\right)\right], \\ S_{\boldsymbol{i}}^z &= S - a_{\boldsymbol{i}}^\dagger a_{\boldsymbol{i}}. \end{aligned} \tag{3.43}$$

Then, it is clear that from terms proportional to S^xS^x, S^yS^y and S^zS^z, we only get processes involving at least four magnons. However, in the non-collinear case [11, 22], the presence of the rotation matrix in the scalar product between the spins, Eq. (3.11), gives rise to terms involving S^xS^z (and S^zS^x) and S^yS^z (and S^zS^y), as can be seen in Eq. (3.12). In the collinear case, where there is no need for a rotation matrix, that is, $\sin\theta_{\boldsymbol{ij}} = 0$, there are no such terms and the lowest order scattering processes involve four magnons.

As demonstrated in recent experiments, the ferromagnetic state has higher magnon thermal conductivity than non-collinear states, such as skyrmion and spiral ones [9]. These experiments directly probe the magnetization via magnetooptical Kerr effect, which

allows to track the magnetization recovery, primarily determined by magnetic thermal conductivity.

Once again, we substitute the Holstein-Primakoff transformation, Eq. (2.22), in the Hamiltonian Eq. (3.14). This time, we collect terms involving three magnons:

$$H^{(3)} = \frac{\sqrt{2S}}{2} \sum_{\boldsymbol{ij}} J_{\boldsymbol{ij}} \sin\theta_{\boldsymbol{ij}} \left[a_{\boldsymbol{i}}^\dagger a_{\boldsymbol{i}} \left(a_{\boldsymbol{j}} + a_{\boldsymbol{j}}^\dagger \right) - \left(a_{\boldsymbol{i}} + a_{\boldsymbol{i}}^\dagger \right) a_{\boldsymbol{j}}^\dagger a_{\boldsymbol{j}} \right. \\ \left. + a_{\boldsymbol{j}}^\dagger a_{\boldsymbol{j}} a_{\boldsymbol{j}} + a_{\boldsymbol{j}}^\dagger a_{\boldsymbol{j}}^\dagger a_{\boldsymbol{j}} - a_{\boldsymbol{i}}^\dagger a_{\boldsymbol{i}} a_{\boldsymbol{i}} - a_{\boldsymbol{i}}^\dagger a_{\boldsymbol{i}}^\dagger a_{\boldsymbol{i}} \right]. \tag{3.44}$$

The last four terms, containing creation and annihilation operators for magnons only on one site, $\boldsymbol{i}$ or $\boldsymbol{j}$, do not contribute. For example, when $\boldsymbol{j} = \boldsymbol{i} + \mathbf{a}$, the two terms with one annihilation and two creation operators give:

$$\sum_{\boldsymbol{i}} J_1 \sin Q \left[a_{\boldsymbol{i}+\mathbf{a}}^\dagger a_{\boldsymbol{i}+\mathbf{a}} a_{\boldsymbol{i}+\mathbf{a}} - a_{\boldsymbol{i}}^\dagger a_{\boldsymbol{i}} a_{\boldsymbol{i}} \right] \tag{3.45}$$

Now we rename $\boldsymbol{i} + \mathbf{a} \to \boldsymbol{i}'$ and the two terms cancel. The same happens when summing over the next-nearest-neighbor $\boldsymbol{j} = \boldsymbol{i}+2\mathbf{a}$ and the nearest-neighbors in the other directions, $\boldsymbol{j} = \boldsymbol{i} + \mathbf{b}$ and $\boldsymbol{j} = \boldsymbol{i} + \mathbf{c}$.
We are left with

$$H^{(3)} = \frac{\sqrt{2S}}{2} \sum_{\boldsymbol{ij}} J_{\boldsymbol{ij}} \sin\theta_{\boldsymbol{ij}} \left[a_{\boldsymbol{i}}^\dagger a_{\boldsymbol{i}} \left(a_{\boldsymbol{j}} + a_{\boldsymbol{j}}^\dagger \right) - \left(a_{\boldsymbol{i}} + a_{\boldsymbol{i}}^\dagger \right) a_{\boldsymbol{j}}^\dagger a_{\boldsymbol{j}} \right] \tag{3.46}$$

and we proceed with the Fourier transform Eq. (3.19):

$$H^{(3)} = \frac{1}{N^{3/2}} \frac{\sqrt{2S}}{2} \sum_{\boldsymbol{ij}} J_{\boldsymbol{ij}} \sin\theta_{\boldsymbol{ij}} \sum_{\boldsymbol{kqp}} \left[a_{\boldsymbol{k}}^\dagger a_{\boldsymbol{q}} e^{-i\boldsymbol{k}\cdot\mathbf{R}_i} e^{i\boldsymbol{q}\cdot\mathbf{R}_j} \left(a_{\boldsymbol{p}} e^{i\boldsymbol{p}\cdot\boldsymbol{R}_i} + a_{\boldsymbol{p}}^\dagger e^{-i\boldsymbol{p}\cdot\boldsymbol{R}_i} \right) \right. \\ \left. - a_{\boldsymbol{k}}^\dagger a_{\boldsymbol{q}} e^{i\boldsymbol{R}_i(\boldsymbol{q}-\boldsymbol{k})} \left(a_{\boldsymbol{p}} e^{i\boldsymbol{p}\cdot\boldsymbol{R}_j} + a_{\boldsymbol{p}}^\dagger e^{-i\boldsymbol{p}\cdot\boldsymbol{R}_j} \right) \right] \tag{3.47}$$

First, we have to sum over $\boldsymbol{j}$. However, because of the $\sin\theta_{\boldsymbol{ij}}$, the sums over $\boldsymbol{j} = \boldsymbol{i} + \mathbf{b}$ and $\boldsymbol{j} = \boldsymbol{i} + \mathbf{c}$ do not contribute, since $\theta_{\boldsymbol{ij}} = 0$ for directions perpendicular to the spiral. We are left with the term $\boldsymbol{j} = \boldsymbol{i} + \mathbf{a}$, that gives:

$$\frac{1}{N^{3/2}} \frac{\sqrt{2S}}{2} \sum_{\boldsymbol{i}} J_1 \sin Q \sum_{\boldsymbol{kqp}} a_{\boldsymbol{k}}^\dagger a_{\boldsymbol{q}} e^{i(\boldsymbol{q}-\boldsymbol{k})\cdot\boldsymbol{R}_i} \left[e^{i(q_x-k_x)a} \left(a_{\boldsymbol{p}} e^{i\boldsymbol{p}\cdot\boldsymbol{R}_i} + a_{\boldsymbol{p}}^\dagger e^{-i\boldsymbol{p}\cdot\boldsymbol{R}_i} \right) \right. \\ \left. + \left(a_{\boldsymbol{p}} e^{i\boldsymbol{p}\cdot\boldsymbol{R}_i} e^{ip_x a} + a_{\boldsymbol{p}}^\dagger e^{-i\boldsymbol{p}\cdot\boldsymbol{R}_i} e^{-ip_x a} \right) \right] \tag{3.48}$$

Making use of Eq. (3.22), we can sum over $\boldsymbol{i}$:

$$\frac{\sqrt{2S}}{\sqrt{N}} J_1 i \sin Q \sum_{\boldsymbol{kq}} \sin k_x a \left(a_{\boldsymbol{k}}^\dagger a_{\boldsymbol{k}+\boldsymbol{q}} a_{\boldsymbol{q}}^\dagger - a_{\boldsymbol{k}+\boldsymbol{q}}^\dagger a_{\boldsymbol{q}} a_{\boldsymbol{k}} \right) \tag{3.49}$$

When $\boldsymbol{j} + \boldsymbol{i} + 2\mathbf{a}$, the result is analogous, with $2Q$ instead of Q, $2\mathbf{a}$ instead of $\mathbf{a}$ and J_2 instead of J_1.
The final Hamiltonian is [11]

$$H^{(3)} = \frac{\sqrt{2S}}{2\sqrt{N}} i \sum_{\boldsymbol{kq}} \left(\beta(k_x) + \beta(q_x) \right) \left(a_{\boldsymbol{k}}^\dagger a_{\boldsymbol{k}+\boldsymbol{q}} a_{\boldsymbol{q}}^\dagger - a_{\boldsymbol{k}+\boldsymbol{q}}^\dagger a_{\boldsymbol{q}} a_{\boldsymbol{k}} \right) \tag{3.50}$$

where we defined

$$\beta(k_x) \equiv J_1 \sin k_x a \sin Q + J_2 \sin 2k_x a \sin 2Q \tag{3.51}$$

and we symmetrized by splitting the sum in two parts and renaming the indices only in the second half; the operators are symmetric under $\boldsymbol{k} \leftrightarrow \boldsymbol{q}$, so they are not affected.
It is now necessary to apply the same Bogoliubov transformation that makes the second-order Hamiltonian diagonal, Eq. (3.35) with $\theta_{\boldsymbol{k}}$ defined as in Eq. (3.39).
Let us start from the first term,

$$\frac{\sqrt{2S}}{2\sqrt{N}} i \sum_{\boldsymbol{kq}} \left(\beta(k_x) + \beta(q_x)\right) a^\dagger_{\boldsymbol{k}} a_{\boldsymbol{k+q}} a^\dagger_{\boldsymbol{q}} \tag{3.52}$$

Writing it in terms of the α operators, and collecting only the terms with two creation and one annihilation operators (the ones with two annihilations and one creation will just give the Hermitian conjugate, and there is no difference in the procedure), we get:

$$\begin{aligned}\frac{\sqrt{2S}}{2\sqrt{N}} i \sum_{\boldsymbol{kq}} \left(\beta(k_x) + \beta(q_x)\right) \Big(& \alpha^\dagger_{\boldsymbol{k}} \alpha^\dagger_{\boldsymbol{-k-q}} \alpha_{\boldsymbol{-q}} \sinh\theta_{\boldsymbol{k+q}} \cosh\theta_{\boldsymbol{k}} \sinh\theta_{\boldsymbol{q}} \\ & + \alpha^\dagger_{\boldsymbol{k}} \alpha_{\boldsymbol{k+q}} \alpha^\dagger_{\boldsymbol{q}} \cosh\theta_{\boldsymbol{k}} \cosh\theta_{\boldsymbol{k+q}} \cosh\theta_{\boldsymbol{q}} \\ & + \alpha_{\boldsymbol{-k}} \alpha^\dagger_{\boldsymbol{-q-k}} \alpha^\dagger_{\boldsymbol{q}} \sinh\theta_{\boldsymbol{k}} \sinh\theta_{\boldsymbol{k+q}} \cosh\theta_{\boldsymbol{q}} \Big)\end{aligned} \tag{3.53}$$

There is still one step to do: we want to always have the same operator, for example $\alpha^\dagger_{\boldsymbol{k-q}} \alpha^\dagger_{\boldsymbol{q}} \alpha_{\boldsymbol{k}}$. To achieve this, we use the fact that $\theta_{\boldsymbol{k}} = \theta_{\boldsymbol{-k}}$ and $\beta(k_x)$ is an odd function in k_x.
For example, in the first term we can define a new index $\boldsymbol{k} + \boldsymbol{p} = \boldsymbol{q}$:

$$\sum_{\boldsymbol{kp}} \left(\beta(k_x) + \beta(p_x - k_x)\right) \alpha^\dagger_{\boldsymbol{p}} \alpha^\dagger_{\boldsymbol{k-p}} \alpha_{\boldsymbol{k}} \sinh\theta_{\boldsymbol{k-p}} \cosh\theta_{\boldsymbol{k}} \sinh\theta_{\boldsymbol{p}} \tag{3.54}$$

and then rename $\boldsymbol{p}$ as $\boldsymbol{q}$.
After collecting all the terms, the Hamiltonian is:

$$H^{(3)} = \frac{\sqrt{2S}}{2\sqrt{N}} i \sum_{\boldsymbol{kq}} C\left(\boldsymbol{k}, \boldsymbol{q}\right) \left(\alpha^\dagger_{\boldsymbol{q}} \alpha^\dagger_{\boldsymbol{k-q}} \alpha_{\boldsymbol{k}} - \alpha_{\boldsymbol{q}} \alpha_{\boldsymbol{k-q}} \alpha^\dagger_{\boldsymbol{k}} \right), \tag{3.55}$$

where we defined

$$\begin{aligned} C\left(\boldsymbol{k}, \boldsymbol{q}\right) \equiv & \left(\beta(q_x) - \beta(k_x)\right) \left(\cosh\theta_{\boldsymbol{k}} \cosh\theta_{\boldsymbol{k-q}} \sinh\theta\boldsymbol{q} + \sinh\theta_{\boldsymbol{k}} \sinh\theta_{\boldsymbol{k-q}} \cosh\theta_{\boldsymbol{q}}\right) \\ & - \left(\beta(k_x - q_x) + \beta(q_x)\right) \left(\sinh\theta_{\boldsymbol{k}} \sinh\theta_{\boldsymbol{k-q}} \sinh\theta_{\boldsymbol{q}} + \cosh\theta_{\boldsymbol{k}} \cosh\theta_{\boldsymbol{k-q}} \cosh\theta_{\boldsymbol{q}}\right) \\ & \left(\beta(k_x) - \beta(k_x - q_x)\right) \left(\sinh\theta_{\boldsymbol{k-q}} \cosh\theta_{\boldsymbol{k}} \cosh\theta_{\boldsymbol{q}} + \sinh\theta_{\boldsymbol{k}} \cosh\theta_{\boldsymbol{q}} \sinh\theta_{\boldsymbol{k-q}}\right). \end{aligned} \tag{3.56}$$

Since β depends on $\sin Q$ and $\sin 2Q$, this interaction Hamiltonian is always zero for a collinear system, as we expected. Its leading terms are linear in Q. Also, we can expect these interactions to be stronger in systems with large spiral pitch $Q = \arccos\left(-\frac{J_1}{4J_2}\right)$ (Eq. (4.6).

The Hamiltonian Eq. (3.55) describes processes where two magnons with momentum $\boldsymbol{q}$ and $\boldsymbol{k} - \boldsymbol{q}$ merge into one with momentum $\boldsymbol{k}$, $\boldsymbol{q} + (\boldsymbol{k} - \boldsymbol{q}) \to \boldsymbol{k}$, as can be seen in Fig. (3.7)(left), or one magnon decays into two, $\boldsymbol{k} \to \boldsymbol{q} + (\boldsymbol{k} - \boldsymbol{q})$, Fig. (3.7)(right).

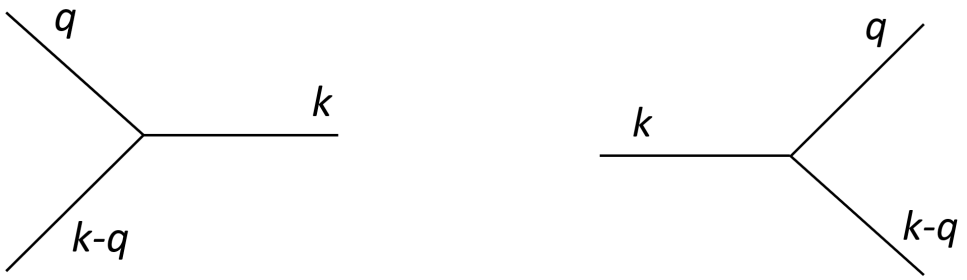

Figure 3.7: Magnon fusion (left) and decay (right) processes induced by spin non-collinearity. Such processes limit magnon lifetime and thermal conductivity.

3.5 Scattering rates

Once the third-order Hamiltonian is found, we can proceed by computing the transition rates due to processes involving three magnons. These rates will then enter in the collision integral in Eq. (2.9)-(2.10).

The transition rate between two states, $|i\rangle$ and $|f\rangle$, is given by the Fermi's Golden Rule:

$$\Gamma_{i\to f} = \frac{2\pi}{\hbar} \left|\langle f| H^{(3)} |i\rangle\right|^2 \delta\left(E_f - E_i\right) \tag{3.57}$$

In our case, we are only interested in the intrinsic rates, so the initial and final states will only be composed by one or two magnons. We will take into account the number of excitations present in the system when writing the collision integral, where the intrinsic rates are multiplied by the factors involving Bose-Einstein distributions. Therefore, we only have to compute the matrix elements where the initial state contains one magnon and the final state contains two, and vice versa. For the decay process $\boldsymbol{k}_1 \to \boldsymbol{k}_2\boldsymbol{k}_3$, with momentum conservation $\boldsymbol{k}_1 = \boldsymbol{k}_2 + \boldsymbol{k}_3$, we have:

$$\langle \boldsymbol{k}_2, \boldsymbol{k}_3| H^{(3)} |\boldsymbol{k}_1\rangle = \frac{\sqrt{2S}}{2\sqrt{N}} i \sum_{\boldsymbol{kq}} C(\boldsymbol{k}, \boldsymbol{q}) \langle \boldsymbol{k}_2, \boldsymbol{k}_3| \alpha^\dagger_{\boldsymbol{k}-\boldsymbol{q}} \alpha^\dagger_{\boldsymbol{q}} \alpha_{\boldsymbol{k}} |\boldsymbol{k}_1\rangle \tag{3.58}$$

that is non-zero only if $\boldsymbol{k}$ is equal to $\boldsymbol{k}_1$:

$$\langle \boldsymbol{k}_2, \boldsymbol{k}_3| H^{(3)} |\boldsymbol{k}_1\rangle = \frac{\sqrt{2S}}{2\sqrt{N}} i \sum_{\boldsymbol{q}} C(\boldsymbol{k}_1, \boldsymbol{q}) \langle \boldsymbol{k}_2, \boldsymbol{k}_3| \alpha^\dagger_{\boldsymbol{k}_1-\boldsymbol{q}} \alpha^\dagger_{\boldsymbol{q}} |0\rangle \tag{3.59}$$

There are now two cases: if the two magnons in the final states are different, $\boldsymbol{k}_2 \neq \boldsymbol{k}_3$, then we can have $\boldsymbol{q} = \boldsymbol{k}_2$ or $\boldsymbol{q} = \boldsymbol{k}_3$, and the matrix element is:

$$\langle \boldsymbol{k}_2, \boldsymbol{k}_3| H^{(3)} |\boldsymbol{k}_1\rangle = \frac{\sqrt{2S}}{2\sqrt{N}} i \left[C(\boldsymbol{k}_1, \boldsymbol{k}_2) + C(\boldsymbol{k}_1, \boldsymbol{k}_3)\right] \delta_{\boldsymbol{k}_1, \boldsymbol{k}_2+\boldsymbol{k}_3} \tag{3.60}$$

While, if $\boldsymbol{k}_2 = \boldsymbol{k}_3$, we use the property $\alpha_{\boldsymbol{k}} |N_{\boldsymbol{k}}\rangle = \sqrt{N_{\boldsymbol{k}}} |N_{\boldsymbol{k}} - 1\rangle$ to get:

$$\begin{aligned} \langle \boldsymbol{k}_2, \boldsymbol{k}_3| H^{(3)} |\boldsymbol{k}_1\rangle =& \frac{\sqrt{2S}}{2\sqrt{N}} i \sum_{\boldsymbol{q}} C(\boldsymbol{k}_1, \boldsymbol{q}) \langle N_{\boldsymbol{k}_2} = 2| \alpha^\dagger_{k_1-q} \alpha^\dagger_q |0\rangle \\ =& \frac{\sqrt{S}}{\sqrt{N}} i C(\boldsymbol{k}_1, \boldsymbol{k}_2) \delta_{\boldsymbol{k}_1, 2\boldsymbol{k}_2} \end{aligned} \tag{3.61}$$

Since $H^{(3)}$ is Hermitian, the matrix element for the fusion process $\boldsymbol{k}_2\boldsymbol{k}_3 \to \boldsymbol{k}_1$ is simply the complex conjugate of the matrix element for the decay, so the rate will be the same as for the decay.

Finally, we substitute 3.60 and 3.61 in Eq. (3.57) to get the transition rates:

$$\begin{aligned}
\Gamma_{\boldsymbol{k}_1\to\boldsymbol{k}_2\boldsymbol{k}_3} &= \Gamma_{\boldsymbol{k}_2\boldsymbol{k}_3\to\boldsymbol{k}_1} = \frac{\pi V}{\hbar} S\left[C(\boldsymbol{k}_1,\boldsymbol{k}_2) + C(\boldsymbol{k}_1,\boldsymbol{k}_3)\right]^2 \delta\left(E_{\boldsymbol{k}_2} + E_{\boldsymbol{k}_3} - E_{\boldsymbol{k}_1}\right) \delta_{\boldsymbol{k}_1,\boldsymbol{k}_2+\boldsymbol{k}_3} \\
\Gamma_{\boldsymbol{k}_1\to\boldsymbol{k}_2\boldsymbol{k}_2} &= \Gamma_{\boldsymbol{k}_2\boldsymbol{k}_2\to\boldsymbol{k}_1} = \frac{2\pi V}{\hbar} S\left[C(\boldsymbol{k}_1,\boldsymbol{k}_2)\right]^2 \delta\left(2E_{\boldsymbol{k}_2} - E_{\boldsymbol{k}_1}\right) \delta_{\boldsymbol{k}_1,2\boldsymbol{k}_2}
\end{aligned} \tag{3.62}$$

Energy conservation law, encoded by δ-function in Eq. 3.62, sets stringent constraints on the possible states participating in the magnon fusion and decay processes. In Fig. (3.9), the upper panel shows the set of points that simultaneously satisfy energy and momentum conservation, $E(\boldsymbol{k}+\boldsymbol{q}) = E(\boldsymbol{k}) + E(\boldsymbol{q})$, with $q_y = q_z = k_y = k_z = 0$. In general, finding such surface in the six-dimensional space $(q_x, q_y, q_z, k_x, k_y, k_z)$ and integrating along it is a difficult problem. Instead, the usual approach [15, 23] is to introduce the energy smearing by replacing the δ-function $\delta(E(\boldsymbol{k}) + E(\boldsymbol{q}) - E(\boldsymbol{k}+\boldsymbol{q}))$ by the Gaussian $\propto \exp\left[-\frac{(E(\boldsymbol{k})+E(\boldsymbol{q})-E(\boldsymbol{k}+\boldsymbol{q}))^2}{\sigma_E^2}\right]$ and performing the integration over the entire space. The lower panel in Fig. (3.9) shows such Gaussian approximation of the δ-function.

The other factors, besides the δ-functions are plotted in Fig. 3.8. They have a rich structure, with a number of peaks, particularly at the positions of Goldstone modes $q = 0, \pm Q$. We note that the rate corresponding to the Goldstone mode at $k = 0$ has zero amplitude despite divergent occupations.

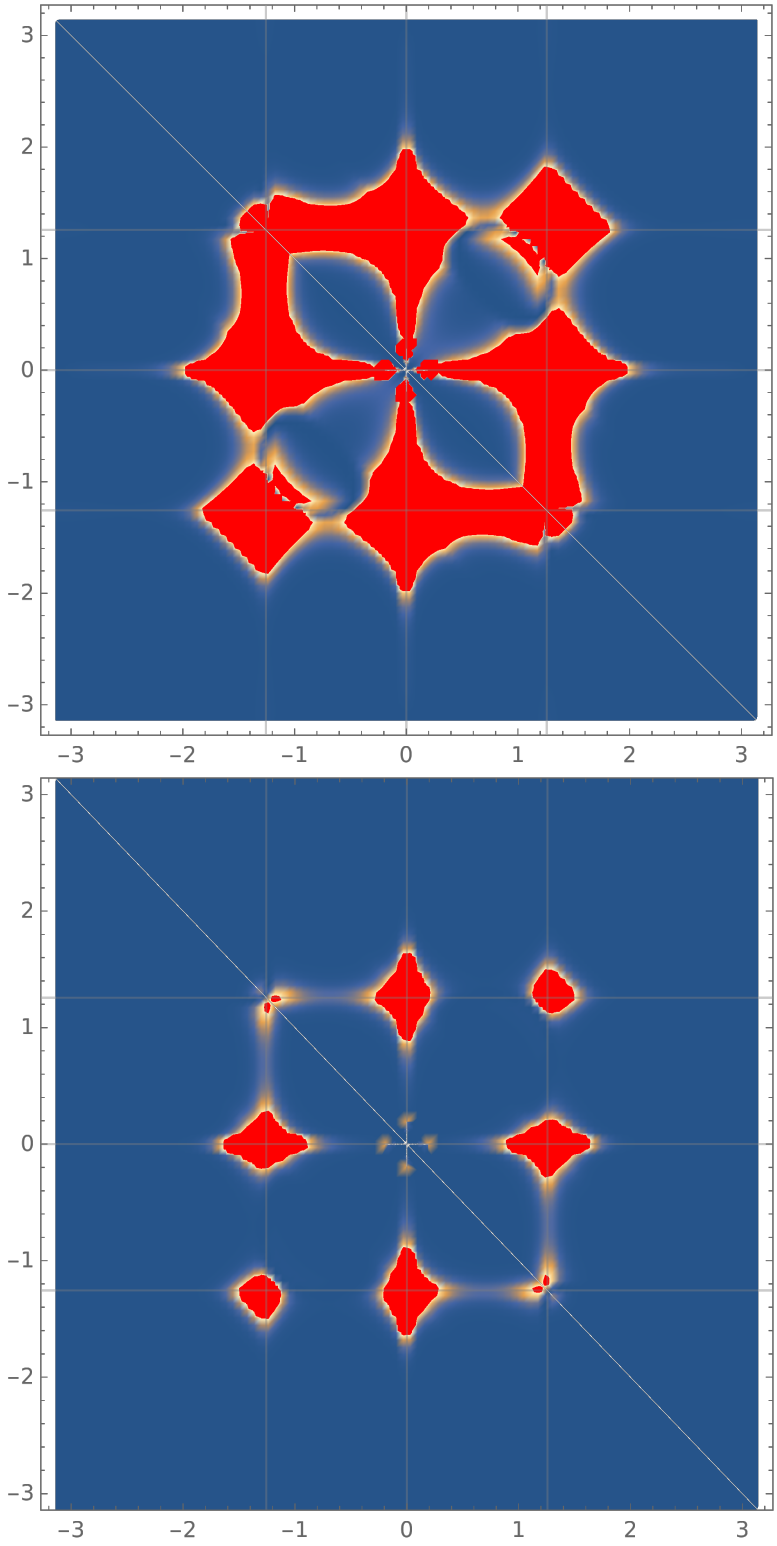

Figure 3.8: Magnon fusion and decay rate in the (q_x, k_x) plane for $q_y = q_z = k_y = k_z = 0$, as given by the matrix elements of Eq. (3.61) multiplied by the occupations of the initial and final states. The overall rate is obtained by additionally multiplying by the δ-function that enforces the energy conservation law, cf. Fig. 3.9. The grid lines mark the values of the spiral wave vector. The colors encode the rate, with blue corresponding to zero rate and red to high rate. The lower panel is mapping a wider range of rates to the color range to show the peak structure in more detail.

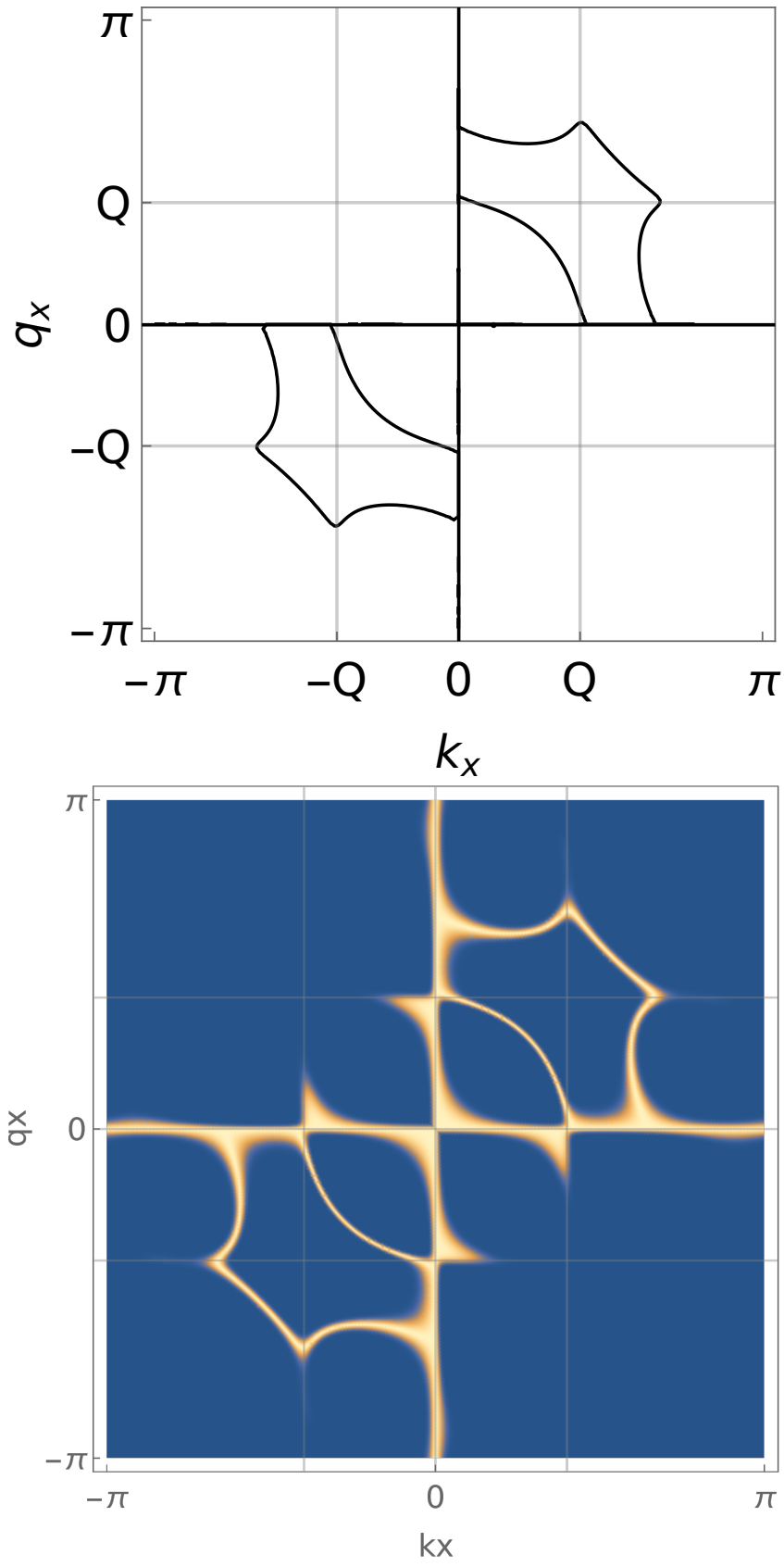

Figure 3.9: The thick black lines in the upper panel show the set of states k_x, q_x that simultaneously satisfy energy and momentum conservation law for the decay $\boldsymbol{k}, \boldsymbol{q} \to \boldsymbol{k}+\boldsymbol{q}$ for $q_y = q_z = k_y = k_z = 0$. Lower panel shows the Gaussian, used to approximate $\delta(E(\boldsymbol{k}) + E(\boldsymbol{q}) - E(\boldsymbol{k}+\boldsymbol{q}))$ in numerical calculations.

Chapter 4

Relaxons

The aim of this Chapter is to find an expression for the thermal conductivity by putting together what we have learned so far about the Boltzmann transport equation (BTE) and the magnetic excitations in spiral magnets.

We will write the collision matrix in the case of processes involving three magnons. The presence of non-diagonal terms in the collision matrix means that the eigenvectors of the BTE are not individual magnons, but linear combinations of many of them. These excitations, called relaxons, are the heat carriers and describe exponential energy relaxation with a well defined relaxation time. Finally, we will derive an expression for the thermal conductivity in the relaxon picture.

4.1 Collision integral with three-magnons scattering

In the case of scattering processes involving three magnons, there are four different cases that we have to take into account in the collision integral. The out-of-equilibrium distribution function $f_{\boldsymbol{k}}$ can increase with time because two magnons, $\boldsymbol{p}$ and $\boldsymbol{q}$, merge into a single magnon with momentum $\boldsymbol{k}$, and because one magnon $\boldsymbol{p}$ decays into two magnons $\boldsymbol{k}$ and $\boldsymbol{q}$:

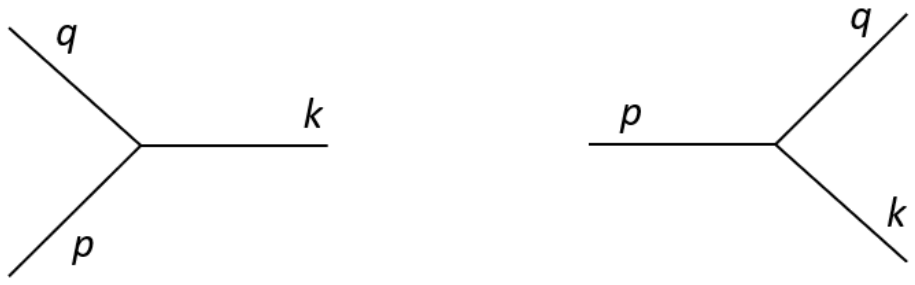

Figure 4.1: Scattering processes that increase the number of magnons with the wave vector $\boldsymbol{k}$.

Additionally, $f_{\boldsymbol{k}}$ can decrease because a magnon with the momentum $\boldsymbol{k}$ decays into $\boldsymbol{q}$ and $\boldsymbol{p}$, and because $\boldsymbol{k}$ and $\boldsymbol{q}$ merge to give $\boldsymbol{p}$:

The collision integral is the sum of these four contributions, weighted with the distribution functions of the magnons involved: for the scattering to happen, the magnons in the initial state must be present in the system, so we multiply every rate by the occupations of the initial states involved. Instead, for a final state $\boldsymbol{k}$, we multiply by $(f_{\boldsymbol{k}} + 1)$:

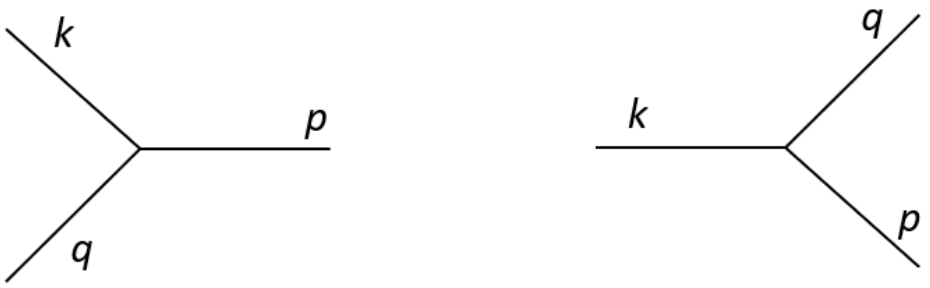

Figure 4.2: Scattering processes that decrease the number of magnons with the wave vector $\boldsymbol{k}$.

the scattering into a state that is already occupied is enhanced. Clearly this is only true for bosons, while for fermions we should multiply by $(1 - f_{\boldsymbol{k}})$ to make sure that the final state was initially empty.

Putting all the contributions together, we arrive at the collision integral in the form:

$$\left(\frac{\partial f_{\boldsymbol{k}}}{\partial t}\right)_{scatt} = \iint \frac{d\boldsymbol{q}}{(2\pi)^3}\frac{d\boldsymbol{p}}{(2\pi)^3}\left[\Gamma^{\boldsymbol{k}}_{\boldsymbol{qp}} f_{\boldsymbol{q}} f_{\boldsymbol{p}}(f_{\boldsymbol{k}}+1) + \Gamma^{\boldsymbol{kq}}_{\boldsymbol{p}} f_{\boldsymbol{p}}(f_{\boldsymbol{q}}+1)(f_{\boldsymbol{k}}+1)\right.$$
$$\left. -\Gamma^{\boldsymbol{p}}_{\boldsymbol{kq}} f_{\boldsymbol{k}} f_{\boldsymbol{q}}(f_{\boldsymbol{p}}+1) - \Gamma^{\boldsymbol{qp}}_{\boldsymbol{k}} f_{\boldsymbol{k}}(f_{\boldsymbol{q}}+1)(f_{\boldsymbol{p}}+1)\right] \quad (4.1)$$

As we discussed in the previous section, the rate for the process $\boldsymbol{k} \to \boldsymbol{q}+\boldsymbol{p}$ is the same as the rate for the inverse process $\boldsymbol{q}+\boldsymbol{p} \to \boldsymbol{k}$, so we can simplify the last expression by collecting these contributions together:

$$\begin{aligned}\left(\frac{\partial f_{\boldsymbol{k}}}{\partial t}\right)_{scatt} &= \iint \frac{d\boldsymbol{q}}{(2\pi)^3}\frac{d\boldsymbol{p}}{(2\pi)^3}\left[\Gamma^{\boldsymbol{k}}_{\boldsymbol{qp}}\left(f_{\boldsymbol{q}} f_{\boldsymbol{p}}(f_{\boldsymbol{k}}+1) - f_{\boldsymbol{k}}(f_{\boldsymbol{q}}+1)(f_{\boldsymbol{p}}+1)\right)\right. \\ &\left. +\Gamma^{\boldsymbol{kq}}_{\boldsymbol{p}}\left(f_{\boldsymbol{p}}(f_{\boldsymbol{q}}+1)(f_{\boldsymbol{k}}+1) - f_{\boldsymbol{k}} f_{\boldsymbol{q}}(f_{\boldsymbol{p}}+1)\right)\right] \\ &\equiv I^{\boldsymbol{k}}_{\boldsymbol{qp}} + I^{\boldsymbol{kq}}_{\boldsymbol{p}},\end{aligned} \quad (4.2)$$

where $I^{\boldsymbol{k}}_{\boldsymbol{qp}}$ ($I^{\boldsymbol{kq}}_{\boldsymbol{p}}$) is the term proportional to $\Gamma^{\boldsymbol{k}}_{\boldsymbol{qp}}$ ($\Gamma^{\boldsymbol{kq}}_{\boldsymbol{p}}$).

In general, $f_{\boldsymbol{k}} = f^0_{\boldsymbol{k}} + \Delta f_{\boldsymbol{k}}$, where $\Delta f_{\boldsymbol{k}}$ is a small deviation and $f^0_{\boldsymbol{k}}$ is, in the case of magnons, the Bose-Einstein distribution,

$$f^0_{\boldsymbol{k}} = \frac{1}{e^{E_{\boldsymbol{k}}/k_B T} - 1}. \quad (4.3)$$

It is useful to use, instead of Δf_k, a new function Φ_k defined as [12, 24]

$$f_{\boldsymbol{k}} = f^0_{\boldsymbol{k}} - \Phi_{\boldsymbol{k}}\frac{\partial f^0_{\boldsymbol{k}}}{\partial \epsilon_{\boldsymbol{k}}}, \quad (4.4)$$

where $\Phi_{\boldsymbol{k}}$ describes the average extra energy that magnons have due to non-equilibrium conditions (temperature gradient, etc).

For magnons,

$$\frac{\partial f^0_{\boldsymbol{k}}}{\partial E_{\boldsymbol{k}}} = -\frac{1}{k_B T} f^0_{\boldsymbol{k}}\left(f^0_{\boldsymbol{k}}+1\right), \quad (4.5)$$

and the out-of-equilibrium distribution can be written as

$$f_{\boldsymbol{k}} = f^0_{\boldsymbol{k}} + \frac{\Phi_{\boldsymbol{k}}}{k_B T} f^0_{\boldsymbol{k}}\left(f^0_{\boldsymbol{k}}+1\right). \quad (4.6)$$

Now, we can plug Eq. (4.6) in the collision integral Eq. (4.2) and collect only terms that are first order in Φ, to get the linearized collision integral.

The zeroth order terms do not contribute, as is to be expected since they describe the situation of equilibrium. To see this, we substitute $f_{\boldsymbol{k}}$ with $f^0_{\boldsymbol{k}}$ in Eq. (4.2), and get terms proportional to $(f_{\boldsymbol{q}} f_{\boldsymbol{p}}(f_{\boldsymbol{k}}+1) - f_{\boldsymbol{k}}(f_{\boldsymbol{q}}+1)(f_{\boldsymbol{p}}+1))$ or $(f_{\boldsymbol{p}}(f_{\boldsymbol{q}}+1)(f_{\boldsymbol{k}}+1) - f_{\boldsymbol{k}} f_{\boldsymbol{q}}(f_{\boldsymbol{p}}+1))$. Since energy is conserved in the scattering, we can prove that the detailed balance,

$$f^0_{\boldsymbol{q}} f^0_{\boldsymbol{p}}(f^0_{\boldsymbol{k}}+1) = f^0_{\boldsymbol{k}}(f^0_{\boldsymbol{q}}+1)(f^0_{\boldsymbol{p}}+1), \tag{4.7}$$

holds, and all terms cancel.

Collecting first order terms, we get, for $I^{\boldsymbol{k}}_{\boldsymbol{qp}}$:

$$\begin{aligned} I^{\boldsymbol{k}}_{\boldsymbol{qp}} &= \iint \frac{d\boldsymbol{q}}{(2\pi)^3}\frac{d\boldsymbol{p}}{(2\pi)^3}\Gamma^{\boldsymbol{k}}_{\boldsymbol{qp}}\left[f_{\boldsymbol{q}} f_{\boldsymbol{p}}(f_{\boldsymbol{k}}+1) - f_{\boldsymbol{k}}(f_{\boldsymbol{q}}+1)(f_{\boldsymbol{p}}+1)\right] = \\ &= \frac{1}{k_B T}\iint \frac{d\boldsymbol{q}}{(2\pi)^3}\frac{d\boldsymbol{p}}{(2\pi)^3}\Gamma^{\boldsymbol{k}}_{\boldsymbol{qp}}\Big[\Phi_{\boldsymbol{k}}\left(f^0_{\boldsymbol{q}} f^0_{\boldsymbol{p}} f^0_{\boldsymbol{k}}(f^0_{\boldsymbol{k}}+1) - f^0_{\boldsymbol{k}}(f^0_{\boldsymbol{k}}+1)(f^0_{\boldsymbol{q}}+1)(f^0_{\boldsymbol{p}}+1)\right) \\ &\qquad + \Phi_{\boldsymbol{p}}\left(f^0_{\boldsymbol{q}} f^0_{\boldsymbol{p}}(f^0_{\boldsymbol{p}}+1)(f^0_{\boldsymbol{k}}+1) - f^0_{\boldsymbol{k}}(f^0_{\boldsymbol{q}}+1) f^0_{\boldsymbol{p}}(f^0_{\boldsymbol{p}}+1)\right) \\ &\qquad + \Phi_{\boldsymbol{q}}\left(f^0_{\boldsymbol{q}} f^0_{\boldsymbol{p}}(f^0_{\boldsymbol{q}}+1)(f^0_{\boldsymbol{k}}+1) - f^0_{\boldsymbol{k}} f^0_{\boldsymbol{q}}(f^0_{\boldsymbol{q}}+1)(f^0_{\boldsymbol{p}}+1)\right)\Big] \end{aligned} \tag{4.8}$$

We can use again the detailed balance, Eq. (4.7), so that, for example, in the first term,

$$\Gamma^{\boldsymbol{k}}_{\boldsymbol{qp}}\Phi_{\boldsymbol{k}}\left(f^0_{\boldsymbol{q}} f^0_{\boldsymbol{p}} f^0_{\boldsymbol{k}}(f^0_{\boldsymbol{k}}+1) - f^0_{\boldsymbol{k}}(f^0_{\boldsymbol{k}}+1)(f^0_{\boldsymbol{q}}+1)(f^0_{\boldsymbol{p}}+1)\right), \tag{4.9}$$

we substitute $f^0_{\boldsymbol{k}}(f^0_{\boldsymbol{q}}+1)(f^0_{\boldsymbol{p}}+1)$ with $(f^0_{\boldsymbol{k}}+1) f^0_{\boldsymbol{q}} f^0_{\boldsymbol{p}}$ and get

$$\Gamma^{\boldsymbol{k}}_{\boldsymbol{qp}}\Phi_{\boldsymbol{k}} f^0_{\boldsymbol{q}} f^0_{\boldsymbol{p}}(f^0_{\boldsymbol{k}}+1) = P^{\boldsymbol{k}}_{\boldsymbol{qp}}\Phi_{\boldsymbol{k}}, \tag{4.10}$$

where $P^{\boldsymbol{k}}_{\boldsymbol{qp}}$ is the equilibrium transition rate,

$$P^{\boldsymbol{k}}_{\boldsymbol{qp}} \equiv \Gamma^{\boldsymbol{k}}_{\boldsymbol{qp}} f^0_{\boldsymbol{q}} f^0_{\boldsymbol{p}}(f^0_{\boldsymbol{k}}+1). \tag{4.11}$$

By doing the same in the second and third terms in the sum, and then swapping the indices $\boldsymbol{q}$ and $\boldsymbol{p}$ in the term, proportional to $\Phi_{\boldsymbol{p}}$, we get:

$$I^{\boldsymbol{k}}_{\boldsymbol{qp}} = \frac{1}{k_B T}\iint \frac{d\boldsymbol{q}}{(2\pi)^3}\frac{d\boldsymbol{p}}{(2\pi)^3} P^{k}_{\boldsymbol{qp}}\left(\Phi_{\boldsymbol{p}} - \frac{\Phi_{\boldsymbol{k}}}{2}\right). \tag{4.12}$$

Similarly, the term proportional to $\Gamma^{\boldsymbol{kq}}_{\boldsymbol{p}}$ is

$$\begin{aligned} I^{\boldsymbol{kq}}_{\boldsymbol{p}} &= \frac{1}{k_B T}\iint \frac{d\boldsymbol{q}}{(2\pi)^3}\frac{d\boldsymbol{p}}{(2\pi)^3}\Gamma^{\boldsymbol{kp}}_{\boldsymbol{q}}\left[f_{\boldsymbol{q}}(f_{\boldsymbol{p}}+1)(f_{\boldsymbol{k}}+1) - f_{\boldsymbol{k}} f_{\boldsymbol{p}}(f_{\boldsymbol{q}}+1)\right] \\ &= \frac{1}{k_B T}\iint \frac{d\boldsymbol{q}}{(2\pi)^3}\frac{d\boldsymbol{p}}{(2\pi)^3}\left[\Gamma^{\boldsymbol{p}}_{\boldsymbol{kq}}\Phi_{\boldsymbol{p}} f^0_{\boldsymbol{k}} f^0_{\boldsymbol{q}}(f^0_{\boldsymbol{p}}+1) - \Gamma^{\boldsymbol{q}}_{\boldsymbol{kp}}\left(f^0_{\boldsymbol{q}}(f^0_{\boldsymbol{p}}+1)(f^0_{\boldsymbol{k}}+1)\right)(\Phi_{\boldsymbol{k}}+\Phi_{\boldsymbol{p}})\right] \\ &= \frac{1}{k_B T}\iint \frac{d\boldsymbol{q}}{(2\pi)^3}\frac{d\boldsymbol{p}}{(2\pi)^3}\left[\Phi_{\boldsymbol{p}}\left(P^{\boldsymbol{p}}_{\boldsymbol{kq}} - P^{\boldsymbol{q}}_{\boldsymbol{kp}}\right) - \Phi_{\boldsymbol{k}} P^{\boldsymbol{q}}_{\boldsymbol{kp}}\right]. \end{aligned} \tag{4.13}$$

The collision integral at the first order in Φ is then:

$$\left(\frac{\partial f_{\boldsymbol{k}}}{\partial t}\right)_{\text{scatt}} = \frac{1}{k_B T}\iint \frac{d\boldsymbol{q}}{(2\pi)^3}\frac{d\boldsymbol{p}}{(2\pi)^3}\left[\Phi_{\boldsymbol{p}}\left(P^{\boldsymbol{k}}_{\boldsymbol{qp}} + P^{\boldsymbol{p}}_{\boldsymbol{kq}} - P^{\boldsymbol{q}}_{\boldsymbol{kp}}\right) - \Phi_{\boldsymbol{k}}\left(\frac{P^{\boldsymbol{k}}_{\boldsymbol{qp}}}{2} + P^{\boldsymbol{q}}_{\boldsymbol{kp}}\right)\right] \quad (4.14)$$

We can now invert Eq. (4.6) and go back to $\Delta f_{\boldsymbol{k}}$:

$$\left(\frac{\partial f_{\boldsymbol{k}}}{\partial t}\right)_{\text{scatt}} = \iint \frac{d\boldsymbol{q}}{(2\pi)^3}\frac{d\boldsymbol{p}}{(2\pi)^3}\left[\frac{\Delta f_{\boldsymbol{p}}}{f^0_{\boldsymbol{p}}(f^0_{\boldsymbol{p}}+1)}\left(P^{\boldsymbol{k}}_{\boldsymbol{qp}} + P^{\boldsymbol{p}}_{\boldsymbol{kq}} - P^{\boldsymbol{q}}_{\boldsymbol{kp}}\right) - \frac{\Delta f_{\boldsymbol{k}}}{f^0_{\boldsymbol{k}}(f^0_{\boldsymbol{k}}+1)}\left(\frac{P^{\boldsymbol{k}}_{\boldsymbol{qp}}}{2} + P^{\boldsymbol{q}}_{\boldsymbol{kp}}\right)\right]. \quad (4.15)$$

Therefore the collision kernel $\Omega(\boldsymbol{k},\boldsymbol{p})$ that satisfies

$$\left(\frac{\partial f_{\boldsymbol{k}}}{\partial t}\right)_{\text{scatt}} = -\int \frac{d\boldsymbol{p}}{(2\pi)^3}\Omega(\boldsymbol{k},\boldsymbol{p})\Delta f_{\boldsymbol{p}} \quad (4.16)$$

takes the form

$$\Omega(\boldsymbol{k},\boldsymbol{p}) = \int \frac{d\boldsymbol{q}}{(2\pi)^3}\left[-\frac{P^{\boldsymbol{k}}_{\boldsymbol{qp}} + P^{\boldsymbol{p}}_{\boldsymbol{kq}} - P^{\boldsymbol{q}}_{\boldsymbol{kp}}}{f^0_{\boldsymbol{p}}(f^0_{\boldsymbol{p}}+1)} + \int \frac{d\boldsymbol{l}}{(2\pi)^3}(2\pi)^3\delta(\boldsymbol{p}-\boldsymbol{k})\frac{P^{\boldsymbol{q}}_{\boldsymbol{kl}} + P^{\boldsymbol{k}}_{\boldsymbol{ql}}/2}{f^0_{\boldsymbol{p}}(f^0_{\boldsymbol{p}}+1)}\right] \quad (4.17)$$

We discretize the equations on a finite grid with N k-points. We convert the integral to a sum as $\int \frac{d\boldsymbol{p}}{(2\pi)^3} = \frac{1}{NV}\sum_{\boldsymbol{p}}$, with V being the unit cell volume. The δ-function $\delta(k-p)$ is replaced by the Kronecker symbol $\delta_{\boldsymbol{k},\boldsymbol{p}}$ as

$$(2\pi)^3\delta(\boldsymbol{k}-\boldsymbol{p}) \to NV\delta_{\boldsymbol{k},\boldsymbol{p}}. \quad (4.18)$$

The kinetic equation then takes the form:

$$\frac{\partial f_{\boldsymbol{k}}}{\partial t} + \mathbf{v}_{\boldsymbol{k}}\cdot\nabla f_{\boldsymbol{k}} = -\frac{1}{NV}\sum_{\boldsymbol{p}}\Omega_{\boldsymbol{k},\boldsymbol{p}}\Delta f_{\boldsymbol{p}}, \quad (4.19)$$

where $N = \sum_k 1$ and the diagonal terms of the scattering matrix are given by

$$\Omega_{\boldsymbol{k},\boldsymbol{k}} = \frac{1}{NV}\sum_{\boldsymbol{q}}\frac{1}{f^0_{\boldsymbol{k}}(f^0_{\boldsymbol{k}}+1)}\left[\left(P^{\boldsymbol{q}}_{\boldsymbol{kk}} - 2P^{\boldsymbol{k}}_{\boldsymbol{qk}}\right) + \sum_{\boldsymbol{p}}\left(\frac{P^{\boldsymbol{k}}_{\boldsymbol{qp}}}{2} + P^{\boldsymbol{q}}_{\boldsymbol{kp}}\right)\right], \quad (4.20)$$

while the off-diagonal terms are

$$\Omega_{\boldsymbol{kp}} = \frac{1}{NV}\sum_{\boldsymbol{q}}\frac{1}{f^0_{\boldsymbol{p}}(f^0_{\boldsymbol{p}}+1)}\left(P^{\boldsymbol{q}}_{\boldsymbol{kp}} - P^{\boldsymbol{k}}_{\boldsymbol{qp}} - P^{\boldsymbol{p}}_{\boldsymbol{kq}}\right). \quad (4.21)$$

So far, this matrix is nonsymmetric because of the factors in the denominator. Since the next step is to diagonalize it, we perform the transformation [14, 25]

$$\begin{aligned}\tilde{\Omega}_{\boldsymbol{kp}} &= \Omega_{\boldsymbol{kp}}\sqrt{\frac{f^0_{\boldsymbol{p}}(f^0_{\boldsymbol{p}}+1)}{f^0_{\boldsymbol{k}}(f^0_{\boldsymbol{k}}+1)}}\\ \tilde{f}_{\boldsymbol{k}} &= \frac{f_{\boldsymbol{k}}}{\sqrt{f^0_{\boldsymbol{k}}(f^0_{\boldsymbol{k}}+1)}}\end{aligned} \quad (4.22)$$

The new matrix $\tilde{\Omega}_{\boldsymbol{kp}}$ is symmetric,

$$\tilde{\Omega}_{\boldsymbol{kp}} = \tilde{\Omega}_{\boldsymbol{pk}} = \frac{1}{NV}\sum_{\boldsymbol{q}}\frac{\left(P^{\boldsymbol{q}}_{\boldsymbol{kp}} - P^{\boldsymbol{k}}_{\boldsymbol{qp}} - P^{\boldsymbol{p}}_{\boldsymbol{kq}}\right)}{\sqrt{f^0_{\boldsymbol{p}}(f^0_{\boldsymbol{p}}+1)f^0_{\boldsymbol{k}}(f^0_{\boldsymbol{k}}+1)}}, \quad (4.23)$$

and we can proceed with diagonalization.

4.2 Relaxons

In the SMA the off-diagonal elements of the scattering matrix are neglected, and consequently the diagonal ones are the inverse lifetimes of magnons. However, in a spin spiral state we cannot neglect the off-diagonal terms, and three-magnon scattering events must be considered. Analyzing the various contributions to thermal conductivity is convenient in the eigenbasis of the symmetrized scattering matrix [23, 25].

We define the eigenvalues and eigenvectors of $\tilde{\Omega}$ as [25]:

$$\frac{1}{NV}\sum_{\boldsymbol{p}}\tilde{\Omega}_{\boldsymbol{kp}}\theta^{\alpha}_{\boldsymbol{p}} = \frac{1}{\tau_\alpha}\theta^{\alpha}_{\boldsymbol{k}} \tag{4.24}$$

Since $\tilde{\Omega}$ was not diagonal to start with, the eigenvectors θ_α do not represent single magnons, but linear combinations of them. These collective excitations, that we label with α and call relaxons [23], are the heat carriers, and have a well defined relaxation time τ_α. It can be shown that $\frac{1}{\tau_\alpha} > 0$.

The deviation from the equilibrium, $\Delta\tilde{f}_{\boldsymbol{k}}$, can be written in the relaxon basis [23, 25]:

$$\Delta\tilde{f}_{\boldsymbol{k}}(\mathbf{x},t) = \sum_{\alpha}\gamma_\alpha(\mathbf{x},t)\theta^{\alpha}_{\boldsymbol{k}}, \tag{4.25}$$

so that the Boltzmann equation,

$$\frac{\partial\tilde{f}^0_{\boldsymbol{k}}}{\partial T}\left(\frac{\partial T}{\partial t}+\mathbf{v}_{\boldsymbol{k}}\cdot\nabla T\right)+\frac{\partial(\Delta\tilde{f}_{\boldsymbol{k}})}{\partial t}+\mathbf{v}_{\boldsymbol{k}}\cdot\nabla(\Delta\tilde{f}_{\boldsymbol{k}}) = -\frac{1}{NV}\sum_{\boldsymbol{p}}\tilde{\Omega}_{\boldsymbol{kp}}\Delta\tilde{f}_{\boldsymbol{p}}, \tag{4.26}$$

becomes:

$$\frac{\partial\tilde{f}^0_{\boldsymbol{k}}}{\partial T}\left(\frac{\partial T}{\partial t}+\mathbf{v}_{\boldsymbol{k}}\cdot\nabla T\right)+\sum_{\alpha}\left[\frac{\partial\gamma_\alpha}{\partial t}\theta^{\alpha}_{\boldsymbol{k}}+\mathbf{v}_{\boldsymbol{k}}\cdot(\nabla\gamma_\alpha)\theta^{\alpha}_{\boldsymbol{k}}\right] = -\sum_{\alpha}\frac{\gamma_\alpha}{\tau_\alpha}\theta^{\alpha}_{\boldsymbol{p}} \tag{4.27}$$

It is useful to introduce a vector, $\theta^0_{\boldsymbol{k}}$, defined as the linear deviation from equilibrium of $\tilde{f}_{\boldsymbol{k}}{}^0$:

$$\frac{\partial\tilde{f}^0_{\boldsymbol{k}}}{\partial T} = \frac{\sqrt{f^0_{\boldsymbol{k}}\left(f^0_{\boldsymbol{k}}+1\right)}E_{\boldsymbol{k}}}{k_BT^2} \tag{4.28}$$

To normalize it to one, we have to multiply it by $\sqrt{\frac{k_BT^2}{C}}$, with the magnon specific heat C defined as

$$C = \int\frac{d\boldsymbol{k}}{(2\pi)^3}C_{\boldsymbol{k}}, \tag{4.29}$$

where we used the expression for the specific heat Eq. (2.18). We get

$$\theta^0_{\boldsymbol{k}} = \frac{\partial\tilde{f}^0_{\boldsymbol{k}}}{\partial T} = \frac{\sqrt{f^0_{\boldsymbol{k}}\left(f^0_{\boldsymbol{k}}+1\right)}E_{\boldsymbol{k}}}{\sqrt{k_BT^2C}}. \tag{4.30}$$

Using this new vector θ^0 and taking the scalar product with a generic eigenvector $\theta^{\alpha'}$, Eq. (4.27) becomes:

$$\sum_{\boldsymbol{k}}\left[\theta^0_{\boldsymbol{k}}\theta^{\alpha'}_{\boldsymbol{k}}\sqrt{\frac{C}{k_BT^2}}\left(\frac{\partial T}{\partial t}+\mathbf{v}_{\boldsymbol{k}}\cdot\nabla T\right)+\sum_{\alpha}\left(\mathbf{v}_{\boldsymbol{k}}\cdot(\nabla\gamma_\alpha)\theta^{\alpha}_{\boldsymbol{k}}\theta^{\alpha'}_{\boldsymbol{k}}\right)\right]+\frac{\partial\gamma_{\alpha'}}{\partial t} = -\frac{\gamma_{\alpha'}}{\tau_{\alpha'}} \tag{4.31}$$

We introduce two velocities, $\mathbf{V}_{\alpha\alpha'}$ and $\mathbf{V}_\alpha$,

$$\begin{aligned}\mathbf{V}_{\alpha\alpha'} &\equiv \frac{1}{NV}\sum_{\boldsymbol{k}} \theta^\alpha_{\boldsymbol{k}} \mathbf{v}_{\boldsymbol{k}} \theta^{\alpha'}_{\boldsymbol{k}},\\ \mathbf{V}_\alpha &\equiv \frac{1}{NV}\sum_{\boldsymbol{k}} \theta^0_{\boldsymbol{k}} \mathbf{v}_{\boldsymbol{k}} \theta^\alpha_{\boldsymbol{k}}.\end{aligned} \tag{4.32}$$

We will see that, if the temperature perturbation in homogeneous, $\mathbf{V}_\alpha$ can be interpreted as a relaxon velocity. The Boltzmann equation becomes:

$$\sqrt{\frac{C}{k_B T^2}}\left(\sum_{\boldsymbol{k}} \theta^0_{\boldsymbol{k}}\theta^{\alpha'}_{\boldsymbol{k}}\frac{\partial T}{\partial t} + \mathbf{V}_{\alpha'}\cdot\nabla T\right) + \sum_\alpha \mathbf{V}_{\alpha\alpha'}\cdot(\nabla\gamma_\alpha)\theta^\alpha_{\boldsymbol{k}}\theta^{\alpha'}_{\boldsymbol{k}} + \frac{\partial\gamma_{\alpha'}}{\partial t} = -\frac{\gamma_{\alpha'}}{\tau_{\alpha'}}. \tag{4.33}$$

Note that different relaxons are only coupled through the matrix $\mathbf{V}_{\alpha\alpha'}$. However, since the system we are studying is infinite, if the temperature perturbation is homogeneous, the response of the system will not depend on space, $\nabla\gamma_\alpha = 0$. Under this condition, both the left and the right hand sides of this equation are diagonal in α, and $\boldsymbol{V}_\alpha$ represents the velocity of the heat carriers α:

$$\sqrt{\frac{C}{k_B T^2}}\left(\sum_{\boldsymbol{k}} \theta^0_{\boldsymbol{k}}\theta^{\alpha}_{\boldsymbol{k}}\frac{\partial T}{\partial t} + \mathbf{V}_{\alpha}\cdot\nabla T\right) + \frac{\partial\gamma_{\alpha}}{\partial t} = -\frac{\gamma_{\alpha}}{\tau_{\alpha}}. \tag{4.34}$$

The equation simplifies further if we consider a steady state and set time derivatives to zero:

$$\sqrt{\frac{C}{k_B T^2}}\mathbf{V}_\alpha\cdot\nabla T = -\frac{\gamma_\alpha}{\tau_\alpha}. \tag{4.35}$$

Expanding for small deviations from equilibrium,

$$\gamma_\alpha = \sum_i \xi^i_\alpha \nabla_i T, \tag{4.36}$$

where i is a Cartesian index, and Eq. (4.35) becomes:

$$\sqrt{\frac{C}{k_B T^2}}V^i_\alpha = -\frac{\xi^i_\alpha}{\tau_\alpha}. \tag{4.37}$$

Finally, we can find an expression for the thermal conductivity κ_{ij}: we start from its definition as a proportionality coefficient between the temperature gradient and heat flux,

$$-\frac{1}{NV}\sum_{\boldsymbol{k}} E_{\boldsymbol{k}} v^i_{\boldsymbol{k}} \Delta f_{\boldsymbol{k}} = \sum_j \kappa_{ij}\nabla_j T \tag{4.38}$$

Using the relation (4.25) between $\Delta\tilde{f}_{\boldsymbol{k}}$ and $\theta^\alpha_{\boldsymbol{k}}$, and the transformation (4.22) from $\Delta f_{\boldsymbol{k}}$ to $\Delta\tilde{f}_{\boldsymbol{k}}$,

$$\Delta f_{\boldsymbol{k}} = \sum_\alpha \sqrt{f^0_{\boldsymbol{k}}(f^0_{\boldsymbol{k}}+1)}\gamma_\alpha(\mathbf{x},t)\theta^\alpha_{\boldsymbol{k}} \tag{4.39}$$

Substituting Eq. (4.36), Eq. (4.37), we obtain:

$$\Delta f_{\boldsymbol{k}} = \sum_\alpha \sqrt{f^0_{\boldsymbol{k}}(f^0_{\boldsymbol{k}}+1)}\sum_i \xi^i_\alpha \nabla_i T\theta^\alpha_{\boldsymbol{k}} = -\sum_\alpha \sqrt{f^0_{\boldsymbol{k}}(f^0_{\boldsymbol{k}}+1)}\sum_l \sqrt{\frac{C}{k_B T^2}}V^l_\alpha \tau_\alpha \nabla_l T\theta^\alpha_{\boldsymbol{k}}, \tag{4.40}$$

and, finally, substituting $\Delta f_{\boldsymbol{k}}$ here, we find

$$\begin{aligned}\kappa_{ij} &= \frac{1}{NV}\frac{\partial}{\partial \nabla_j T}\sum_{\boldsymbol{k}} E_{\boldsymbol{k}} v^i_{\boldsymbol{k}} \sum_{\alpha} \sqrt{f^0_{\boldsymbol{k}}(f^0_{\boldsymbol{k}}+1)} \sum_{l} \sqrt{\frac{C}{k_B T^2}} V^l_\alpha \tau_\alpha \nabla_l T \theta^\alpha_{\boldsymbol{k}} \\ &= C \sum_\alpha V^i_\alpha V^j_\alpha \tau_\alpha,\end{aligned} \tag{4.41}$$

which allows to compute the thermal conductivity from the kinetic equation with the full scattering matrix. We note that the contribution of every relaxon involves the total specific heat from all magnon modes.

Chapter 5

Results

To obtain numerical results, we implemented the theoretical approach, developed here, in the Mathematica code listed in Appendix A. Due to limitations on performance and on the number of simultaneously running Mathematica kernels, we followed up by porting the program to C++ and used OpenMP for parallelization. We have verified that the two programs give identical results for small k-grid sizes. For a given k grid, the program fills the collision matrix with the diagonal (4.20) and off-diagonal elements (4.21), transformed with (4.22) so that it is symmetric. Then, it diagonalizes the matrix. Once we have

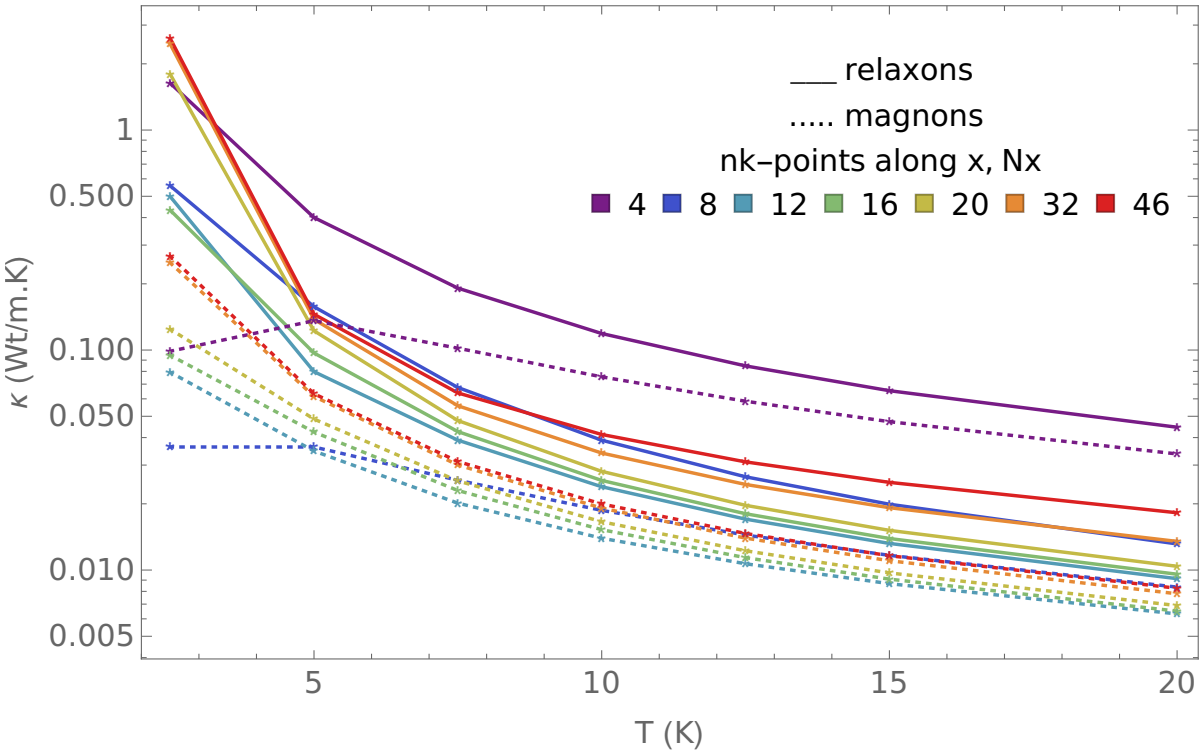

Figure 5.1: Temperature dependence of the thermal conductivity in a quasi-one dimensional model with spin spiral ordering, with spiral pitch $Q = \frac{2\pi}{5}$ and easy plane anisotropy $\Delta = 0.1$ meV. Colors indicate the results for different k-grids, $N_x \times 4 \times 4$, with N_x corresponding to each curve indicated in the legend. Solid lines correspond to the complete scattering matrix (relaxons), while the dashed lines are computed in a single magnon mode approximation (only diagonal elements). Thermal conductivity computed with the complete scattering matrix is higher than that computed in a single mode approximation.

eigenvectors and eigenvalues, it is easy to compute thermal conductivity using Eq. (4.41).

We run the code for different temperatures, k-grids and spiral pitches Q, using the scripts, listed in Appendix A. The results for $Q = 2\pi/5$ (period 5) and $\Delta = 0.1$ meV are summarized in the Figures 5.1–5.14. Thermal conductivity as a function of temperature for different k-grids (represented by different colors) is reported in Fig. (5.1). We compute it both in the relaxon picture (solid lines), with the complete scattering matrix, and in the single mode approximation (dashed lines), with only diagonal elements.

We find a significant difference between the magnon and relaxon-based calculations of thermal conductivity. The thermal conductivity, computed with the complete scattering matrix is always higher than in the single mode approximation. Therefore, single-mode approximation to the kinetic equation is insufficient for short spiral periods.

The parallel version of the code allowed us to preform calculations for dense k-grids. The dependence of the thermal conductivity on the inverse grid size is shown in Fig. 5.2 and Fig. 5.3. We see that the convergence requires a dense grid, which is a consequence of the rich structure of the scattering matrix, as seen in Fig. 5.15. We generally find that the finite size scaling plots become linear at $L_x = 20 \dots 30$.

Relaxon formalism allows to study individual contributions to the thermal conductivity. Figures 5.11–5.14 show contributions of relaxons and magnons κ_i/κ. A few relaxons with the longest relaxation time and velocity account for the significant part of the thermal conductivity. That qualitative conclusion also holds for calculations at higher temperatures, although our low-order $1/S$ expansion is only expected to work at temperatures well below the ordering transition. In the mean-field approximation the ordering temperature can be estimated as $T_c = \frac{1}{4} k_{\mathrm{B}} S(S+1)(2J_1 \cos Q + 2J_2 \cos 2Q + 2J_3 + 2J_4) \approx 16$ K for $Q = 2\pi/5, S = 1, J_2 = 1$ meV.

The variation of magnon occupations, corresponding to relaxons that give the largest contributions to the thermal conductivity, is shown in Fig. 5.5 and Fig. 5.6. They contribute 38% and 24% of thermal conductivity, respectively. It is apparent that these relaxons are odd, that is, the occupation change satisfies the condition $\theta_{\boldsymbol{k}} = -\theta_{-\boldsymbol{k}}$. Even relaxons, that satisfy $\theta_{\boldsymbol{k}} = \theta_{-\boldsymbol{k}}$, describe same positive changes of magnon occupations for both $+\boldsymbol{k}$ and $-\boldsymbol{k}$, and therefore have zero velocity, $\mathbf{V}_\alpha = 0$, and do not contribute to the thermal conductivity. An example of such a relaxon is shown in Fig. 5.9.

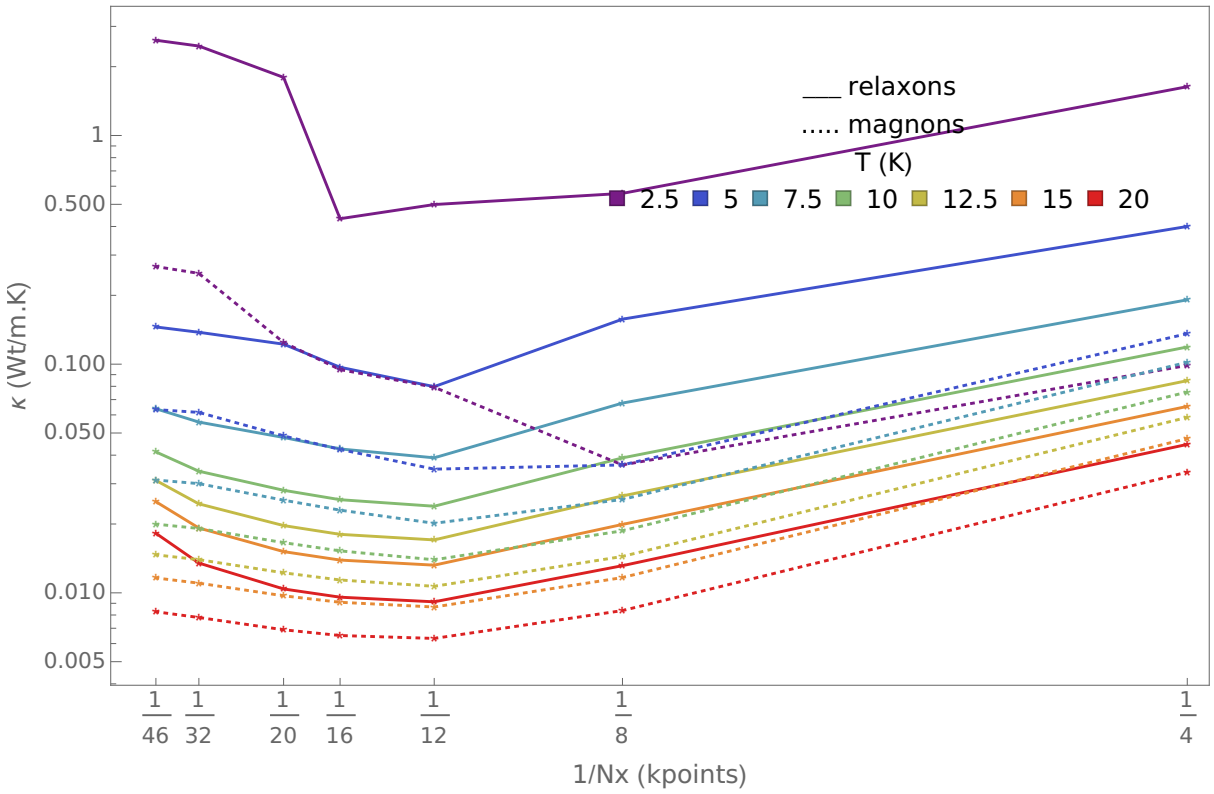

Figure 5.2: Finite grid size scaling of computed thermal conductivity, $\log \kappa(1/N_x)$, in a quasi-one dimensional model with spin spiral ordering, with spiral pitch $Q = \frac{2\pi}{5}$ and easy plane anisotropy $\Delta = 0.1$ meV. The k-grid used is $N_x \times 4 \times 4$, with $1/N_x$ on the horizontal axis. Curves of different colors correspond to different temperatures, as indicated in the legend. Solid lines correspond to the complete scattering matrix (relaxons), while the dashed lines are computed in a single magnon mode approximation (only diagonal elements). Convergence is seen towards $N_x = 46$. At higher temperatures our $1/S$ expansion becomes less precise.

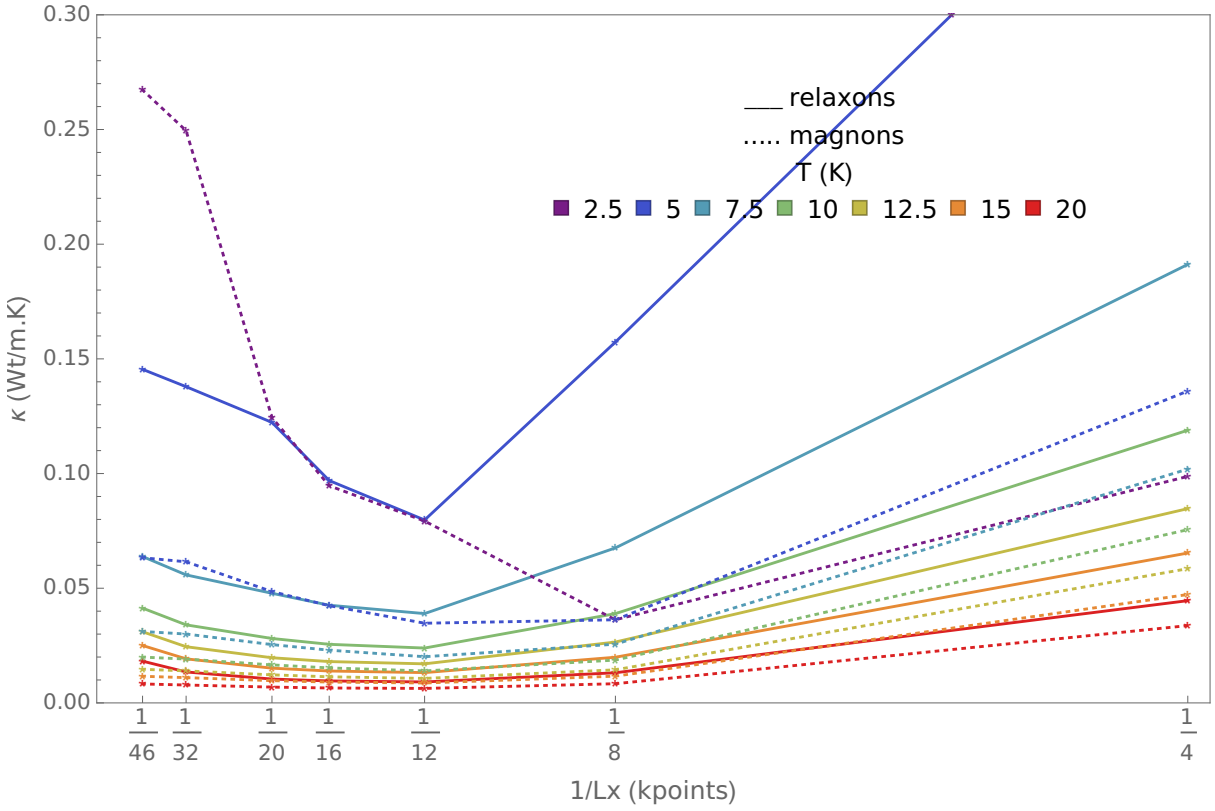

Figure 5.3: Finite grid size scaling of computed thermal conductivity, $\kappa(1/N_x)$, in a quasi-one dimensional model with spin spiral ordering, with spiral pitch $Q = \frac{2\pi}{5}$ and easy plane anisotropy $\Delta = 0.1$ meV. The k-grid used is $N_x \times 4 \times 4$, with $1/N_x$ on the horizontal axis. Curves of different colors correspond to different temperatures, as indicated in the legend. Solid lines correspond to the complete scattering matrix (relaxons), while the dashed lines are computed in a single magnon mode approximation (only diagonal elements). Convergence is seen towards $N_x = 46$. At higher temperatures our $1/S$ expansion becomes less precise.

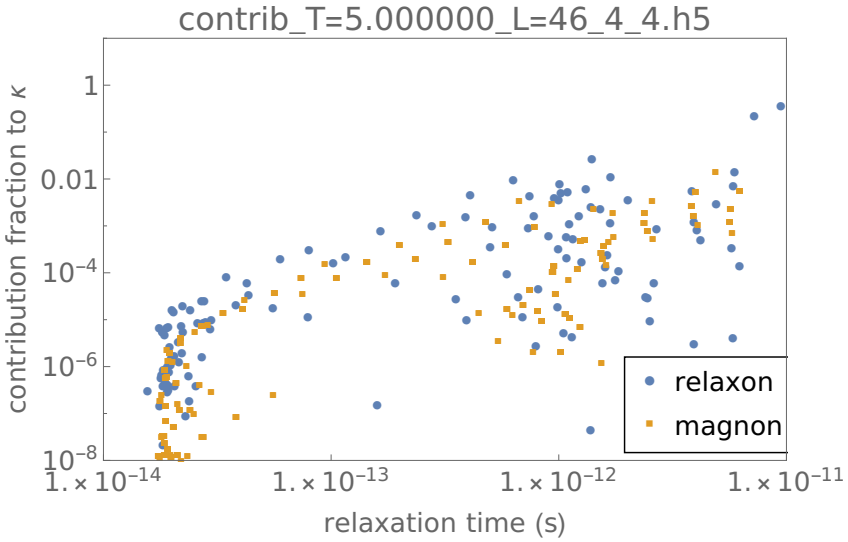

Figure 5.4: Contribution fractions $\kappa_i/\kappa_{\text{tot}}$ of relaxons (blue dots) and magnons (yellow dots) to the thermal conductivity plotted against their relaxation time. The calculations are performed in a quasi-one dimensional model with spin spiral ordering, with spiral pitch $Q = \frac{2\pi}{5}$ and easy plane anisotropy $\Delta = 0.1$ meV, for $T = 5$ K, and using the k-grid of $46 \times 4 \times 4$. Relaxon contributions are seen to exceed those of magnons.

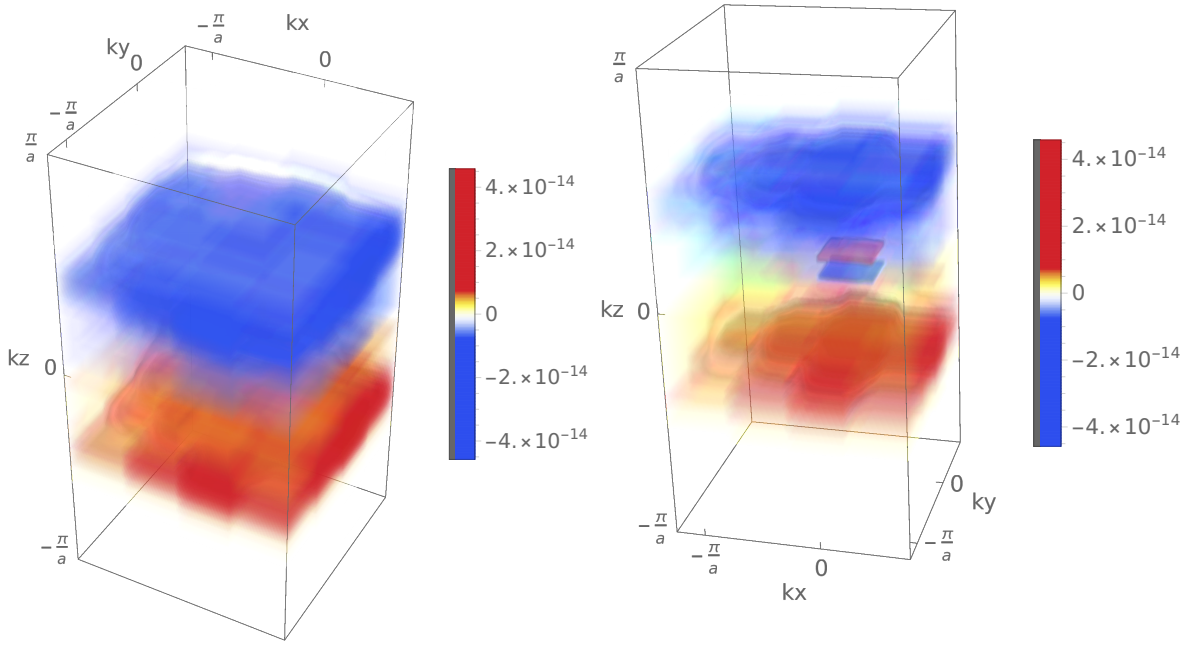

Figure 5.5: The wave function of the relaxon with the largest contribution to the thermal conductivity (38%). The colors for each pixel (k_x, k_y, k_z) encode the change of the occupation of individual magnons (k_x, k_y, k_z), as indicated by the legend. The calculations are performed in a 3D model with spin spiral ordering, with spiral pitch $Q = \frac{2\pi}{5}$ and easy plane anisotropy $\Delta = 0.1$ meV, for $T = 5$ K, and using the k-grid of $46 \times 4 \times 4$. The lifetime of the relaxon is 9.4 ps.

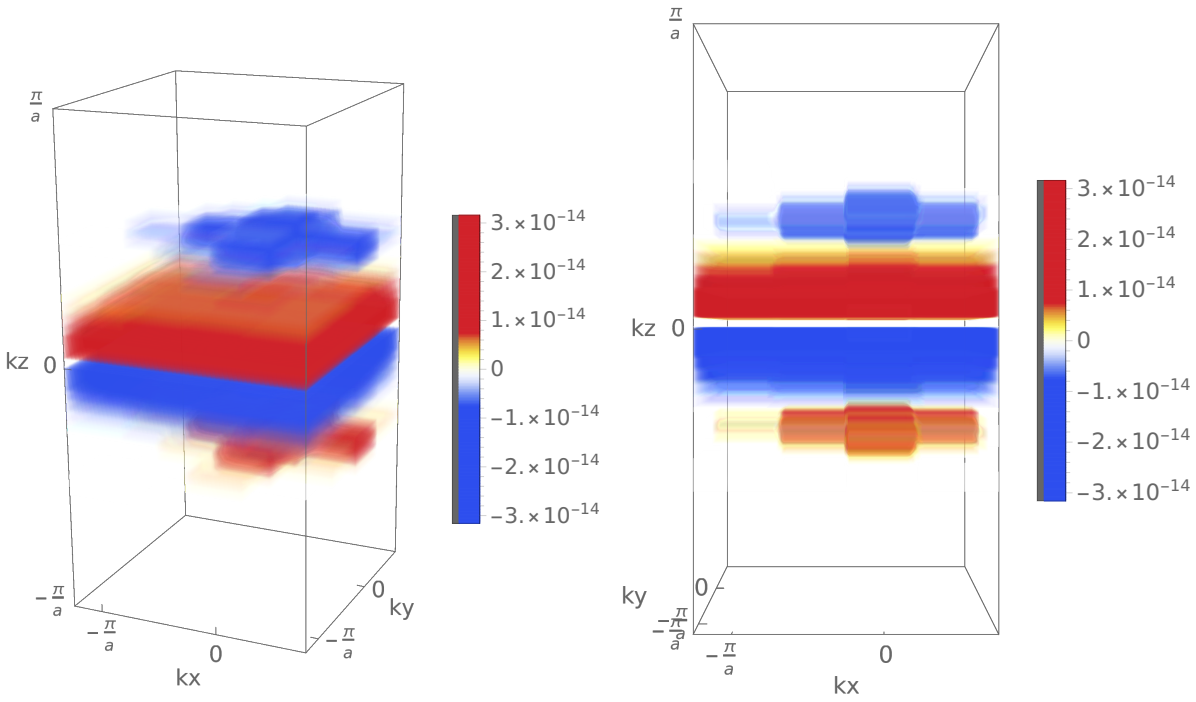

Figure 5.6: The wave function of the relaxon with the second largest contribution to the thermal conductivity (24%). The colors for each pixel (k_x, k_y, k_z) encode the change of the occupation of individual magnons (k_x, k_y, k_z), as indicated by the legend. The calculations are performed in a 3D model with spin spiral ordering, with spiral pitch $Q = \frac{2\pi}{5}$ and easy plane anisotropy $\Delta = 0.1$ meV, for $T = 5$ K, and using the k-grid of $46 \times 4 \times 4$. The lifetime of the relaxon is 7 ps.

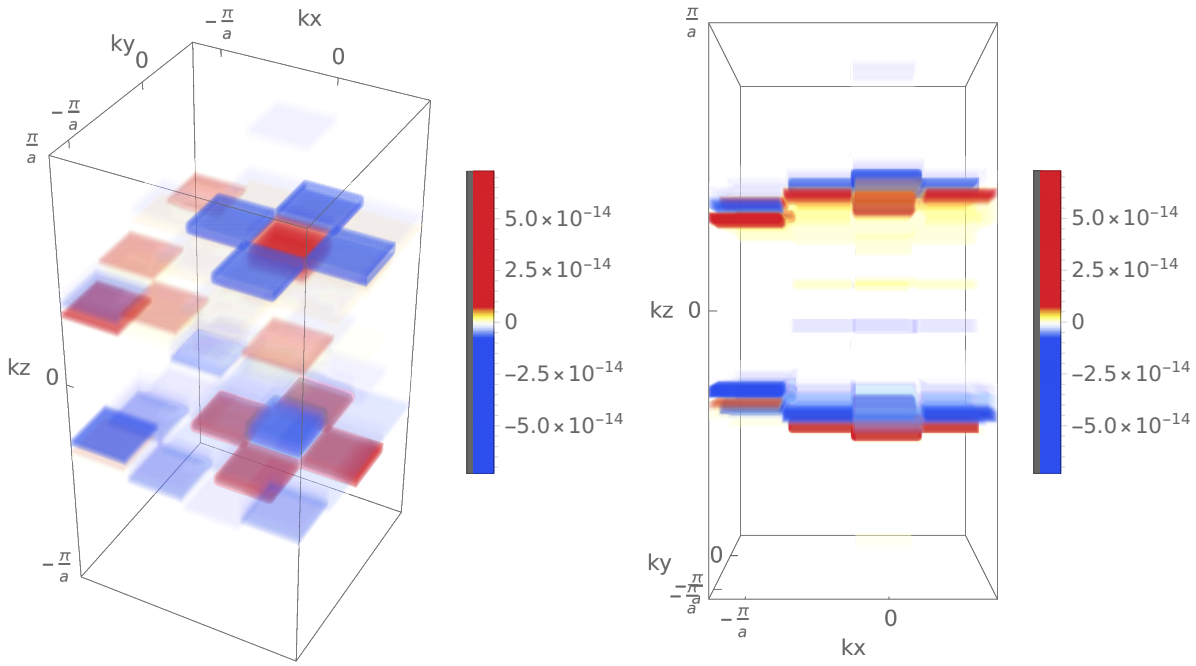

Figure 5.7: The wave function of the relaxon with the seventh largest contribution to the thermal conductivity (1%). The colors for each pixel (k_x, k_y, k_z) encode the change of the occupation of individual magnons (k_x, k_y, k_z), as indicated by the legend. The calculations are performed in a 3D model with spin spiral ordering, with spiral pitch $Q = \frac{2\pi}{5}$ and easy plane anisotropy $\Delta = 0.1$ meV, for $T = 5$ K, and using the k-grid of $46 \times 4 \times 4$. The lifetime of the relaxon is 0.6 ps.

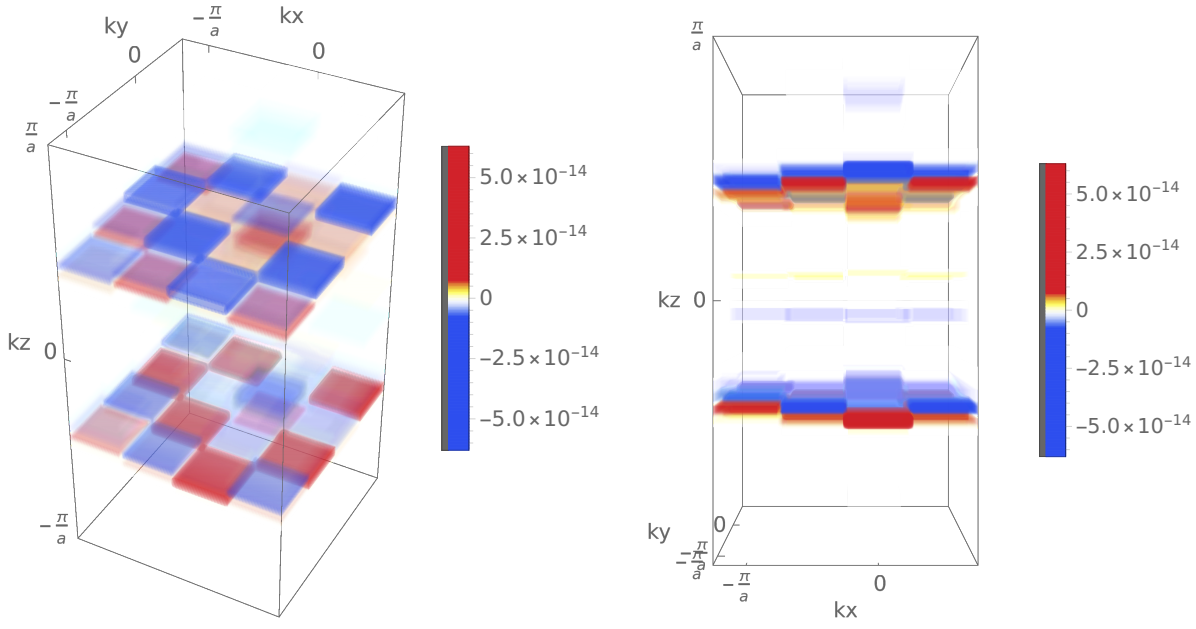

Figure 5.8: The wave function of the relaxon with the eights largest contribution to the thermal conductivity (0.4%). The colors for each pixel (k_x, k_y, k_z) encode the change of the occupation of individual magnons (k_x, k_y, k_z), as indicated by the legend. The calculations are performed in a 3D model with spin spiral ordering, with spiral pitch $Q = \frac{2\pi}{5}$ and easy plane anisotropy $\Delta = 0.1$ meV, for $T = 5$ K, and using the k-grid of $46 \times 4 \times 4$. The lifetime of the relaxon is 0.4 ps.

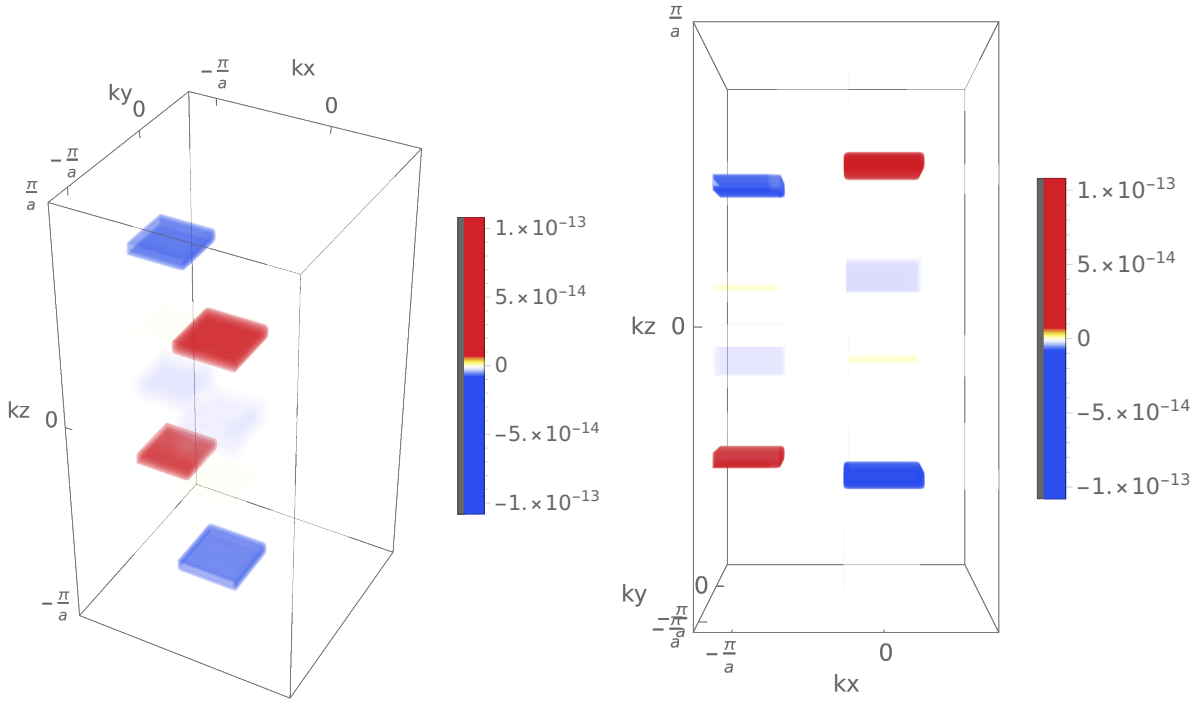

Figure 5.9: The wave function of the least contributing relaxon (0%). The colors for each pixel (k_x, k_y, k_z) encode the change of the occupation of individual magnons (k_x, k_y, k_z), as indicated by the legend. The calculations are performed in a 3D model with spin spiral ordering, with spiral pitch $Q = \frac{2\pi}{5}$ and easy plane anisotropy $\Delta = 0.1$ meV, for $T = 5$ K, and using the k-grid of $46 \times 4 \times 4$. The lifetime of the relaxon is 0.16 ps.

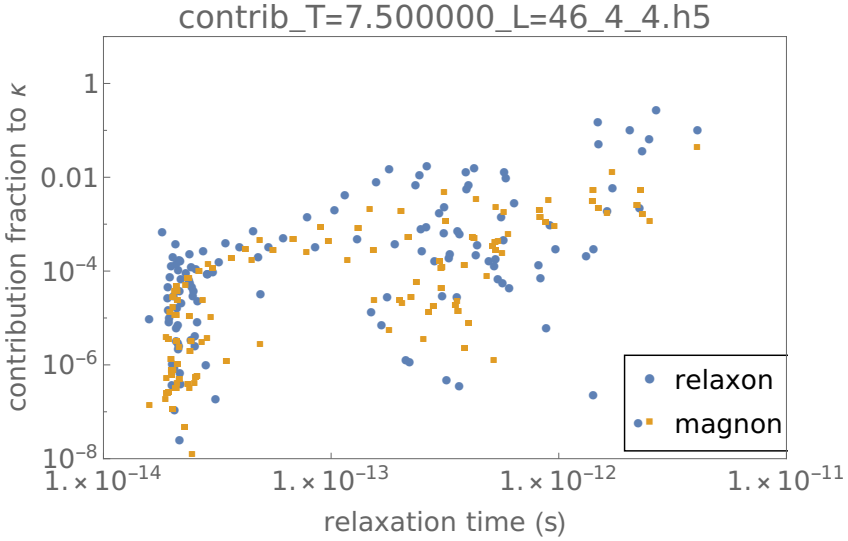

Figure 5.10: Contribution fractions $\kappa_i/\kappa_{\text{tot}}$ of relaxons (blue dots) and magnons (yellow dots) to the thermal conductivity plotted against their relaxation time. The calculations are performed in a quasi-one dimensional model with spin spiral ordering, with spiral pitch $Q = \frac{2\pi}{5}$ and easy plane anisotropy $\Delta = 0.1$ meV, for $T = 7.5$ K and using the k-grid of $46 \times 4 \times 4$. Relaxon contributions are seen to exceed those of magnons.

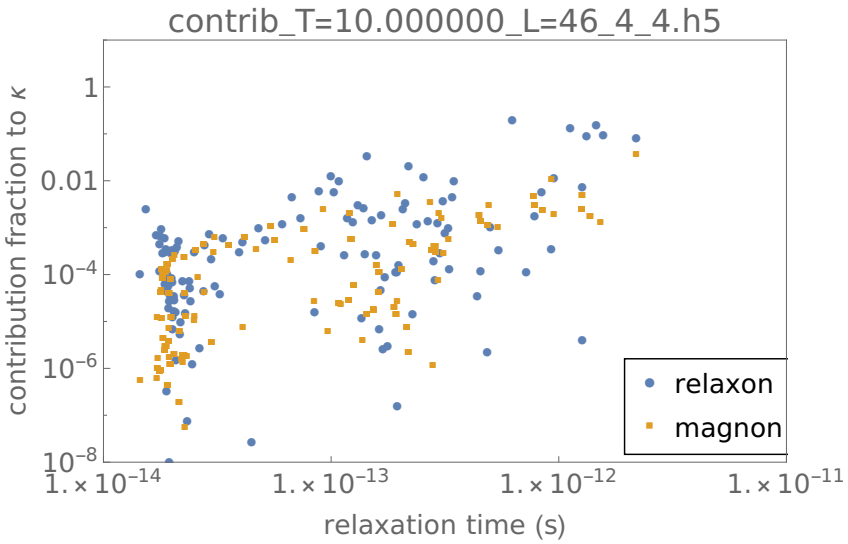

Figure 5.11: Contribution fractions $\kappa_i/\kappa_{\text{tot}}$ of relaxons (blue dots) and magnons (yellow dots) to the thermal conductivity plotted against their relaxation time. The calculations are performed in a quasi-one dimensional model with spin spiral ordering, with spiral pitch $Q = \frac{2\pi}{5}$ and easy plane anisotropy $\Delta = 0.1$ meV, for $T = 10$ K, and using the k-grid of $46 \times 4 \times 4$. Relaxon contributions are seen to exceed those of magnons.

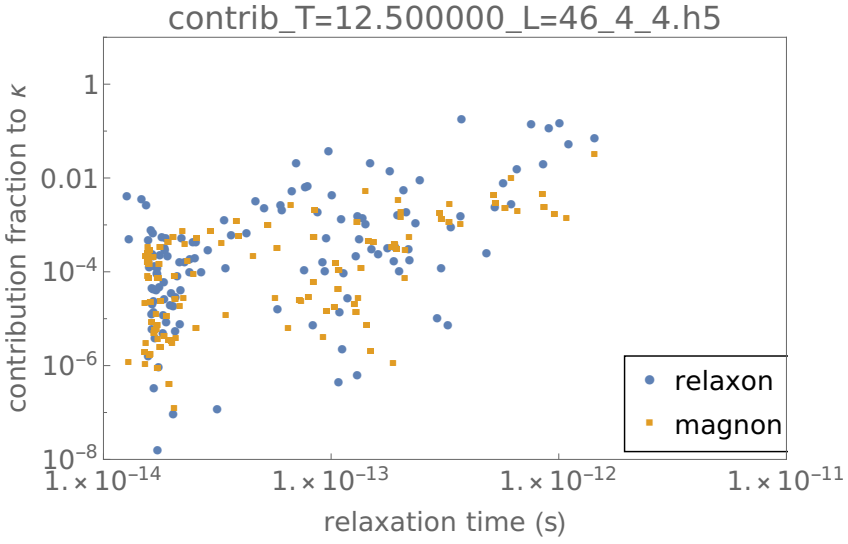

Figure 5.12: Contribution fractions $\kappa_i/\kappa_{\text{tot}}$ of relaxons (blue dots) and magnons (yellow dots) to the thermal conductivity plotted against their relaxation time. The calculations are performed in a quasi-one dimensional model with spin spiral ordering, with spiral pitch $Q = \frac{2\pi}{5}$ and easy plane anisotropy $\Delta = 0.1$ meV, for $T = 12.5$ K, and using the k-grid of $46 \times 4 \times 4$. Relaxon contributions are seen to exceed those of magnons.

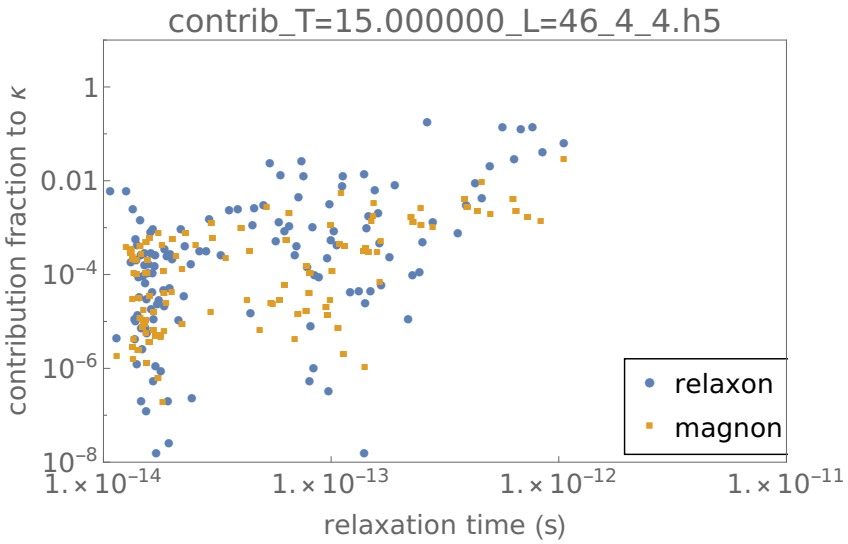

Figure 5.13: Contribution fractions $\kappa_i/\kappa_{\text{tot}}$ of relaxons (blue dots) and magnons (yellow dots) to the thermal conductivity plotted against their relaxation time. The calculations are performed in a quasi-one dimensional model with spin spiral ordering, with spiral pitch $Q = \frac{2\pi}{5}$ and easy plane anisotropy $\Delta = 0.1$ meV, for $T = 15$ K, and using the k-grid of $46 \times 4 \times 4$. Relaxon contributions are seen to exceed those of magnons.

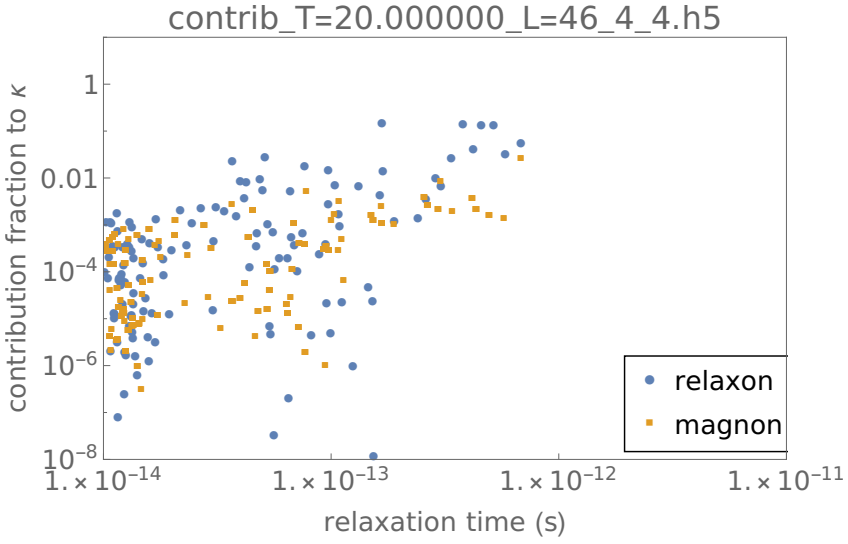

Figure 5.14: Contribution fractions $\kappa_i/\kappa_{\text{tot}}$ of relaxons (blue dots) and magnons (yellow dots) to the thermal conductivity plotted against their relaxation time. The calculations are performed in a quasi-one dimensional model with spin spiral ordering, with spiral pitch $Q = \frac{2\pi}{5}$ and easy plane anisotropy $\Delta = 0.1$ meV, for $T = 20$ K, and using the k-grid of $46 \times 4 \times 4$. Relaxon contributions are seen to exceed those of magnons.

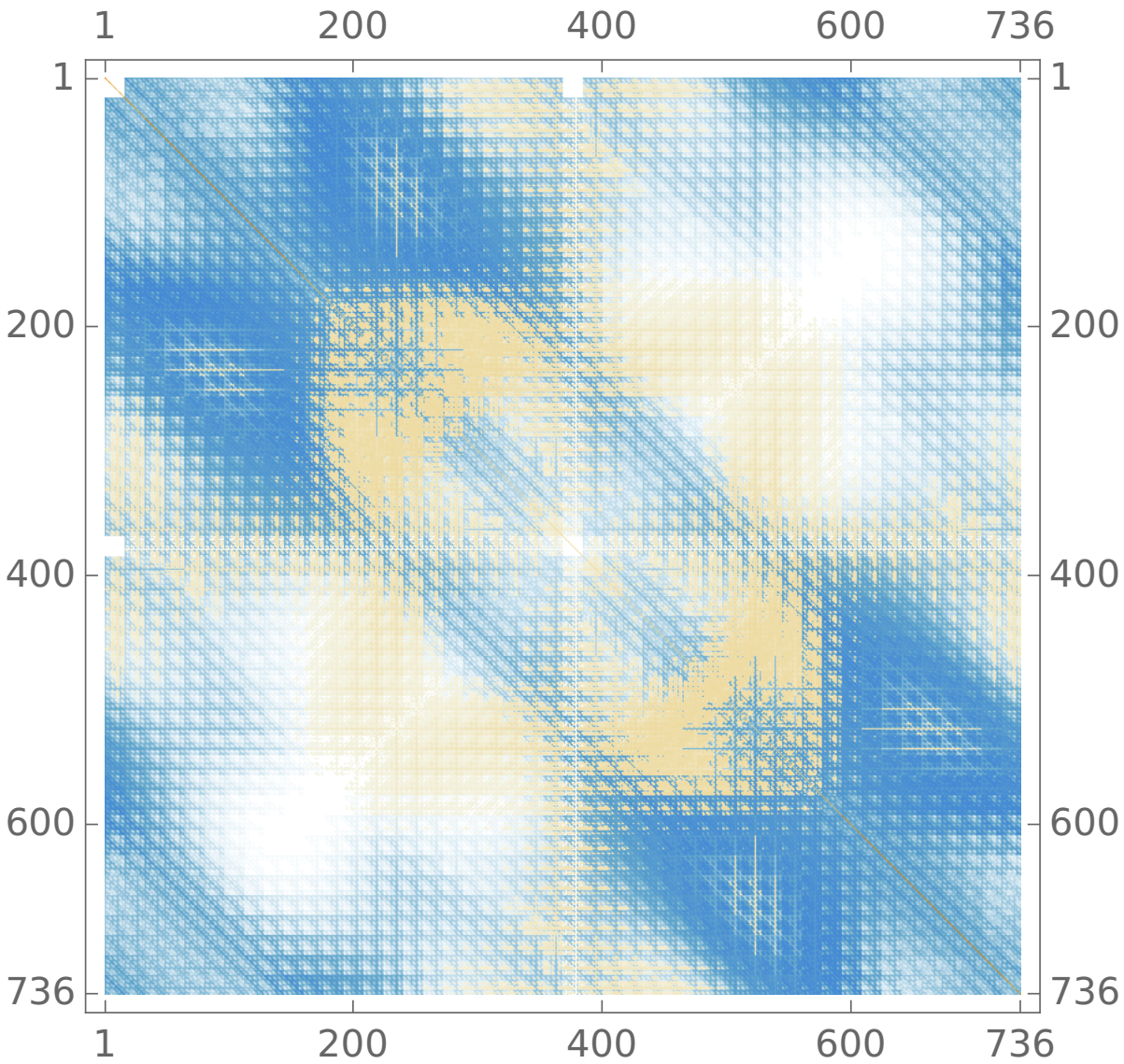

Figure 5.15: The plot of a scattering matrix used in the calculation of thermal conductivity for the k-grid $46 \times 4 \times 4$ for a spiral with $Q = 2\pi/5$ at $T = 5$ K. The matrix was flattened. The yellow shades represent positive matrix elements, while the blue – negative. The rich structure justifies the need for dense reciprocal space grids.

5.1 Conclusions

In this work we have developed the scheme to compute thermal conductivity in spiral magnets, which are the most basic non-collinear spin systems. We have seen that the spin non-collinearity leads to three-magnon scattering events and therefore limits the magnon mean free path. However, considering magnons as heat carriers is a poor approximation – full solution of Boltzmann equation gives much larger thermal conductivity than the single-mode approximation for magnons, since sets of magnons diagonalizing the collision matrix describe energy transport and relaxation. Their relaxation time is much longer than the scattering time for magnons. Hence using the magnon scattering time as energy relaxation time, as done in the single mode approximation, leads to an underestimation of thermal conductivity. This tells us that it is more precise to consider linear combinations of magnons, diagonalizing the scattering matrix – relaxons – as the heat carriers.

The approach can be extended to other important non-collinear spin textures, such as domain walls and even skyrmions, topological spin textures that are proposed as an essential ingredient of race-track memories and skyrmion-based logic devices. Realistic spin textures always involve domain walls, that may scatter magnons. Hence, analyzing their role is important for thermal transport modelling in real systems. The possibility of thermal current, induced perpendicular to the temperature gradient ("Thermal Hall effect"), can also be studied.

I would like to thank Dr. Foggetti and Prof. Mostovoy who I learned a lot from for illuminating discussions.

Appendix A

C++/OpenMP code

The code is launched with the following command line arguments:

```
./magcond.x T Lx Ly Lz Qx A
```

where T is the temperature in Kelvin; Lx Ly Lz define a reciprocal space grid with L_x, L_y, L_z points along the three directions; Qx is the spiral wave vector Q_x, equal to the rotation angle between the nearest spins in radians; A is the easy plane anisotropy in meV.

The code uses relaxon formalism and saves the results in HDF5 format appending the temperature and grid parameters to the file names:

1. `M_T=10.000000_L=46_4_4.h5` – scattering matrix
2. `Mph_T=10.000000_L=46_4_4.h5` – scattering matrix in SMA
3. `thetak_T=10.000000_L=46_4_4.h5` – relaxon wave functions
4. `contrib_T=10.000000_L=46_4_4.h5` – relaxon contributions to the thermal conductivity, records {lifetime (sec), $\kappa_i/\kappa_{\text{tot}}$}
5. `contribph_T=10.000000_L=46_4_4.h5` – fraction of thermal conductivity due to individual phonons, records {lifetime (sec), $\kappa_i/\kappa_{\text{tot}}$}
6. `slurm-242420.out` – standard output contains the computed values of thermal conductivity, specific heat as well as other information

```
1  #include <cstdio>
2  #include <cstdlib>
3  #include <cmath>
4  #include <complex>
5  const std::complex<double> I(0.,1.);
6  #include "omp.h"
7  #include "err.h"
8
9  #include <iostream>
10 #include <iomanip>
11 #include <armadillo>
12
```

```
13 #include <boost/program_options.hpp>
14 #include <vector>
15
16 using namespace std;
17 using namespace arma;
18
19 #define ARMA_NO_DEBUG
20 ivec L({2,2,2});
21 vec sigmak;
22 vec Q({0, 0, 0});
23
24 double j2 = 1., J1 = -4.*j2*cos(Q(0)), j3 = -0.1, j4 = ↩
      -0.1, epa = 0.1, hbar = 1.E-34, T;
25 double a=4E-10, eps0;
26 vec vmax=vec({0., 0., 0.});
27
28 inline double sqr(double x)
29 { return x*x; }
30
31 inline double funA(const vec& k) {
32    return 2*(J1*cos(k(0))*(cos(Q(0)) + 1) + j2*cos(2*k(0))↩
         *(cos(2*Q(0)) + 1) -
33          2*(J1*cos(Q(0)) + j2*cos(2*Q(0))) + 2*j3*cos(k(1))↩
               +
34          2*j4*cos(k(2)) - 2*j3 - 2*j4) + epa;
35 }
36
37 inline double funB(const vec& k) {
38    return -(2*(J1*cos(k(0))*(cos(Q(0)) - 1) + j2*cos(2*k(0)↩
         )*(cos(2*Q(0)) - 1)) - epa);
39 }
40
41 //dispersion relation
42 inline double epsilon(const vec& k) {
43    if (dot(k,k)>0.01/L.max())
44       return sqrt( sqr(funA(k)) - sqr(funB(k)) )/2;
45    else return eps0;
46 }
47
48 //converts grid index to momentum
49 inline double momx(int xi) { return (xi*2*M_PI/L(0) - M_PI)↩
      ; }
50 inline double momy(int xi) { return (xi*2*M_PI/L(1) - M_PI)↩
      ; }
51 inline double momz(int xi) { return (xi*2*M_PI/L(2) - M_PI)↩
      ; }
52
53 //Bose-Einstein distribution
```

```
54 inline double BE(const vec& k) { return 1./(exp(11.6*↩
     epsilon(k)/T)-1); } //1meV/kb Kelvin=11.6
55
56 vec k0;
57
58 //coefficients of the Bogoliubov transformation
59 inline double theta(const vec& k) {
60    if (abs(funB(k)/funA(k))<1) return atanh(funB(k)/funA(k)↩
        )/2;
61    else return 0;
62 }
63
64 inline double beta(const vec& k) {
65    return J1*sin(Q(0))*sin(k(0)) + j2*sin(2*Q(0))*sin(2*k↩
        (0));
66 }
67
68 inline double ch(const vec& k) { return cosh(theta(k)); }
69 inline double sh(const vec& k) { return sinh(theta(k)); }
70
71 inline double funC(const vec& k, const vec& q) {
72    return beta(q)*(ch(q) + sh(q))*(ch(k - q)*ch(k) + sh(k)*↩
        sh(k - q)) +
73           beta(k - q)* (ch(k - q) + sh(k - q))*(ch(k)*ch(q) ↩
              + sh(k)*sh(q)) -
74           beta(k)*(sh(k) + ch(k))*(ch(q)*sh(k - q) + sh(q)*↩
              ch(k - q));
75 }
76
77 static double normk, sigmaE;
78 size_t nveck;
79 mat veck;
80
81 //transition rates computed with Fermi Golden Rule
82 //2 Pi (meV)^2/hbar=1.529E-9 s^-1
83 //meV/hbar=1.519E12 s^-1
84 inline double P21(const vec& k1, const vec& k2, const vec& ↩
     k3) {
85    //    double k4c=(exp(-0.5*(sqr(k3(0) - (fmod(k1(0) + k2↩
        (0) +3* M_PI, 2*M_PI) - M_PI))/sqr(sigmak(0))+
86    //                    sqr(k3(1) - (fmod(k1(1) + k2(1) ↩
        +3* M_PI, 2*M_PI) - M_PI))/sqr(sigmak(1))+
87    //                sqr(k3(2) - (fmod(k1(2) + k2(2) +3* ↩
        M_PI, 2*M_PI) - M_PI))/sqr(sigmak(2))))/normk);
88    double k4c= arma::approx_equal(k3, vec({fmod(k1(0) + k2↩
        (0) +3* M_PI, 2*M_PI) - M_PI,
89       fmod(k1(1) + k2(1) +3* M_PI, 2*M_PI) - M_PI,
90       fmod(k1(2) + k2(2) +3* M_PI, 2*M_PI) - M_PI}), "↩
```

```
          absdiff", 0.01/L.max());
91    if (!arma::approx_equal(k1, k2, "absdiff", 0.01/L.max())↩
        )
92       return 1.529E-9*sqr(2*(funC(k3, k1) + funC(k3, k2)))*
93             (BE(k1)*BE(k2)*(BE(k3) + 1.)) *
94             exp(-0.5*sqr(1.519E12*(epsilon(k3) - epsilon(k1↩
                 ) - epsilon(k2))/sigmaE))/
95             (sqrt(2*M_PI)*sigmaE*hbar) * k4c;
96    else return 1.529E-9*sqr(2*sqrt(2)*funC(k3, k1))*
97          (BE(k1)*BE(k2)*(BE(k3) + 1.))*
98          exp(-0.5*sqr(1.519E12*(epsilon(k3) - epsilon(k1) -↩
                epsilon(k2))/sigmaE))/
99          (sqrt(2*M_PI)*sigmaE*hbar) * k4c;
100 }
101
102 // specific heat per magnon
103 inline double cimu(const vec& k)
104 { return (BE(k)*(BE(k) + 1.)*sqr(epsilon(k))*134.7/sqr(T));↩
     }
105 //(meV)^2/((1K)^2*Boltzmann constant)=134.7 Boltzmann ↩
    constants
106 //meV*4 Angstrom/hbar=607.7 m/s
107
108 //magnon velocity (computed in Mathematica)
109 inline vec vmagnon(const vec& k) {
110    if (dot(k,k)>0.01/L.max()) return a*607.7/(4.E-10)*vec↩
       ({(-4*(J1 + cos(Q(0))*(J1 + 8*j2*cos(k(0))*cos(Q(0)))↩
       )*
111          (epa - 4*(j3 + j4) + 4*j3*cos(k(1)) + 4*j4*cos(k↩
             (2)) + 2*J1*cos(k(0))*(1 + cos(Q(0))) -
112             4*(cos(Q(0))*(J1 - j2*cos(2*k(0))*cos(Q(0)))↩
                  + j2*cos(2*Q(0))))*sin(k(0)) -
113             4*sin(k(0))*(J1 - J1*cos(Q(0)) + 8*j2*cos(k↩
                (0))*sqr(sin(Q(0))))*
114             (-epa + 2*J1*cos(k(0))*(-1 + cos(Q(0))) - 4*↩
                  j2*cos(2*k(0))*sqr(sin(Q(0)))))/
115       (8.*sqrt(2)*sqrt((epa - 2*(j3 + j4) + 2*J1*cos(k(0)) ↩
          + 2*j2*cos(2*k(0)) + 2*j3*cos(k(1)) + 2*j4*cos(k↩
          (2)) - 2*J1*cos(Q(0)) -
116             2*j2*cos(2*Q(0)))*(-j3 - j4 + j3*cos(k(1)) + j4↩
                *cos(k(2)) + J1*(-1 + cos(k(0)))*cos(Q(0)) -
117             2*j2*cos(2*Q(0))*sqr(sin(k(0))))),-((j3*
118             (epa - 4*(j3 + j4) + 4*j3*cos(k(1)) + 4*j4*cos(↩
                k(2)) + 2*J1*cos(k(0))*(1 + cos(Q(0))) -
119             4*(cos(Q(0))*(J1 - j2*cos(2*k(0))*cos(Q(0)))↩
                  + j2*cos(2*Q(0))))*sin(k(1)))/
120             (sqrt(2)*sqrt((epa - 2*(j3 + j4) + 2*J1*cos(↩
                k(0)) + 2*j2*cos(2*k(0)) + 2*j3*cos(k(1))↩
```

```
                    + 2*j4*cos(k(2)) - 2*J1*cos(Q(0)) -
121                 2*j2*cos(2*Q(0)))*(-j3 - j4 + j3*cos(k(1)) +↩
                     j4*cos(k(2)) + J1*(-1 + cos(k(0)))*cos(Q↩
                    (0)) -
122                 2*j2*cos(2*Q(0))*sqr(sin(k(0))))))),-((j4*
123                 (epa - 4*(j3 + j4) + 4*j3*cos(k(1)) + 4*j4*↩
                    cos(k(2)) + 2*J1*cos(k(0))*(1 + cos(Q(0))↩
                    ) -
124                 4*(cos(Q(0))*(J1 - j2*cos(2*k(0))*cos(Q(0)))↩
                     + j2*cos(2*Q(0))))*sin(k(2)))/
125                 (sqrt(2)*sqrt((epa - 2*(j3 + j4) + 2*J1*cos(↩
                    k(0)) + 2*j2*cos(2*k(0)) + 2*j3*cos(k(1))↩
                     + 2*j4*cos(k(2)) - 2*J1*cos(Q(0)) -
126                 2*j2*cos(2*Q(0)))*(-j3 - j4 + j3*cos(k(1)) +↩
                     j4*cos(k(2)) + J1*(-1 + cos(k(0)))*cos(Q↩
                    (0)) -
127                 2*j2*cos(2*Q(0))*sqr(sin(k(0))))))});
128     else return vec({0,0,0});
129 }
130
131 double theta0(const vec& k, const double& citot) {
132     return sqrt(BE(k)*(BE(k) + 1.))*epsilon(k)*11.6/(T*sqrt(↩
          citot)); //1meV/k_B Kelvin=11.6
133 }
134 // relaxon velocity
135 vec vrelaxon(const vec& alpha, const double& citot) {
136     vec res(3, fill::zeros);
137     for (int i=0; i<nveck; i++) {
138         res+=theta0(veck.col(i), citot)*vmagnon(veck.col(i))*↩
              alpha(i);
139     }
140     return res/(pow(a,3)*nveck);
141 }
142
143 int main(int argc, char **argv) {
144     int vL[3];
145     if (argc==7) {
146         sscanf(argv[1],"%lf", &T);
147         sscanf(argv[2], "%d", vL);
148         sscanf(argv[3], "%d", vL+1);
149         sscanf(argv[4], "%d", vL+2);
150         sscanf(argv[5], "%lf", Q.memptr());
151         sscanf(argv[6], "%lf", &epa);
152     } else {
153         cout << "usage: " << argv[0] << " Temperature Lx Ly ↩
              Lz Qx Anisotropy" << endl;
154         exit(0);
155     }
```

```
156    L(0)=vL[0]; L(1)=vL[1]; L(2)= vL[2];
157    cout << " T= " << T << " Anisotropy= " << epa <<" L= " ↩
          << L.t() << " Q= " << Q.t() << endl;
158    sigmak = 2*M_PI/arma::conv_to<vec>::from(L);
159    cout << "sigmak=" << sigmak.t() << endl;
160    // infrared momentum cutoff
161    k0=M_PI/2./arma::conv_to<vec>::from(L);
162    // number of kpoints
163    nveck=L(0)*L(1)*L(2);
164    veck.resize(3,nveck);
165    // compute J1 so that cos Q=-J1/4J2
166    J1 = -4.*j2*cos(Q(0));
167
168    cout << "using the cutoff k(0,0,0)->2Pi/L" << endl;
169    // energy cutoff (Bose-Einstein diverges at k=0)
170    eps0 = sqrt( sqr(funA(k0)) - sqr(funB(k0)) )/2;
171    cout << "eps0= " << eps0 << endl;
172
173    //maximum magnon velocities computed with Mathematica
174    //vmax=vec({1601.61, 314.143, 314.143}); //Q=2Pi/5
175    //vmax=vec({3678.93, 193.319, 193.319}); //Q=Pi/4
176    //vmax=vec({1063.04, 258.589, 258.589}); //Q=Pi/3
177    vmax=vec({5810.31, 124.567, 124.567}); //Q=Pi/10
178
179    // list all kvectors
180    for (size_t x=0, i=0;x<L(0);x++)
181       for (size_t y=0;y<L(1);y++)
182          for (size_t z=0;z<L(2);z++,i++) {
183             veck.col(i)=vec({momx(x), momy(y), momz(z)});
184          }
185    // energy smearing for Fermi Golden Rule
186    sigmaE = sigmak(0)*vmax(0)/a; //sigmaE/hbar
187
188    // compute the normalization for the Gaussian used for k↩
          smearing in P21
189    normk = 0;
190    for (int i=0; i<nveck; i++) {
191       normk+=exp(-0.5*(sqr(veck(0,i)/sigmak(0))+
192             sqr(veck(1,i)/sigmak(1))+
193             sqr(veck(2,i)/sigmak(2))));
194    }
195    cout << "sigmaE/hbar= " << sigmaE << " T= " << T << " ↩
          normk= " << normk << endl;
196
197    // M is the collision matrix (relaxons picture)
198    // Mmag is the diagonal part of it (magnons picture)
199    mat M(nveck,nveck,fill::zeros), Mmag(nveck,nveck,fill::↩
          zeros);
```

```
200
201     cout << "**********************************" << endl;
202
203     //filling M with its non diagonal elements
204 #pragma omp parallel for
205     for (int x=0; x<nveck; x++) {
206        for (int y=0; y<=x; y++) {
207           for (int z=0; z<nveck; z++) {
208
209              M(x, y)+=(P21(veck.col(x), veck.col(y), veck.↩
                    col(z)) -
210                 P21(veck.col(x), veck.col(z), veck.col(y)↩
                       ) -
211                 P21(veck.col(y), veck.col(z), veck.col(x)↩
                       ))/
212                 (sqrt(  BE(veck.col(y))* (BE(veck.col(y))↩
                        + 1.) * BE(veck.col(x)) * (BE(veck.↩
                       col(x)) + 1.)))/nveck;
213           }
214           M(y,x)=M(x,y);
215        }
216     }
217
218     //filling M and Mmag with the diagonal elements
219 #pragma omp parallel for
220     for (int x=0; x<nveck; x++) {
221        for (int y=0; y<nveck; y++)
222           for (int z=0; z<nveck; z++) {
223              Mmag(x,x)+=(P21(veck.col(x), veck.col(y), veck.↩
                    col(z)) + 0.5*P21(veck.col(y), veck.col(z), ↩
                    veck.col(x)))/
224                 ( BE(veck.col(x)) * (BE(veck.col(x)) + ↩
                       1.))/nveck;
225           }
226        M(x,x)+=Mmag(x,x);
227     }
228     // saving M and Mmag matrices
229     M.save(hdf5_name(string("M_T=")+to_string(T)+"_L="+↩
        to_string((int)L(0))+"_"+to_string((int)L(1))+"_"+↩
        to_string((int)L(2))+".h5","M"));
230     Mmag.save(hdf5_name(string("Mmag_T=")+to_string(T)+"_L="↩
        +to_string((int)L(0))+"_"+to_string((int)L(1))+"_"+↩
        to_string((int)L(2))+".h5","Mmag"));
231
232     // rescale M before diagonalizing to suppress numerical ↩
        noise
233     double scale = M.max();
234     cout << "scale=" << scale << endl;
```

```
235     vec freq; //eigenvalues of M
236     mat thetak1; //eigenvectors of M
237     // compute eigenvalues of M as scale/eig(scale/M)
238     eig_sym( freq, thetak1, inv(M/scale) );
239     freq = scale/freq;
240     // compute normalized eigenvectors of M and save
241     mat thetak=thetak1*pow(a,3./2)*pow(nveck, 1./2);
242     thetak.save(hdf5_name(string("thetak_T=")+to_string(T)+"_L="+to_string((int)L(0))+"_"+to_string((int)L(1))+"_"+to_string((int)L(2))+".h5","M"));
243
244     double citot=0.; // total specific heat due to all modes
245 #pragma omp parallel for reduction(+:citot)
246     for (int i=0; i<nveck; i++)
247         citot += cimu(veck.col(i));
248
249     citot/=pow(a,3);
250     citot/=nveck;
251     cout << "citot[J/(K.m^3)] = " << citot*1.38E-23 << endl;
252     //a^3=normalization volume
253
254     mat cond(3,3,fill::zeros); //thermal conductivity tensor
255     //components of thermal conductivity along the direction of the spiral
256     double cond00=0, condmag00=0;
257
258     //thermal conductivity in relaxons picture
259 #pragma omp parallel for reduction(+:cond00)
260     for (int alpha=0; alpha<nveck; alpha++) {
261         cond00+=vrelaxon(thetak.col(alpha),citot)(0)*vrelaxon(thetak.col(alpha),citot)(0)/freq(alpha);
262     }
263
264     cond00*=1.38E-23*citot;
265
266     cout << "cond_xx = " << cond00 << endl;
267
268     //contributions of different relaxons to thermal conductivity
269     mat contrib(2,nveck);
270 #pragma omp parallel for
271     for (int alpha=0; alpha<nveck; alpha++) {
272         contrib.col(alpha) = vec({1/freq(alpha), 1.38E-23*citot*(vrelaxon(thetak.col(alpha),citot)(0)*vrelaxon(thetak.col(alpha),citot)(0))/freq(alpha)/cond00});
273     }
274     contrib.save(hdf5_name(string("contrib_T=")+to_string(T)
```

```
      +"_L="+to_string((int)L(0))+"_"+to_string((int)L(1))+"_"+to_string((int)L(2))+".h5","contrib"));

   // same for the diagonal part of M -- single mode approximation
   double scalemag = Mmag.max();
   vec freqmag; //eigenvalues of Mmag
   mat thetakmag1; //eigenvectors of Mmag
   eig_sym( freqmag, thetakmag1, inv(Mmag/scalemag));
   mat thetakmag=thetakmag1*pow(a,3./2)*pow(nveck, 1./2); //normalized eigenvectors of Mmag
   freqmag = scalemag/freqmag;
   //(meV)^2/((1K)^2*Boltzmann constant)=134.7 Boltzmann constants

   mat condmag(3,3,fill::zeros);
   //thermal conductivity in magnons picture
#pragma omp parallel for reduction(+:condmag00)
   for (int alpha=0; alpha<nveck; alpha++)
      condmag00+=vrelaxon(thetakmag.col(alpha), citot)(0)*vrelaxon(thetakmag.col(alpha),citot)(0)/freqmag(alpha);

   condmag00*=1.38E-23*citot;

   cout << "condmag_xx = " << condmag00 << endl;
   mat contribmag(2,nveck);
#pragma omp parallel for
   for (int alpha=0;alpha<nveck;alpha++)
      contribmag.col(alpha)=vec({1/freqmag(alpha),1.38E-23*citot*(vrelaxon(thetakmag.col(alpha),citot)(0)*vrelaxon(thetakmag.col(alpha),citot)(0))/freqmag(alpha)/cond00});
   contribmag.save(hdf5_name(string("contribmag_T=")+to_string(T)+"_L="+to_string((int)L(0))+"_"+to_string((int)L(1))+"_"+to_string((int)L(2))+".h5","contrib"));

   return 0;
}
```

The code is compiled with the help of the following `Makefile`:

```
CC=g++
SHELL:=/bin/bash
LD_LIBRARY_PATH=$LD_LIBRARY_PATH:/opt/Applications/arma/
MKL=/opt/intel/compilers_and_libraries_2016.1.150/linux/mkl
COMP=/opt/intel/compilers_and_libraries_2016.1.150/linux/compiler
```

```
MATHINCL=/usr/local/Wolfram/Mathematica/10.3/SystemFiles/IncludeFiles
all:
	. /usr/share/Modules/init/bash; \
	module load gcc/gcc8; \
	module load mkl/2016.1.056; \
	$(CC) magcond3dopt-kappa.cpp -o magcond.x -O3 -march=native \
	-fopenmp -larmadillo -L/usr/lib64/ -lboost_filesystem-mt \
	-lboost_system -lboost_filesystem -lboost_program_options \
	-L/opt/software/boost/lib/ \
	-I $(MKL)/include/ -I $(MATHINCL)/C/ -L$(MKL)/lib/intel64_lin/ \
	-lmkl_intel_lp64 -lmkl_intel_thread -lmkl_core -lm -lpthread \
	-L$(COMP)/lib/intel64_lin/ -liomp5 -march=native -fopenmp

#-std=gnu++11 -lstdc++ -fPIC -shared -o

clean:
	rm magcond.x
```

The runs at various values of temperature, anisotropy and for different grid sizes are launched by the following `02runAll.sh` script:

```
#!/bin/bash
for Anis in 0.1; do
for T in 5 10 12.5 15 20 7.5; do
for Lx in 4 8 12 16 20 32 46 72 128; do
#    for ((T=10; T<=100; T+=10)); do
        if (($Lx<=64)); then tasksPerNode=$Lx;
        else tasksPerNode=64;
        fi;
        sbatch <<EOF
#!/bin/bash
#SBATCH -N 1 --ntasks-per-node=$tasksPerNode --time=24:00:00 -J cL${Lx}T${T} -p amd-hp

module load gcc/gcc8 mkl/2018.1.163
export LD_LIBRARY_PATH=\$LD_LIBRARY_PATH:/opt/Applications/arma
export OMP_NUM_THREADS=$tasksPerNode
time ./magcond.x $T $Lx 4 4 0.314159 $Anis
EOF
    done
done
```

```
done
```

`03summary.sh` prints the summary of the completed calculations:

```
#!/bin/bash
for s in slurm-*.out; do
    awk '/T=.*L=/{printf("\n" $0 "\t")}/cond.*_xx =/||/citot/{printf $0 " "}' $s;
done
echo
```

Appendix B

Mathematica code

This section provides a Mathematica code, developed to calculate the magnetic contribution to thermal conductivity in a spiral magnet. This simplified version uses relaxon formalism and saves the results in .mx files in the following order:

1. M – scattering matrix
2. freq – relaxation rates of relaxons
3. thetak – wavefunctions of relaxons
4. cond – thermal conductivity
5. relcontrib – contributions of individual relaxons to thermal conductivity
6. Mmag – scattering matrix in SMA
7. freqmag – relaxation rates of magnons in SMA
8. thetakmag – wavefunctions of magnons
9. condmag – thermal conductivity from SMA
10. magcontrib fractions of thermal conductivity due to individual magnons

```
48  Print[$ScriptCommandLine]
49 toN[str_]:=Read[StringToStream@str, Number]
50 LL={toN@$ScriptCommandLine[[2]]};
51 Tmin=toN@$ScriptCommandLine[[3]];
52 a=4 10^(-10);
53
54 (* parameters of the spiral *)
55 Q=2 Pi/5;
56 j2 = 1.`100; (* meV *)
57 j1=-4 j2 Cos[Q]; (* meV *)
58
59
60 hbar=10^(-34);
61 (* range of temperatures to be computed*)
```

```
Tmin=1`100;
Tmax=10`100;

Nstep=10; (* number of temperatures *)
deltaT=(Tmax-Tmin)/Nstep;
(* vector that will be filled with values of temperatures considered *)
Temperature=Table[0,{i,Nstep}];
(* vector that will be filled with values of thermal conductivities *)
cond=Table[0,{i,Nstep}];

funA[k_]:=2(j1 Cos[k] (Cos[Q]+1)+j2 Cos[2 k] (Cos[2 Q]+1))-4(j1 Cos[Q]+j2 Cos[2 Q]);
funB[k_]:=2(j1 Cos[k] (Cos[Q]-1)+ j2 Cos[2 k] (Cos[2 Q]-1));

(*coefficients of the Bogoliubov transformation*)
theta[k_]:= Piecewise[{{ArcTanh[funB[k]/(funA[k])]/2,funA[k]!=funB[k]&&funA[k]!=-funB[k]}}];

ch[k_]:=Cosh[theta[k]];
sh[k_]:= Sinh[theta[k]];

beta[k_]:=j1 Sin[Q] Sin[k]+j2 Sin[2 Q] Sin[2 k];

(*dispersion relation*)
eps[k_]:= Sqrt[funA[k]^2 - funB[k]^2]/2;

funC[k_,q_]:=Piecewise[{{beta[q] (ch[q]+sh[q]) (ch[k-q] ch[k]+sh[k] sh[k-q])+beta[k-q] (ch[k-q]+sh[k-q]) (ch[k] ch[q]+sh[k] sh[q])-beta[k] (sh[k]+ch[k]) (ch[q] sh[k-q]+ sh[q] ch[k-q]),k!=q}}];

(*magnon velocities*)
vmagnon[k_]:=607.7`100  eps'[k]; (*meV*4 Angstrom/hbar=607.7 m/s*)
vmax=FindMaximum[vmagnon[k],{k,-Pi,Pi}];


SpiralCond=Table[{Temperature,cond}=Transpose@Table[

(* inverse lifetimes of relaxons -- eigenvalues of the collision matrix *)
freq=Table[0,{i,1,L}];

(* eigenvectors of the collision matrix *)
thetak=Table[0,{i,1,L},{j,1,L}];
```

```
100
101 (* converts k-grid index into momentum *)
102 mom[xi_]:=((xi-1) Pi 2/L-Pi);
103
104 veck={};
105 (* fills veck with all the k-vectors except for Golstone ↩
    modes *)
106 For[i=1,i<=L,i++,
107 If[mom[i]!=0&&Abs[mom[i]]!=Q,
108  veck=Append[veck,mom[i]];
109 ]
110 ];
111
112 (* momentum and energy smearings, to be used in Fermi ↩
    Golden Rule *)
113 sigmak=2Pi/L;
114 sigmaE=sigmak vmax[[1]]/a; (*sigmaE/hbar*)
115
116 T=Tmin+deltaT (idx-1);
117
118 (* Bose-Einstein distibution *)
119 BE[k_]:=1/(E^(11.6 eps[k]/T)-1); (*1meV/kb Kelvin=11.6*)
120
121 (* instead of a Kronecker delta for momentum conservation, ↩
    here we use a Gaussian *)
122 (* normalization for the Gaussian on momenta *)
123 norm=Sum[E^(-0.5`100 veck[[idk]]^2/sigmak^2),{idk,↩
    Dimensions[veck][[1]]}];
124 (*meV 2 Pi/hbar=9.546\[Times]10^12 s^-1*)
125
126 (* scattering rates, computed with Fermi Golden Rule *)
127 P21[kx_,ky_,kz_]:=Piecewise[{
128   {1.529`100*10^-9  Abs[2 I (funC[kz,kx]+funC[kz, ky])]^2 *
129   (BE[kx] BE[ky] (BE[kz]+1)) (1/Dimensions[veck][[1]]) *
130   E^(-0.5`100 (1.519`100*10^12 *
131    (eps[kz]-eps[kx]-eps[ky])/sigmaE)^2)/(Sqrt[2 Pi] sigmaE ↩
       hbar)*
132   (E^(-0.5`100 ((kz-(Mod[kx+ ky-Pi,2Pi]-Pi))/(sigmak))^2)/↩
      norm), kx!=ky},
133
134   {1.529`100*10^-9  Abs[2 I Sqrt[2] funC[kz,kx]]^2 *
135   (BE[kx] BE[ky] (BE[kz]+1)) (1/Dimensions[veck][[1]]) *
136   E^(-0.5`100 (1.519`100*10^12 *
137     (eps[kz]-eps[kx]-eps[ky])/sigmaE)^2)/(Sqrt[2 Pi] sigmaE↩
        hbar)*
138   (E^(-0.5`100 ((kz-(Mod[kx+ ky-Pi,2Pi]-Pi))/(sigmak))^2)/↩
      norm),
139   kx==ky}}];
```

```
140
141 (* collision matrix in relaxons picture *)
142 M=Table[0, {i,1, Dimensions[veck][[1]]}, {j,1, Dimensions[↩
    veck][[1]]}];
143 (* collision matrix in magnons picture *)
144 Mmag=Table[0, {i,1, Dimensions[veck][[1]]}, {j,1, ↩
    Dimensions[veck][[1]]}];
145
146 (* filling the collision matrix for relaxons *)
147 M=Normal@SparseArray@Flatten@ParallelTable[
148     {xx,yy}->Sum[(P21[veck[[xx]],veck[[yy]],veck[[zz]]]-
149     P21[veck[[xx]],veck[[zz]],veck[[yy]]]-
150     P21[veck[[yy]],veck[[zz]],veck[[xx]]])/(Sqrt[BE[veck[[↩
        yy]]](BE[veck[[yy]]]+1)BE[veck[[xx]]](BE[veck[[xx↩
        ]]]+1)])/Dimensions[veck][[1]]
151 ,{zz,Length[veck]}],
152 {xx,Length[veck]},{yy,xx}
153 ];
154 M+=M\[Transpose]-DiagonalMatrix@Diagonal[M]; (* M is ↩
    symmetric *)
155
156 (* adding to M the diagonal terms *)
157 M+=DiagonalMatrix[ParallelTable[
158 Sum[(P21[veck[[xx]],veck[[yy]],veck[[zz]]]+
159     1/2P21[veck[[yy]],veck[[zz]],veck[[xx]]])/
160     (BE[veck[[xx]]](BE[veck[[xx]]]+1)BE[veck[[xx]]](BE[veck↩
        [[xx]]]+1))/Dimensions[veck][[1]],
161 {yy,Length[veck]},{zz,Length[veck]}]
162 ,{xx,Length[veck]}]];
163
164 (* filling the collision matrix for magnons *)
165 Mmag=DiagonalMatrix@ParallelTable[
166 Sum[(P21[veck[[xx]],veck[[yy]],veck[[zz]]]+1/2 P21[veck[[yy↩
    ]],veck[[zz]],veck[[xx]]])/(BE[veck[[xx]]](BE[veck[[xx↩
    ]]]+1)BE[veck[[xx]]](BE[veck[[xx]]]+1))/Dimensions[veck↩
    ][[1]],
167 {yy,Length[veck]},{zz,Length[veck]}],{xx,Length[veck]}];
168
169 (* we scale the M matrix and compute eigenvalues of the ↩
    inverse to improve numerical stability *)
170 scale=Max[Flatten[M]];
171
172 {freq,thetak}= Eigensystem[Inverse[M/scale]];
173 freq=scale/freq;
174
175 (* specific heat per magnon *)
176 (*(meV)^2/((1K)^2*Boltzmann constant)=134.7 Boltzmann ↩
    constants*)
```

```
177 cimu[k_]:=(BE[k] (BE[k]+1) eps[k]^2 134.7)/(T^2);(*Subscript[C, \[Mu]]/Subscript[k, B]*)
178
179 (*total specific heat due to all modes *)
180 citot=(1/a^3) Sum[cimu[veck[[i]]],{i,1,Dimensions[veck][[1]]}];(*Subscript[C, tot]/Subscript[k, B]*) (*a^3=norm volume*)
181
182 theta0[i_]:=Sqrt[BE[veck[[i]]] (BE[veck[[i]]]+1)] eps[veck[[i]]] 11.6/(T Sqrt[citot]);
183
184 (* relaxon velocity *)
185 vrelaxon[alpha_]:=(1/a^3)Sum[theta0[i] vmagnon[veck[[i]]] a^(3/2)thetak[[alpha,i]],{i,1,Dimensions[veck][[1]]}];
186
187 (* computing thermal conductivity for relaxons *)
188 cond=1.38 10^(-23) citot Sum[vrelaxon[alpha]^2 /(freq[[alpha]]),{alpha,1,Dimensions[veck][[1]]}];
189
190
191 scalemag=Max[Flatten[Mmag]];
192
193 {freqmag,thetakmag}= Eigensystem[Inverse[Mmag/scalemag]];
194 freqmag=scalemag/freqmag;
195
196 vrelaxonph[alpha_]:=(1/a^3)Sum[theta0[i] vmagnon[veck[[i]]] a^(3/2)thetakmag[[alpha,i]],{i,1,Dimensions[veck][[1]]}];
197
198 condmag=1.38 10^(-23) citot Sum[vrelaxonmag[alpha]^2 /(freqmag[[alpha]]),{alpha,1,Dimensions[veck][[1]]}];
199
200 relcontrib=Table[{1/(freq[[alpha]]),1.38 10^(-23) citot vrelaxon[alpha]^2 /(freq[[alpha]])},{alpha,1,Dimensions[veck][[1]]}];
201
202 magcontrib=Table[{1/(freqmag[[alpha]]),1.38 10^(-23) citot vrelaxonmag[alpha]^2 /(freqmag[[alpha]])},{alpha,1,Dimensions[veck][[1]]}];
203
204 DumpSave["outL"<>ToString[L]<>"T"<>ToString[Tmin]<>".mx",{M,freq,thetak,cond,relcontrib,Mmag,freqmag,thetakmag,condmag,magcontrib}];
205 {T,cond},{idx,1,Nstep}
206 ],{L,LL}]
```

References

[1] Hosho Katsura, Naoto Nagaosa, and Alexander V. Balatsky. "Spin current and magnetoelectric effect in noncollinear magnets". In: *Physical Review Letters* (2005). ISSN: 00319007. DOI: 10.1103/PhysRevLett.95.057205.

[2] Maxim Mostovoy. "Ferroelectricity in Spiral Magnets". In: *Phys. Rev. Lett.* 96 (6 2006), p. 067601. DOI: 10.1103/PhysRevLett.96.067601. URL: https://link.aps.org/doi/10.1103/PhysRevLett.96.067601.

[3] I. A. Sergienko and E. Dagotto. "Role of the Dzyaloshinskii-Moriya interaction in multiferroic perovskites". In: *Phys. Rev. B* 73 (9 2006), p. 094434. DOI: 10.1103/PhysRevB.73.094434. URL: https://link.aps.org/doi/10.1103/PhysRevB.73.094434.

[4] Sang-Wook Cheong and Maxim Mostovoy. "Multiferroics: a magnetic twist for ferroelectricity". In: *Nature materials* 6.1 (2007), pp. 13–20.

[5] Andrei Pimenov et al. "Possible evidence for electromagnons in multiferroic manganites". In: *Nature physics* 2.2 (2006), pp. 97–100.

[6] Alexander Kirillovich Tagantsev, L Eric Cross, and Jan Fousek. *Domains in ferroic crystals and thin films*. Vol. 13. Springer, 2010.

[7] Louis Ponet et al. "Topologically protected magnetoelectric switching in a multiferroic". In: *Nature* 607.7917 (2022), pp. 81–85.

[8] Jan Seidel. "Topological structures in ferroic materials". In: *Switzerland: Springer International Publishing* (2016).

[9] Fumiya Sekiguchi et al. "Slowdown of photoexcited spin dynamics in the noncollinear spin-ordered phases in skyrmion host GaV4S8". In: *Nature Communications* 13.1 (2022), pp. 1–8.

[10] Junichi Iwasaki, Masahito Mochizuki, and Naoto Nagaosa. "Universal current-velocity relation of skyrmion motion in chiral magnets". In: *Nature communications* 4.1 (2013), pp. 1–8.

[11] D. V. Dmitriev and V. Ya. Krivnov. "Frustrated ferromagnetic spin-$\frac{1}{2}$ chain in a magnetic field". In: *Phys. Rev. B* 73 (2 Jan. 2006), p. 024402. DOI: 10.1103/PhysRevB.73.024402. URL: https://link.aps.org/doi/10.1103/PhysRevB.73.024402.

[12] E.M. Lifshitz and L.P. Pitaevskii. *Physical Kinetics: Volume 10*. Course of theoretical physics. Elsevier Science, 1995. ISBN: 9780750626354. URL: https://books.google.it/books?id=HgRBAQAAIAAJ.

[13] Wolfram Research Inc. *Mathematica, Version 13.1*. Champaign, IL, 2022. URL: https://www.wolfram.com/mathematica.

[14] Robert J. Hardy. "Energy-Flux Operator for a Lattice". In: *Phys. Rev.* 132 (1 1963), pp. 168–177. DOI: 10.1103/PhysRev.132.168. URL: https://link.aps.org/doi/10.1103/PhysRev.132.168.

[15] Giorgia Fugallo et al. "Ab initio variational approach for evaluating lattice thermal conductivity". In: *Phys. Rev. B* 88 (4 July 2013), p. 045430. DOI: 10.1103/PhysRevB.88.045430. URL: https://link.aps.org/doi/10.1103/PhysRevB.88.045430.

[16] Naoto Nagaosa. *Quantum field theory in condensed matter physics*. Springer Science & Business Media, 1999.

[17] Assa Auerbach. *Interacting electrons and quantum magnetism*. Springer Science & Business Media, 2012.

[18] T. Holstein and H. Primakoff. "Field Dependence of the Intrinsic Domain Magnetization of a Ferromagnet". In: *Phys. Rev.* 58 (12 Dec. 1940), pp. 1098–1113. DOI: 10.1103/PhysRev.58.1098. URL: https://link.aps.org/doi/10.1103/PhysRev.58.1098.

[19] Hung T Diep. *Statistical Physics: Fundamentals and Application to Condensed Matter*. World Scientific, 2015.

[20] N. Bogolyubov. In: *J. Phys. USSR* 11 (1947), p. 292.

[21] N. D. Mermin and H. Wagner. "Absence of Ferromagnetism or Antiferromagnetism in One- or Two-Dimensional Isotropic Heisenberg Models". In: *Phys. Rev. Lett.* 17 (22 Nov. 1966), pp. 1133–1136. DOI: 10.1103/PhysRevLett.17.1133. URL: https://link.aps.org/doi/10.1103/PhysRevLett.17.1133.

[22] Z. Z. Du et al. "Magnetic excitations in quasi-one-dimensional helimagnets: Magnon decays and influence of interchain interactions". In: *Phys. Rev. B* 94 (13 Oct. 2016), p. 134416. DOI: 10.1103/PhysRevB.94.134416. URL: https://link.aps.org/doi/10.1103/PhysRevB.94.134416.

[23] Andrea Cepellotti and Nicola Marzari. "Thermal Transport in Crystals as a Kinetic Theory of Relaxons". In: *Phys. Rev. X* 6 (4 2016), p. 041013. DOI: 10.1103/PhysRevX.6.041013. URL: https://link.aps.org/doi/10.1103/PhysRevX.6.041013.

[24] John M Ziman. *Electrons and phonons: the theory of transport phenomena in solids*. Oxford university press, 2001.

[25] Robert J. Hardy. "Phonon Boltzmann Equation and Second Sound in Solids". In: *Phys. Rev. B* 2 (4 Aug. 1970), pp. 1193–1207. DOI: 10.1103/PhysRevB.2.1193. URL: https://link.aps.org/doi/10.1103/PhysRevB.2.1193.